Université d'Ottawa · University of Ottawa

To Janet ,

Andrew and Richard

Abstract

The work presented in the following pages is the culmination of four years of research in the area of gas phase ion chemistry. During this period mass spectrometry and ab initio molecular orbital calculations were employed to investigate the unimolecular decomposition of proton-bound complexes between acetonitrile and methanol, ethanol, n-propanol, i-propanol, n–butanol, s-butanol, i-butanol, and t-butanol. Common to these systems, is a competition between dissociation of the hydrogen bond in the proton-bound dimer and isomerization to $(CH_3CNR)(H_2O)^+$ (R=CH_3, CH_2CH_3, $CH_2CH_2CH_3$, $CH(CH_3)_2$, butyl). The minimum energy reaction pathways for the isomerization in these systems are presented and compared. The dominant isomerization pathway for these ions is an internal S_N2 reaction that proceeds via an intermediate $CH_3CN\bullet\bullet\bullet ROH_2^+$ ion (R=CH_3, CH_2CH_3, $CH_2CH_2CH_3$, $CH(CH_3)_2$). The mass spectra for the four butanol containing dimers (n-, s-, i-, and t-butanol) show similar behaviour.

The effect of chlorine substitution on the acetonitrile on the four systems methanol, ethanol, n– and i- propanol were also investigated. The theoretical and experimental studies reveal a potential energy surface which is very similar to that obtained for the CH_3CN containing analogues $(CH_3CN)(CH_3OH)H^+$, $(CH_3CN)(CH_3CH_2OH)H^+$, $(CH_3CN)(CH_3CH_2CH_2OH)H^+$ and $(CH_3CN)((CH_3)_2CHOH)H^+$. The effect of chloro-substitution of the acetonitrile does not significantly affect the height of the rate limiting isomerization barrier which governs the water loss channel. The chloro-substitution however, lowers the proton affinity of the chloroacetonitrile and hence where there is competition between simple cleavage and isomerization, the protonated alcohol outcompetes the protonated chloroacetonitrile in the MI mass spectra.

The dimer ion of acetonitrile and oxygen exhibit three peaks at m/z 32 (O_2), m/z 41 (CH_3CN and $^{\bullet}CH_2CNH^+$) and m/z 56 (-OH) in its MI mass spectrum. When O_2 (triplet ground state) encounters a $CH_3CN^{+\bullet}$ or $^{\bullet}CH_2CNH^+$ ion, the resulting complex $(C_2H_3N)(O_2)^{+\bullet}$ can take on either a doublet or quartet character. RRKM calculations predict a fast forward isomerization of $CH_3CN^{+\bullet}$ to $^{\bullet}CH_2CNH^+$. The fact the dissociation and isomerization compete on the microsecond timescale is an indication that the reactions do not occur statistically and that RRKM theory does not apply.

Acknowledgments

This is more than a compilation of scientific research conducted over a four year period. It is the totality of varying and unexpected circumstances and the influence and input of many people, each of whom have contributed a significant role which made this thesis a reality.

I am deeply grateful to my supervisor, Dr Paul M. Mayer, for providing me with an enthusiastic and productive environment which enabled me to bring my study to a successful completion. I have gained a solid background in mass spectrometry and ab initio theory because of his patience and putting up with me. I have been privileged to have been a member of your group. I would like to thank Prof John Holmes for his very useful discussions and chats.

A big thank you to Dr A. A. Mommers (Sander), for all the instrumental problems he always solved even at very short notice. Many thanks to Dr Clem Kazakoff for the very interesting chats. The study period would be less enjoyable if it were not for my colleagues, post-docs and students Julie, Christiane, Jie, Don, Natalia, Danielle, Xiang, Janeen, Vladimir and Little Clem.

Lastly I would like to thank my family and close friends for their support and encouragement throughout this journey.

Table of Contents

List of Figures

List of Tables

List of Abbreviations

CI:	Chemical ionization
CID:	Collision induced dissociation
CIDI:	Collision induced dissociative ionization
$\Delta_f H^0$:	Standard heat of formation
ESA:	Electrostatic analyzer
FFR:	Field free region
IE:	Ionization energy
KER:	Kinetic energy release
MI :	Metastable ion
PA:	Proton affinity
PES:	Potential energy surface
HF:	Hartree-Fock theory
MP2:	Mφller-Plesset pertubation theory
B3-LYP:	Becke-Lee-Young and Parr gradient-corrected correlation functional
CI:	Configuration integration
ACIMS	Active chemical ionization mass spectrometry

CHAPTER 1

INTRODUCTION AND FOCUS

1.1 Introduction

Mass spectrometry is a powerful analytical technique that is used to quantify known materials, and to elucidate the structural and chemical properties of molecules. Detection of compounds can be accomplished with very minute quantities of samples (down to 10^{-15} g or 10^{-12} mole for a compound of mass 1000 Daltons). This means that compounds can be identified at very low concentrations (one part in 10^{12}) in samples that are complex mixtures of chemicals. Mass spectrometry provides valuable information to a wide range of professionals: physicians, law enforcement officials, process control engineers, chemists, astronomers, and biologists, to name a few.

The basis of mass spectrometry is the production of ions from neutral compounds and the examination of the subsequent decomposition of these ions. The techniques now available in this field however, have greatly expanded upon this basic function. The steady increase in the number of mass spectrometers for research and their constant modifications have led to a rapid expansion of this discipline.

As its name implies, a mass spectrometer measures mass (or strictly speaking mass-to-charge ratio) and gives no direct information on ion structures. In mass spectrometric terms, structure is defined as the arrangement of atoms only, how they are bound together in the ion or neutral,

and not to the bond lengths and angles between atoms. Without further analysis of 'mass' selected ions, little more than their elemental composition is available. For ions containing more than a very few atoms the number of possible structure assignments is very large, and further analysis is required.

In mass spectrometry, structures are based on the indirect evidence of thermochemical arguments, decomposition products, and isotopic labelling. The experimentally obtained heats of formation and barriers to dissociation may reflect the stability and characteristic pathways to ion dissociation. These values may be compared with experimental values from similar systems or theoretically calculated systems. With the increasing accuracy of ab initio molecular orbital theory calculations, the latter comparisons have been given a steadily increasing weight. The observed decomposition products, structure characteristic fragments of the precursor, may be considered on their own merits or by comparison with the fragmentation pathway of other, reference, precursors. In either case, the analysis of isotopic derivatives can also serve to underline the proposed structure.

Such interpretations for the structural assignment are necessary to properly assign heats of formation and to devise mechanisms for gas-phase ion reactions. In the early years of ion chemistry, structures and reaction mechanisms were proposed using analogies from condensed phase organic chemistry. Such analogies have been found to be unjustified; whole classes of ions, having no neutral counterpart, have been found to be stable species in the gas-phase and thermodynamic properties of organic ions do not follow the same trends as for neutral organic

molecules. The generation of a solid reference base, including the structure and thermochemistry of common and not so common gas-phase ions and neutrals, is essential for the continued expansion of the field of gas-phase ion chemistry.

1.2 The Focus

Reactions of ions in the gas phase contribute to the formation of molecules in the atmospheres of planets, including the terrestrial atmosphere (TA), and in the interstellar clouds (ISC) that occupy the space between the stars. The observations of ions and molecules in these diverse regions and the laboratory studies of the reactions between ions and neutral atoms and molecules (studies in which mass spectrometry has been indispensable) have established the important role of ion-neutral reactions in these chemistries.[1] Gas-phase ion chemistry occurs in all these regions, because there are sources of ionization that act on the ambient atmospheres to continuously generate very reactive ionic species.

Following the development of our understanding of the ionization phenomena in gases in the early part of the 20 th Century, and before the advent of rocket-born mass spectrometry, it was assumed that the positive ions in the terrestrial atmosphere were simply those derived from the major atmospheric components N_2 and O_2, i.e. N^+, N_2^+, O^+ and O_2^+. Well how wrong could one be. It immediately became apparent following the flight of the first rocket-born mass spectrometers into the upper TA [2] that NO^+ was the major ambient species, and that gas-

phase ion chemistry was occurring (Figure 1). Subsequent flights into the lower atmosphere (the mesosphere) [3,4] showed that hydrated hydronium ions, $H_3O^+(H_2O)_n$ were the dominant positive ion species (Figure 1). These pioneering observations triggered the major new discipline of atmospheric ion chemistry and the development of new laboratory techniques to study the complex ion chemistry of the TA. Measured ion profiles in the ionosphere, have detected a clear chemical boundary between 82 and 85 km. The nature of this boundary is such that the region above 85 km (the E-region) is dominated by the ions O_2^+, NO^+ and M^+ (where M^+ is either Na^+, Al^+ or Fe^+), whereas below 82 km (the D-region), the dominant ions are of the form $H^+(H_2O)_n$ with n=1-8 being the most abundant.

Species such as $H^+(H_2O)_2$ are cluster ions. Cluster ions can range in size from simple dimers such as $(He)_2^+$ to large polymolecular species such as water hydrates, $H_3O^+(H_2O)_n$. Interest in their chemistry stems from their occurrence in the earth's atmosphere and from the study of the early stages of the effects of solvation. A central issue when studying the chemistry of gaseous ions is their propensity for rearrangement prior to reaction. Over the last 20 years work in organic mass spectrometry has lead to the discovery of a variety of thermodynamically stable structures including distonic ions [5,6] (e.g.,$CH_2OH_2^{+\bullet}$), ion/neutral complexes [7,8] (e.g.,$CH_2{=}CH_2)H_2O^{+\bullet}$ and bridged ions [9] (e.g.,$(H_2O)H^+(H_2O)$). These ion structures are ubiquitous to ion dissociation mechanisms, and indeed, the isomerization of gas-phase organic ions appears to be a common occurrence. However, the isomerization reactions of cluster ions have not been extensively studied.

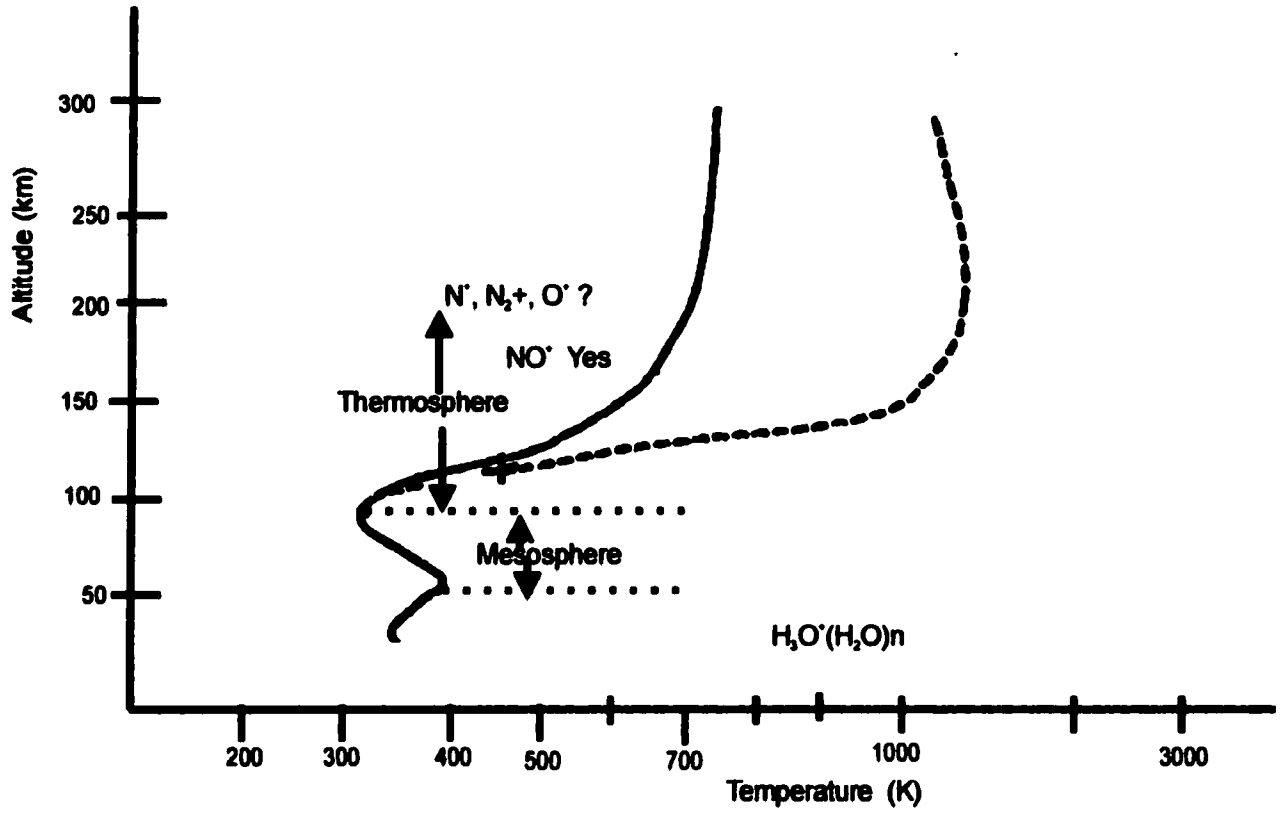

Figure 1:A typical altitudinal profile profile of the neutral gas temperature, T_g (solid curve) and the electron temperature T_e, (dashed curve) in the terrestrial atmosphere plotted using a logarithmic scale.

The focus of this thesis has been on the study of proton-bound cluster ions of acetonitrile-alcohols, chloroacetonitrile-alcohols and an odd electron cluster of acetonitrile and oxygen. All of these have at least one common feature, they exhibit in their unimolecular chemistry the competition between simple-bond dissociations and rearrangement reactions. The competition by the two channels means that there is a fine balancing of thresholds for dissociation with barriers to isomerization.

1.3 Outline of Thesis

As the title of this thesis implies, theoretical and mass spectrometric analysis were used in the study. Chapters 1 and 2 are introductory chapters. They provide the reader with some concepts which are basic to the understanding of gas phase ion chemistry and the theory of unimolecular reactions.

Chapter 3 deals with the computational procedures employed in this study and some aspects of theoretical quantum chemistry are discussed. Chapter 4 provides the reader with some of the major turning points in the history of mass spectrometry in general and a detailed description of the VG-ZAB-2HF mass spectrometer used in this work, and a discussion of the experiments used to study the cluster ions of interest. Chapter 5 deals with an experimental and theoretical study of the unimolecular reactions of proton-bound dimers of CH_3CN and alcohols. Chapter 6 looks at the effect of chlorine substitution of acetonitrile on the internal S_N2 isomerization of proton-

bound dimers of $(ClCH_2CN)(ROH)H^+$ [R=CH_3, C_2H_5, and C_3H_7]. Finally Chapter 7 is a study of a combined theoretical and experimental study of the unimolecular chemistry of the acetonitrile-oxygen dimer complex.

References

[1] D. Smith and P. Spanel, Mass Spec. Rev. 14 (1995) 255.

[2] C. Y. Johnson, J. Geophys. Res. 71 (1966) 330.

[3] R. S. Narcisi and A. O. Bailey, J. Geophys. Res. 70 (1965) 3687.

[4] E. Kopp and U. Herman, Ann. Geophysicae 2 (1984) 83.

[5] B. F. Yates, W. J. Bouma and L. Radom, Tetrahedron 22 (1986) 6225.

[6] H. E. Audier, J. Fossey, D. Leblanc, P. Morgues and V. Troude, ed. Intermediates in ionic gas phase organic reactions: distonic ions Kluwer Academic publishers, Netherlands, 1999.

[7] D. Harnish and J. L. Holmes, J. Am. Chem. Soc. 113 (1991) 9729.

[8] T. H. Morton, Org. Mass Spectrom. 26 (1991) 18-23.

[9] N. Heinrich and H. Schwarz, Role of ion-molecule complexes in the reactions of gaseous ions in ion and cluster ion spectroscopy (Amsterdam, Elsevier, 1989). [10] J. E. Szulejko and T. B. McMahon, Org. Mass Spectrom. 28 (1993) 1009.

[11] V. Aviyente, M. Iraqi, T. Peres and C. Liftshitz, J. Am. Soc. Mass Spectrom. 2 (1991) 113.

CHAPTER 2

SOME BASIC CONCEPTS

2.1 Ion Chemistry as a Function of Ion Internal Energy

Most often, the chemistry of an ion depends on its internal energy. In relation to fragmentation reactions, each fragmentation product requires a particular minimum energy (Figure 2). An ion with an energy 'P' can only access reaction channels A, B, and C and not D and E. The relative importance of A - C will change with internal energy since the rate of each process varies with energy in a unique fashion. We can determine the rate constant at a particular internal energy by modeling the dissociation using statistical theories, and the one applied in this thesis is the Rice-Ramsperger-Kassel and Marcus Quasi equilibrium theory (RRKM/QET). The theory is based on the following assumptions [1]:

(1) Ions generated represent isolated systems; thus the rate of a process is a function of the excitation energy only.

(2) The time required for ionization by electron impact is short with respect to that for dissociation; the removal of an electron occurs within ~ 10^{-16}s while the maximum rate of decomposition corresponds to one vibrational period and is of the order ~ 10^{-14}s.

(3) The rate of dissociation is slow relative to the redistribution of the excitation energy over all degrees of freedom of the molecular ions ground state; thus the rate of dissociation will be independent of the mode of ionization.

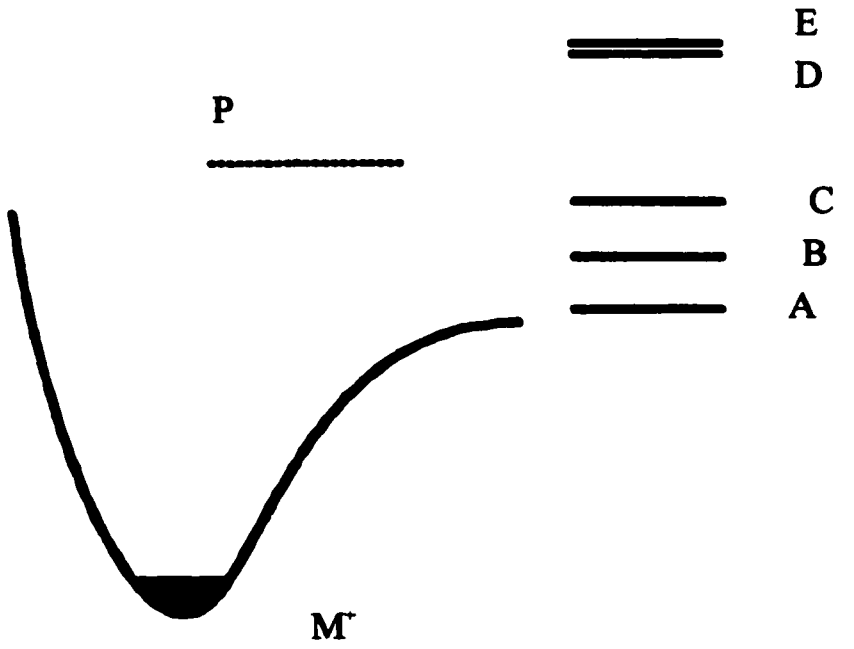

Figure 2:Reaction channel accessibility as a function of internal energy

2.2 The Theory of Unimolecular Reactions

The theory of unimolecular reactions has been referred to as both QET [2] and the RRKM version of statistical theory. [3-6] Mass spectrometry is a useful tool in testing the assumptions of the theory because reactions can take place in collision-free conditions (isolated reactants and products), and the ionic species can be selected and identified with high specificity. [7]

2.3 The RRKM/QET Equation

The RRKM/QET equation, which yields the rate constant for a unimolecular reaction for a molecule at a given internal energy E, is proportional to the ratio of the number of states in the transition state above the activation energy, E_o, to the density of states in the reactant at a given energy [8]:

$$k(E) = \frac{\sigma N^{\ddagger}(E-E_o)}{h \rho(E)} \qquad (1)$$

where $N^{\ddagger}(E-E_o)$ is the sum-of-states of the transition state and represents the probability that a reaction will proceed to products. The reactant ion density of states, $\rho(E)$, reflects the probability that the energy in the ion will "get lost" among the various rotational-vibrational modes and not get into the mode responsible for taking the reaction to the transition state and σ is the symmetry number. As a result, k(E) increases with increasing $N^{\ddagger}$ and decreases with increasing $\rho(E)$.

2.4 Variation of k(E) with E

The rate constant of a given decomposition process rises rapidly with increasing internal energy near threshold, levels off at higher energies, and reaches a constant value at higher energies. This is expected because the shortest decomposition time of an excited ion is of the order of one vibrational period, $\sim 10^{-13} - 10^{-14}$ s. Metastable ions (as observed on a VG ZAB mass spectrometer) decompose predominantly but not exclusively with rate constants between 5×10^5 and 5×10^6 s, while stable ions decompose at lower rates. Thus the terms 'stable' , 'unstable' , or metastable, are defined by the time- scale of a given instrument, wherein a range of rate constants are involved in fragmentations. The time-scale of events applicable to the VG ZAB-2HF mass spectrometer (described in the next chapter) for a typical species of m/z 100 at 8 keV accelerating voltage, is shown in Table 1. Rearrangement reactions generally have low critical energies and low frequency factors due to the unfavourable entropy change necessary to reach the transition state. Simple bond cleavage reactions often have higher critical energies and higher frequency factors than do rearrangement reactions. Ions dissociating via competitive rearrangement and simple cleavage reactions generally dissociate via the rearrangement process at low internal energies (due to a lower critical energy), whereas at higher internal energies, the simple cleavage reaction tends to dominate due to a higher frequency factor [7].

Table 1 **Time-scale of events, VG ZAB-2HF mass spectrometer (ion m/z 100, acceleration voltage 8kV)**

Event	Total time elapsed(s)
Ionization (EI/CI)	10^{-16}
Vibration	10^{-14}-10^{-12}
Rotation	10^{-8}
Ions leave source	10^{-6}
Ions reach 1st field-free region	3×10^{-6}
Ions reach collision cell (2nd field-free region)	13×10^{-6}
Collisional excitation	10^{-14}-10^{-16}
Time for ions to traverse collision cell	10^{-7}
Time for ions to traverse 3rd field-free region	12×10^{-6}
Ions reach collector	41×10^{-6}

2.5 Entropy of Activation and the Transition State

The vibrational frequencies of the reacting ion and the transition state give the entropy of activation $\Delta S^{\ddagger}$. The $\Delta S^{\ddagger}$ is a convenient way of describing the nature of the reaction.[8] Transition states which are less ordered " or looser " than the reactant ion are characterized by positive $\Delta S^{\ddagger}$ values. Simple bond cleavage reactions typically have loose transition states. Transition states which are more ordered than the reactant ion have negative values for $\Delta S^{\ddagger}$. These "tight" transition states are usually associated with rearrangement processes. So, if the vibrational frequencies of the reactant ion and the transition states are known, the nature of the process can be surmised.[8] Conversely, if the nature of the process is known, the transition state frequencies can be estimated so as to obtain $\Delta S^{\ddagger}$ values of the appropriate sign. The entropy of activation is given by the expression[8]:

$$\Delta S^{\ddagger} = k_B \ln \frac{Q^{\ddagger}}{Q} + \frac{U^{\ddagger} - U}{T} = k_B \ln \frac{\prod \overset{\ddagger}{q}_i}{\prod q_i} + \frac{U^{\ddagger} - U}{T} \quad (2)$$

where Q is the total vibrational partition function $q_1 q_2 q_3$ ...., and

$$q_i = \frac{1}{1 - \exp(-\frac{h\nu_i}{k_B T})} \quad (3)$$

and U is the average internal energy. The average internal energies U and $U^{\ddagger}$ can be calculated from the usual formulae by using the vibrational partition functions. Typically, $\Delta S^{\ddagger}$ values are reported at specific temperatures, either 600 or 1000K.

The effects of both E_o and $\Delta S^{\ddagger}$ on the rate constant as a function of energy are complimentary. The E_o is largely responsible for the magnitude of k(E) (Figure 3)[8], whereas $\Delta S^{\ddagger}$ is largely responsible for the slope of k vs E (Figure 4) [8]. Tight transition states($\Delta S^{\ddagger} < 0$) have k(E) curves which increase gradually with increasing energy, while loose transition states ($\Delta S^{\ddagger} > 0$) have k(E) curves that increase more rapidly. If neither E_o nor the transition state structure are known, both of these parameters can be adjusted to obtain an appropriate fit to experimental rate constant versus energy data. The assignment of $\Delta S^{\ddagger}$ affects the value of E_o, which needs to be used to obtain a satisfactory fit to experimental data (Figure 4). Ideally, the transition state of a reaction can be calculated by ab initio calculations and vibrational frequencies therein obtained. This will fix $\Delta S^{\ddagger}$, leaving only E_o to be adjusted to fit the experimental data, because at low levels of theory the calculated vibrational frequencies are more reliable than the relative energies. The transition state frequencies may themselves be estimated if necessary. The usual technique is to use the reacting ion vibrational frequencies less one to represent the reaction coordinate. The transition state can be made loose or tight by scaling the lowest five or six vibrational frequencies (which contribute the most to the calculated sum of states) by a common factor (less than 1.0 will produce $\Delta S^{\ddagger} > 0$, whereas greater than 1.0 will produce $\Delta S^{\ddagger} < 0$).

2.6 Understanding Mass Spectra

The application of both mechanistic and kinetic theories have been considered in the interpretation of the relative abundances of molecular and fragment ions in the mass spectrum of a given molecule. The ultimate goal of any kinetic theory is to calculate the rate of reaction. However, the Quasi-Equilibrium Theory, (QET) developed by Rosenstock et. al. [2] in 1952, also offered a theoretical concept for enabling such phenomena as kinetic shifts and the dependence of the fragment intensities on energies of activation and on lifetime to be predicted and explained.

The mechanistic approach involves the rationalization of mass spectral behaviour by using generalizations about reaction mechanisms from physical organic chemistry. Accordingly, the relative fragment ion abundances are determined by the following:

(a) The stability of the reaction products; those ions corresponding to dissociation processes which generate products of lowest total energy, $\sum \Delta_f H^{\cdot}$, will preferentially be produced.

(b) The strength of the bond cleaved.

The validity of this concept has been discussed in detail by R. W. A. Johnstone [7], however, it is not always possible to extrapolate conventional views of bonding in neutral organic molecules to ions in the gas phase, where the existence of nonclassical structures, such as CH_5^+, are well known, and moreover, an increasing number of other nonconventional species, such as ylid and distonic ions, are being discovered.

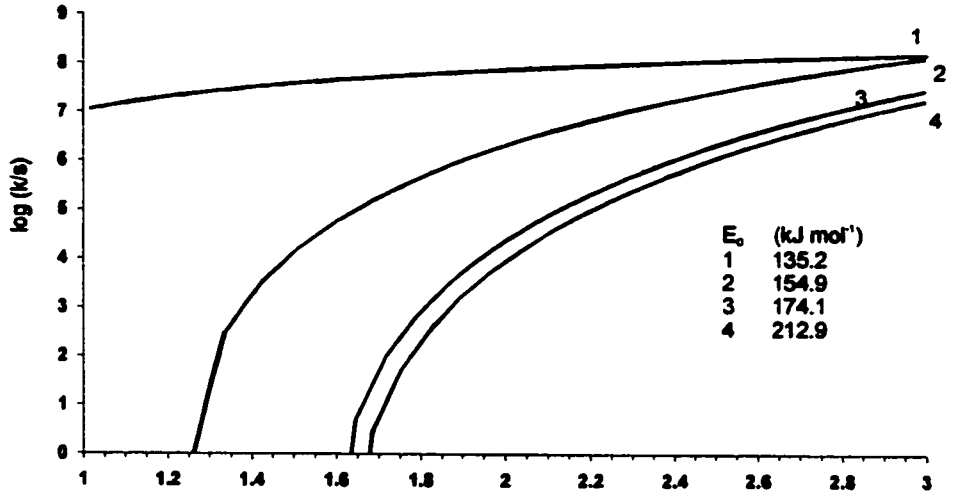

Figure: 3 An illustration of the variation of k(E)with increasing internal energy as E_0 changes

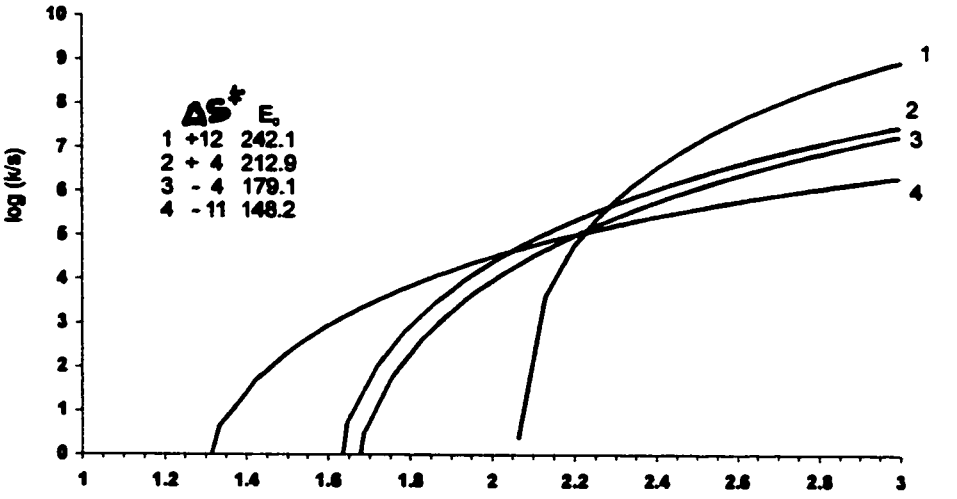

Figure: 4 An illustration of the variation of k(E)with increasing internal energy as $\Delta S^{\ddagger}$ changes

2.7 Isomerization

Energized molecular and fragment ions are not limited to only decomposition. A wide range of excess internal energies is transferred on ionization and so it is also possible for the molecular and fragment ions to rearrange to various isomeric structures, of classical or non-classical form. These isomerization reactions can greatly complicate the interpretation of mass spectra and thus some understanding of the parameters involved is very important. The relative energy barriers for dissociation, (E_{diss}), and isomerization, (E_{iso}), are the parameters which principally determine whether and to what extent an ion A^+ rearranges to an isomeric ion B^+ at a given internal energy E. Figure 5 shows an illustration of this process.

In the case of (a) where $E_{iso} >> E_{diss}$, for all dissociations X, no isomerization is possible below the threshold energy for dissociation, and in general, even above this threshold, decompositions will be much faster than isomerization (due to the greater sum of states in the corresponding activated complexes). In (b) where $E_{iso} << E_{diss}$, at internal energies above E_{iso}, there will be a mixture of rapidly interconverting structures A^+ and B^+. At increased internal energies decomposition becomes possible, however, having been preceded by a number of interconversions, the original placement of the atoms with respect to one another may have been altered several times resulting in partial or full randomization of the initial structure. Thus for (a), isomerization will not hinder the structural elucidation of A^+ and B^+, whereas for (b) the investigation of the dissociation of these ions will give no information unique to one or the other

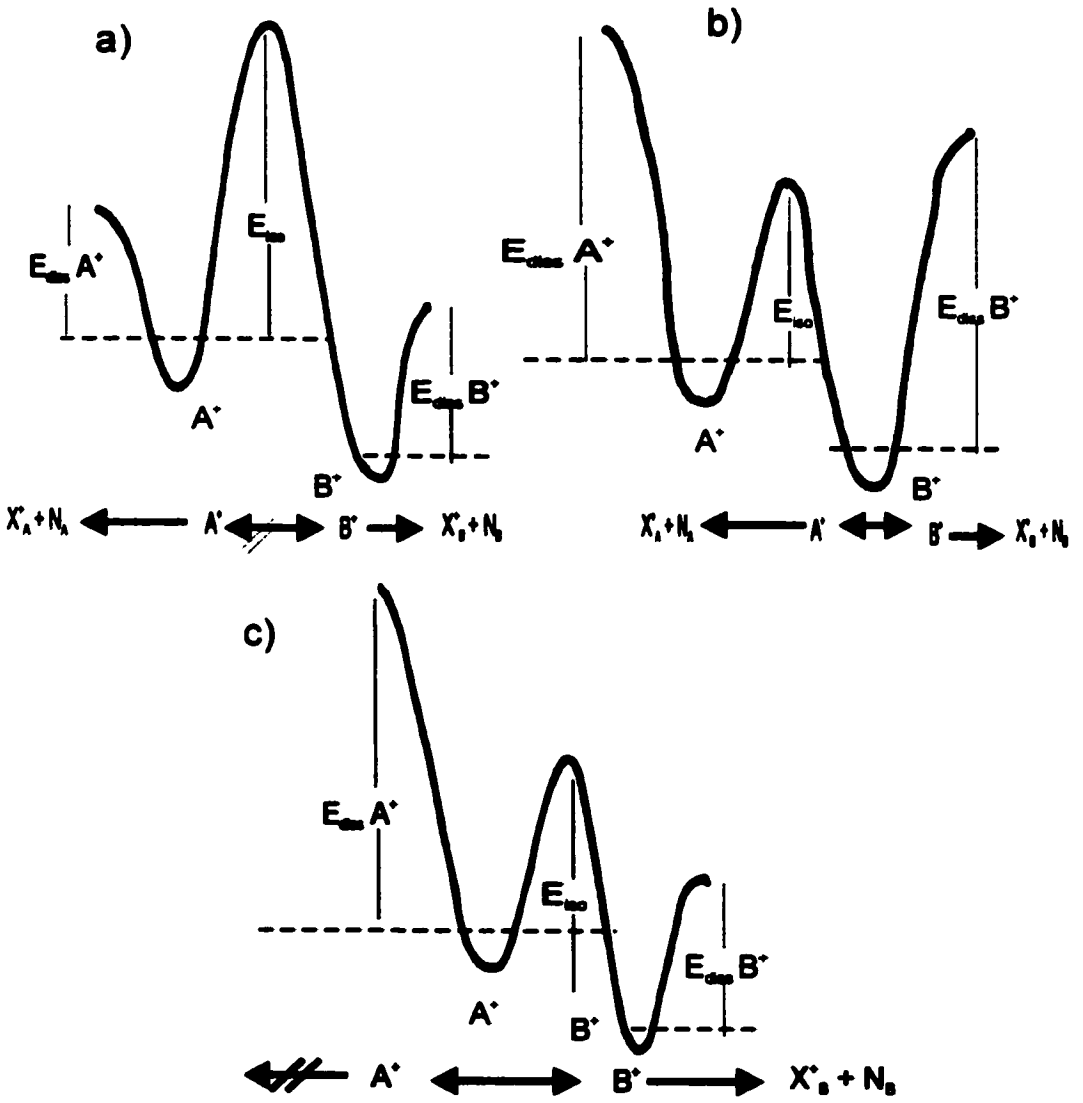

Figure 5:Schematic potential energy diagrams illustrating possible isomerization between ions A^+ and B^+, versus their dissociation products $X_A^+ + N_A$ and $X_B^+ + N_B$ respectively

structure. Intermediate situations between these limiting cases are also a possibility. In (c) A^+ must isomerize to B^+ prior to dissociation and thus both A^+ and B^+ will generate similar mass spectral results.

2.8 Assigning Structures to Ions in the Gas Phase by Mass Spectrometric Methods

In this section, I will give a brief description of some recent techniques used in mass spectrometry in assigning structure to ions in the gas phase. This is largely based on a review article written by Holmes [9]. In this section the term "structure' will imply which atoms are joined together and the probable (formal) locations of radical and / or charge sites. Details of geometry, such as bond lengths, bond angles and charge distribution are not yet accessible to experiments of polyatomic ions, and these can only be obtained from ab initio molecular orbital calculations.[10]

The three main experimental methods currently available are:

(a) Ion thermochemistry

(b) Ion dissociation characteristics: a) Spontaneous

b) Collision-induced

(c) Ion reactivity

Each of these may involve the use of isotopically labelled compounds, the time-honoured method that has proved to be of immense value in unravelling the complexities of ion fragmentation mechanisms [11]. The objective of method (b) is concerned with the fragmentation behaviour

of the ion of interest, and is summarized in Figure 6. The ion whose structure is to be unraveled is the radical cation $[M_1]^{+\bullet}$, which, in this example, may be generated by either direct ionization of a stable neutral molecule, M_1, or as a fragment ion in the dissociative ionization of a suitable neutral precursor species, M_1B, i.e,

$$M_1 + e \rightarrow [M_1]^{+\bullet} + 2e;\ M_1B + e \rightarrow [M_1B]^{+\bullet} + 2e \rightarrow\rightarrow [M_1]^{+\bullet} + B + 2e$$

2.8.1 Ion Thermochemistry

Ionization and appearance energy (IE and AE) measurements are used to establish the energy levels shown as bold horizontal lines in Figure 6. The determination of the heat of formation ΔH°_f of the ion $[M_1]^{+\bullet}$ involves the measurement of the adiabatic IE (M_1) and the standard enthalpy of formation of the neutral molecule. A reliable $\Delta H^\circ_f([M_1]^{+\bullet})$ is then obtained from Eq. 2.1

$$\Delta H^\circ_f([M_1]^{+\bullet}) = IE(M_1) + \Delta H^\circ_f(M_1) \qquad (2.1)$$

When $[M_1]^{+\bullet}$ results from a dissociative ionization (Figure 6) then ancillary ΔH°_f values are required; Eq. (2.2) now applies:

$$\Delta H^\circ_f([M_1]^{+\bullet}) = AE([M_1]^{+\bullet}) - \Delta H^\circ_f(B) + \Delta H^\circ_f(M_1B) \qquad (2.2)$$

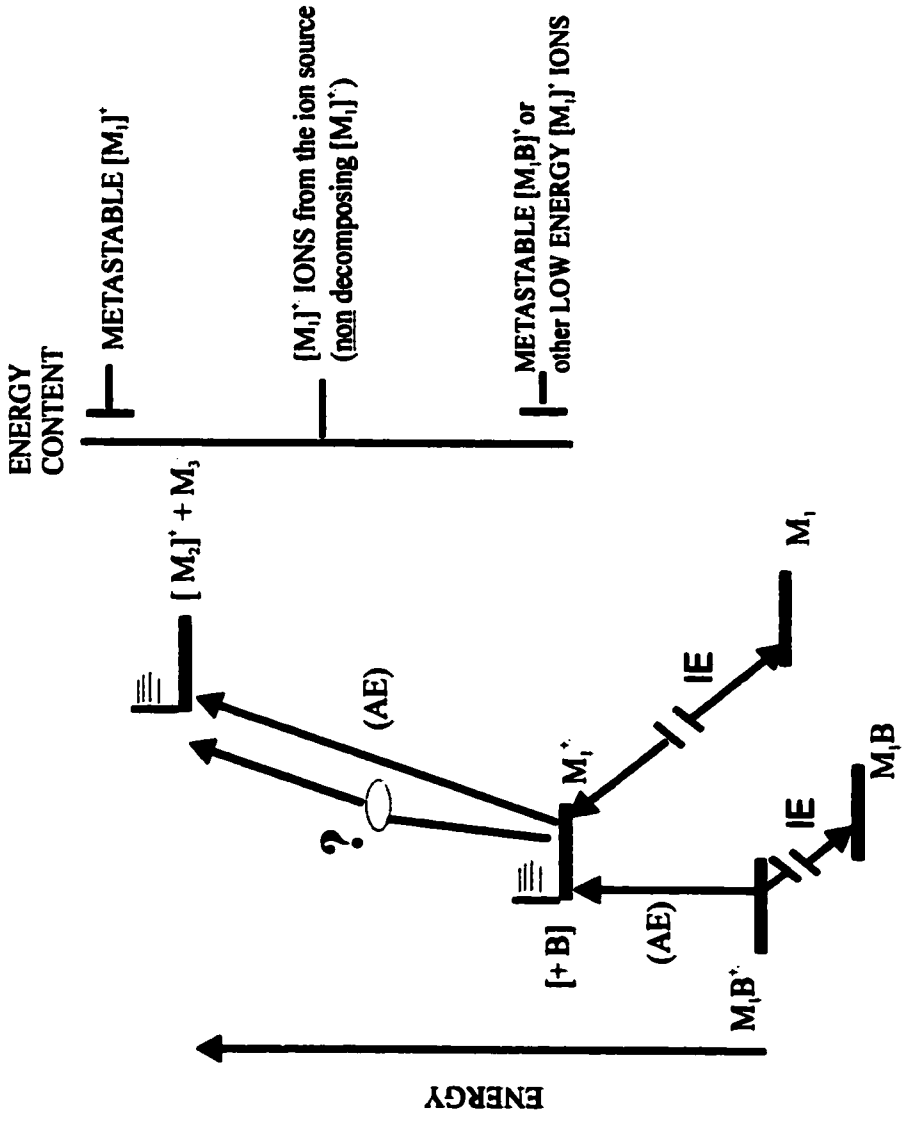

Figure 6:Energy diagram for the generation and fragmentation of an $[M_1]^+$ ion.[9]

The ionic heat of formation obtained from the IE value will be specific for an ion having at least initially the same structure as the neutral molecule. The ion enthalpy derived from equation 2.2 will be the same as that from (2.1), if the daughter ion has the structure $[M_1]^{+\bullet}$ and provided that (i) the fragmentation reaction of $[M_1B]^{+\bullet}$ has no kinetic shift [12] and (ii) that the reverse reaction

$$B + [M_1]^{+\bullet} \rightarrow [M_1B]^{+\bullet} \qquad (2.3)$$

has no energy barrier. A third unresolved problem concerns the difficulty of assigning a precise temperature to the fragmentation products at threshold and hence to correct the AE for the heat capacity effects. This matter, recently discussed by Treager and McLoughlin [13] may not be of great importance unless high precision is required. Although the contributions from (i) and (ii) are a priori unpredictable, some useful general guidelines are given by Holmes.[9] A fragmentation reaction will have a significant kinetic shift when its rate constant rises only slowly with increase in internal energy. In practice this means that the measured AE value will depend quite strongly upon the time scale of the method used for its measurement and it therefore will not lead to a reliable heat of formation, but rather to an upper limit. The same holds for reactions having a significant barrier for their reverse reaction, but in contrast to a kinetic shift this can be inferred from the inspection of the shape of the metastable peak.

2.8.2 Metastable Dissociations

Bearing in mind the earlier assumption that $[M_1]^{+\bullet}$ is uniquely and solely generated from M_1B, then the shape of the metastable peak for the fragmentation $[M_1]^{+\bullet} \rightarrow [M_2]^{+} + [M_3]^{\bullet}$ will be characteristic of the structure $[M_1]^{+\bullet}$, provided that this is the reacting configuration for the dissociation. The term "reacting configuration" refers to that stable ion structure (i.e., a structure which exists in a potential well) which leads directly to the transition state for dissociation. [15,16] If isotopic labelling experiments are performed it may well be discovered that the simplest mechanism required to describe the reaction leads to the proposal that $[M_1]^{+\bullet}$ need undergo no rearrangement. Under these circumstances, the metastable peak shape can provisionally be accepted as an observation criterion for structure $[M_1]^{+\bullet}$. However, although the range of $[M_1]^{+\bullet}$ energies involved is small, the ions nevertheless have relatively high internal energies above the threshold for $[M_1]^{+\bullet}$ formation and therefore it is in general possible that prior to this fragmentation $[M_1]^{+\bullet}$ ions rearrange to another structure. Thus a metastable peak may not be characteristic of the ground state structure but it may arise from an excited state or from a different reacting configuration produced by rearrangement of the original ion. If the known stable isomers of $[M_1]^{+\bullet}$ also fragment by loss of $[M_3]^{\bullet}$, then the metastable peak for this common fragmentation alone may suffice unequivocally to identify the isomeric ions.

2.8.3 Collision-Induced Fragmentations

The principles of the method are outlined with reference to Figure 6. The collision gas cell is usually situated in the same field-free region as that in which metastable dissociations are observed (see Figure 8). Thus mass-selected ions which suffer collisional activation are ions, originating in the ion source, which have insufficient energy to fragment on the microsecond (metastable) time-scale. These non-decomposing $[M_1]^{+\bullet}$ ions, as shown in Figure 6, possess a broad range of internal energies. If it is initially assumed that $[M_1]^{+\bullet}$ ions retain their structure irrespective of their internal energy within this range, then the collisional activation (CA) mass spectrum for these ions can tentatively be taken as structure-specific. However, to substantiate this assumption it is highly recommended to inspect $[M_1]^{+\bullet}$ ions of low internal energy. This can be done in several ways: (i) by transmitting metastably generated $[M_1]^{+\bullet}$ ions (from $[M_1B]^{+\bullet}$, see Figure 6); this can be achieved by adjusting the magnetic field strength so as to transmit ions of apparent mass $m_i^* = M_1^2/(M_1B)$; (ii) by lowering the ionizing electron energy to the lowest value compatible with a reasonable signal-to noise ratio and transmitting the resulting source-generated low-energy $[M_1]^{+\bullet}$ ions; or (iii) by collisionally deenergizing the ions within the source by having present a large pressure of inert gas, such as He.

References

[1] K. G. Kay, J. Chem. Phys. 65 (1976) 3813.

[2] H. M. Rosenstock, M. B. Wallenstein, A. L. Wahrhafit and H. Eyring , 1952; Vol. 38, pp 667.

[3] L. S. Kassel, J. Phys. Chem. 32 (1928) (c) 1617.

[4] R. A. Marcus, J. Chem. Phyics. 20 (1952) .

[5] O. K. Rice and H. C. Ramsperger, J. Am. Chem Soc. 49 (1927) 1617.

[6] T. Baer and W. L. Hase, Unimolecular Reaction Dynamics, Theory and Experiments Editor (Ed.) Oxford University Press, New York, 1996.

[7] K. L. Busch, G. L. Glish and S. A. McLuckey, ed. Mass Spectrometry/Mass Spectrometry VCH Publishers, New York, 1988.

[8] T. Baer and P. M. Mayer, J. Am. Soc. Mass Spectrom. 8 (1997) 103.

[9] J. L. Holmes, Org. Mass Spectrom 20 (1985) 169.

[10] W. J. Bouma and L. Radom, J. Am. Chem. Soc. 107 (1985) 345.

[11] J. L. Holmes, Mass Spectrometry In M.T.P. International Review of Science, Physical Chemistry Series Two Maccoll, A., ed. (London, Butterworths, 1975).

[12] W. A. Chupka, J. Chem. Physics. 30 (1959) 191.

[13] J. C. Traeger and R. G. McLoughlin, J. Am. Chem. Soc. 103 (1981) 3647.

[14] R. P. Morgan, J. H. Beynon, R. H. Bateman and B. N. Green, Int. J. Mass Spectrom. Ion Phys. 28 (1978) 1978.

[15] P. J. Derrrick and K. F. Donchi, ed. Comprehensive Chemical Kinetics Amsterdam, 1983.

[16] J. L. Holmes, and J. K. Terlouw, Org. Mass Spectrom. 15 (1980) 383.

[17] J. A. Hipple and E. U. Condon, Phys. Rev. 68 (1945) 54.

[18] J. A. Hipple, R. E. Cox and E. U. Condon, Phys. Rev. 69 (1946) 347.

[19] R. G. Cooks, J. H. Beynon, R. M. Caprioli and G. R. Lester, ed. Metastable Ions Elsevier Sci. Pub. Co., Amsterdam (1973).

CHAPTER 3

COMPUTATIONAL CHEMISTRY

3.1 Introduction

In order to provide a background for the studies in this thesis, I will first give an introduction to some aspects of theoretical quantum chemistry which can be studied in more detail from standard textbooks [1].

3.2 Theoretical Chemistry

In this section a review is given of the theoretical techniques referred to in the studies given in this thesis. It will start with Hartree-Fock theory and describe methods such as UHF and RHF, Mφller-Plesset perturbation theory and Density Functional Theory. The objective will not be to give detailed derivations, but rather characterize the various methods, and to emphasize their weak and strong points. In discussing the various theoretical methods it is assumed that the Hamiltonian is non-relativistic and that the Born-Oppenheimer approximation is valid, [2] resulting in a description of the motion of electrons with respect to fixed nuclei.

3.2.1 Single Configuration Wavefunctions; Hartree-Fock Theory

The Hartree-Fock theory is a variational theory in quantum mechanics [3-5] in which the n-electron wavefunction of a molecular system is represented as a single determinant wave-function. The variational concept is used to optimize the orbitals in Hartree-Fock wavefunctions. An individual molecular orbital (MO) ψ_j can be expressed as a linear combination of a finite set of N one electron functions known as basis functions, $\varphi_1,\varphi_2...,\varphi_N$. In the case where atomic orbitals of constituent atoms are used as basis functions, one speaks of a linear combination of atomic orbitals (LCAO) theory. The individual orbitals ψ_j can be written as

$$\psi_j = \sum_{\mu=1}^{N} c_\mu \phi_\mu \qquad (3.1)$$

where the MO expansion coefficients $c_{\mu i}$ are adjusted to minimize the expectation value of the total energy E. The final value of E will be as close to the exact energy as is possible within the limitations of Hartree-Fock theory, namely the limitations of a single determinant wavefunction and of the particular basis set chosen. The variational conditions lead to a set of algebraic equations for $c_{\mu i}$, which were derived independently for closed shell wavefunctions by Roothan [6] and Hall [7]. These Roothan-Hall equations are;

$$\sum_{\nu=1}^{N} (F_{\mu\nu} - \varepsilon_i S_{\mu\nu}) c_{\mu i} = 0, \mu = 1,2,...N \qquad (3.2)$$

where, $_i$ is the one-electron energy or orbital energy of molecular orbital ψ_i, $S_{\mu\nu}$ are the elements of an N x N matrix termed the overlap matrix and $F_{\mu\nu}$ are the elements of another N x N matrix, the Fock matrix. F_ν itself depends on the molecular orbital coefficients, and so a solution can only be achieved by an iterative process. The resulting molecular orbitals are derived from their own effective potential, and the method is therefore frequently called the self consistent field (SCF) method.

For open shell systems, the Roothan-Hall equations need to be modified, which can be done in two ways. The first is described as spin restricted Hartree-Fock (RHF) theory [8]. In this approach, a single set of molecular orbitals is used, some of them being doubly occupied and some being singly occupied with electrons of either all α spin or all β spin. The corresponding n-electron wave-function is a single determinant wave function representing a pure doublet, triplet and so on, spin state, that is it is an eigen-function of spin operator S^2. This is an advantage since exact wave functions are also pure spin states. On the other hand, the RHF method shows in some cases bad convergence or no convergence is reached at all. It is then hard to tell whether this is caused by a Hartree-Fock deficiency or by other factors like poor starting geometries or poor starting vectors, etc.

The second type of molecular orbital theory in common use for open shell systems is the spin unrestricted Hartree-Fock(UHF) theory [1]. In this approach the orbitals associated with α and β electrons are treated independently. The two sets of molecular orbitals are defined by

$$\varphi i^{\alpha} = \sum_{\mu=1}^{N} c_{\mu i^{\alpha}} \phi_{\mu}; \qquad \varphi i^{\beta} = \sum_{\mu=1}^{N} c_{\mu i^{\beta}} \phi_{\mu} \tag{3.3}$$

The coefficients $c_{\mu i}$, are varied independently, leading to the UHF generalizations of the Roothan-Hall equations, the Pople-Nesbet equations [8],

$$\sum_{\nu=1}^{N} (F_{\mu\nu^{\alpha}} - \varepsilon i^{\alpha} S_{\mu\nu}) c_{\mu i^{\alpha}} = 0; \qquad \sum_{\nu=1}^{N} (F_{\mu\nu^{\beta}} - \varepsilon_{i}^{\beta} S_{\mu\nu}) c_{\mu i^{\beta}} = 0 \mu = 1,2,\ldots,N \tag{3.4}$$

The advantages of the UHF method are that it is capable of providing a qualitatively correct description of bond dissociation, and converges more easily than the RHF method. However the principal disadvantage of the resulting wavefunction is that it is no longer spin pure. An UHF calculation a system with an extra α electron might lead to a wavefunction that is a mixture of a doublet and a quartet, or higher components rather than a pure doublet. The amount of spin contamination is reflected in the expectation value of the S^2 operator $\langle S^2 \rangle$. For a pure doublet this is 0.75 and the results will be the least suspect. As a criterion for the acceptability of an UHF wavefunction it has been proposed that the $\langle S^2 \rangle$ deviation be less than 10% [9]. Whether these deviations are of the right order of magnitude is hard to say and this point is rarely discussed in the literature. It is possible there is no obvious relationship between the accuracy of the total energy calculated and the deviation of $\langle S^2 \rangle$ from its exact value, which makes the whole problem extremely difficult to discuss. Which of the two methods should be used depends on the shell and process being investigated. RHF is better defined theoretically, but UHF has a better convergence

behaviour which makes UHF in some cases very useful.

3.2.2 Multiple - Determinant Wavefunctions

Hartree-Fock theory is very useful for providing initial, first level predictions for many systems. It is also reasonably good at computing the structures and vibrational frequencies of stable molecules and some transition states. As such, it is a good base-level theory. However, the primary deficiency of Hartree-Fock theory is the inadequate treatment of correlation between the motions of electrons [1]. While correlation of the motions of electrons with the same spin is partially taken into account by virtue of the determinantal form of the wave functions, single configuration wave-functions do not take into account the correlation between electrons with opposite spin. This means that the calculated Hartree-Fock energies will be greater than the exact values. By convention, the difference between the Hartree-Fock and exact (non-relativistic Born-Oppenheimer approximated) energies is called the correlation energy [1],

$$E_{(exact)} = E_{(Hartree\text{-}Fock)} + E_{(correlation)} \qquad (3.5)$$

The neglect of correlation between electrons of opposite spins leads to a number of qualitative deficiencies in the description of electronic structures. One very important consequence is that the closed shell Hartree-Fock function often does not dissociate correctly when nuclei are moved to infinite separation.

3.2.3 Møller-Plesset Perturbation Theory.

One different approach to the correlation problem is the Møller-Plesset (MP) perturbation theory [9], closely related to many body perturbation theory (MBPT). This method has been used extensively in this thesis.

In Perturbation Theory the electronic Hamiltonian, H, is divided into a zero order Hamiltonian (H_0) and a perturbation V, according to :

$$H = H_0 + \lambda V \qquad (3.6)$$

ψ_λ and E_λ, the exact or full configuration interaction, CI, (within a given basis set) ground state wavefunction and energy for a system described by the Hamiltonian H, may now be expanded in powers of λ according to Raleigh-Schrodinger perturbation theory [9].

$$\Psi_\lambda = \Psi(0) + \lambda\,\Psi(1) + \lambda^2\,\Psi(2) + \ldots$$

$$E_\lambda = E^{(0)} + \lambda E^{(1)} + \lambda^2 E^{(2)} + \ldots \qquad (3.7)$$

In Møller-Plesset theory, H_0 is taken to be the sum of the one-electron Fock operators. The eigenvalue, E_s, corresponding to a particular determinant, Ψ_s is the sum of the one-electron energies $_i$, for the spin orbitals which are occupied in Ψ_s.

Practical perturbation methods may now be formulated by truncation of the series in Eq. (3.7)

to various orders and by setting the parameter $\lambda = 1$. In the literature these methods are referred to by the highest-order energy term allowed, that is truncation after second order as MP2, after third order as MP3 and so forth, and one usually uses a spin unrestricted form (UMP).

The leading terms in expansions (3.7) are

$$\Psi^{(0)} = \Psi_0 \qquad (3.8)$$

$$E^{(0)} = \sum_{i}^{occ} \varepsilon_i \qquad (3.9)$$

$$E^{(0)} + E^{(1)} = \sum_{i} + \langle \Psi_0 | V | \Psi_0 \rangle = E_{HF} \qquad (3.10)$$

where Ψ_0 is the Hartree-Fock wavefunction and $_i$ are the one-electron energies defined by Eq. (3.2). The first order Mφller-Plesset energy is thus the Hartree-Fock energy. Higher terms in the expansion involve other matrix elements of the operator V.

The first order contribution to the wavefunction is

$$\Psi^{(1)} = \sum_{s>0} a_s^{(1)} \Psi_s \qquad (3.11)$$

with

$$a_s^{(1)} = (E_0 - E_s)^{-1} V_{s0} \qquad (3.12)$$

V_{s0} vanishes unless it corresponds to a double substitution, so that only such substitutions contribute to the first-order wavefunction and the third order energy [1].

At the fourth-order level of theory, single, triple and quadruple substitutions also contribute, since

they have nonzero Hamiltonian matrix elements with double substitutions. The triple substitutions are the most difficult computationally, and some computations have been carried out using only singles, doubles and quadruples. This partial fourth-order level of theory is termed MP4SDQ [1]. MP2, MP3 and MP4 energy expressions again satisfy some, but not all of the model conditions. They are well defined and can be applied widely. They are size consistent at any order. In general perturbation theory results, terminated at any order, are no longer variational, since they are not derived as expectation values of the Hamiltonian. The Møller-Plesset method, however, does provide a variational upper bound to the energy for all odd orders [10].

3.2.4 Density Functional Theory Methods

Density functional theory-based methods ultimately derive from quantum mechanics research from the 1920's, especially from the Thomas-Fermi-Dirac model, and from Slater's fundamental work in quantum chemistry in the 1950's. The DFT approach is based upon a strategy of modeling electron correlation via general functionals of the electron density [11].

Such methods owe their modern origins to the Hohenberg-Kohn theorem published in 1964 [11] which demonstrated the existence of a unique functional which determines the ground state energy and density exactly. The theorem does not provide the form of this functional, however.

Following on the work of Kohn and Sham [11], the appropriate functionals employed by current DFT methods partition the electronic energy into several terms:

$$E = E^T + E^V + E^J + E^{XC} \qquad (3.12)$$

where E^T is the kinetic energy term (arising from the motion of the electrons), E^V includes terms describing the potential energy of the nuclear-electron attraction and of the repulsion between pairs of nuclei, E^J is the electron-electron repulsion term (it is also described as the Coulomb self-interaction of the electron density), and E^{XC} is the exchange-correlation term and includes the remaining part of the electron-electron interactions [11].

In the last few years, methods based on Density Functional Theory (DFT) have gained steadily in popularity. The best DFT methods achieve significantly greater accuracy than Hartree-Fock theory at only a modest increase in cost (far less than MP2 for medium-size and larger molecular systems [11]). They do so by including some of the effects of electron correlation much less expensively than traditional perturbation methods.

A variety of functionals have been defined, generally distinguished by the way that they treat the exchange and correlation components:

(1) Local exchange and correlation functionals involve only the values of the electron spin densities. Slater and X_α are well-known local exchange functionals and the local spin density treatment of Vosko, Wilk and Nusair (VWN) is a widely-used local correlation functional [11].

(2) Gradient-corrected functionals involve both the values of the electron-spin densities and their gradients. Such functionals are also sometimes referred to as non-local in the literature. A popular gradient-corrected exchange functional is one proposed by Becke in 1988 [11]; a widely-used gradient-corrected correlational functional is the LYP functional of Lee, Yang and Parr. The combination of the two forms gives the B-LYP method (available via the BLYP keyword in Gaussian). Perdew has also proposed some important gradient-corrected functionals, known as Perdew 86 and Perdew-Wang 91 [11].

There are also several hybrid functionals, which define the exchange functional as a linear combination of Hartree-Fock, local, and gradient-corrected exchange terms. This exchange functional is then combined with a local and/or gradient-corrected correlation functional. The best known of these hybrid functionals is Becke's three-parameter formulation; hybrid functionals based on it are available in Gaussian via the B3-LYP and B3-PW91 keywords. Becke-style hybrid functionals have proven to be superior to the traditional functionals defined so far.

3.3 Model Chemistries

Model chemistries are characterized by the combination of theoretical procedure and basis set. For example, every calculation performed with GAUSSIAN [11] must specify the desired theoretical model in addition to specifying the molecular system to consider and which results to

compute for it. The Gaussian program contains a hierarchy of procedures corresponding to different approximation methods (commonly referred to as different levels of theory). Theoretical descriptions for each of them may be found in computational chemistry books. The ones used in this thesis are listed in Table 2. More accurate methods become correspondingly more expensive computationally.

3.3.1 Basis Set Effects

A basis set is the mathematical description of the orbitals within a system (which in turn combine to approximate the total electronic wavefunction) used to perform the theoretical calculation. Larger basis sets more accurately approximate the orbitals by imposing fewer restrictions on the locations of the electrons in space. In the true quantum mechanical picture, electrons have a finite probability of existing anywhere in space [11]. Standard basis sets for electronic structure calculations use linear combinations of Gaussian functions to form the orbitals. GAUSSIAN offers a wide range of pre-defined basis sets, which may be classified by the number and types of basis functions that they contain. Basis sets assign a group of basis functions to each atom within a molecule to approximate its orbitals. These basis functions themselves are composed of a linear combination of Gaussian functions; such basis functions are referred to as contracted functions, and the component Gaussian functions are referred to as primitives. A basis function consisting of a single function is termed uncontracted [11].

Table 2: A list of procedures corresponding to different approximation methods (commonly referred to as different levels of theory) [13].

Keyword	Method	Availability
HF	Hartree-Fock Self-Consistent Field	Through 2nd derivatives
B3LYP	Becke-style 3-Parameter Density Functional Theory (using the Lee-Yang correlation function)	Through 2nd derivatives
MP2	2nd order Mφller-Plesset Perturbation Theory	Through 2nd derivatives
MP4	4th Order Mφller-Plesset Perturbation Theory (including Singles, Doubles, Triples and Quadrupoles by default)	Energies only
QCISD(T)	Quadratic CI (Singles, Doubles & Triples)	Energies only

3.3.2 Minimal Basis Sets

Minimal basis sets contain the minimum number of basis functions needed for each atom, as in these examples:

H: 1s

C: 1s, 2s, $2p_x$, $2p_y$, $2p_z$

Minimal basis sets use fixed-size atomic-type orbitals. The STO-3G basis set is a minimal basis set (although it is not the smallest possible basis set). It uses three Gaussian primitives per basis function, which accounts for the "3G" in its name. "STO" stands for "Slater-type orbitals," and the STO-3G basis set approximates Slater orbitals with Gaussian functions.

3.3.3 Split Valence Basis Sets

The first way that a basis set can be made larger is to increase the number of basis functions per atom. Split valence basis sets, such as 3-21G and 6-31G, have two (or more) sizes of basis function for each valence orbital. For example, hydrogen and carbon are represented as:

H: 1s, 1s'

C: 1s, 2s, 2s', $2p_x$, $2p_y$, $2p_z$, $2p_x'$, $2p_y'$, $2p_z'$

where the primed and unpaired orbitals differ in size.

The double zeta basis sets, such as the Dunning-Huzinga basis set (D95), form all molecular

orbitals from linear combinations of two sizes of functions for each atomic orbital. Similarly, triple split valence basis sets, like 6-311G, use three sizes of contracted functions for each orbital-type.

3.3.4 Polarized Basis Sets

Split valence basis sets allow orbitals to change size, but not to change shape. Polarized basis sets remove this limitation by adding orbitals with angular momentum beyond what is required for the ground state to the description of each atom. For example, polarized basis sets add d functions to carbon atoms and f functions to transition metals, and some of them add p functions to hydrogen atoms.

An example of a polarized basis set is 6-31G(d). Its name indicates that it is the 6-31G basis set with d functions added to heavy atoms. This basis set is becoming very common for calculations involving up to medium-sized systems. This basis set is also known as 6-31G*. Another popular polarized basis set is 6-31G(d,p) also known as 6-31G**, which adds p functions to hydrogen atoms in addition to the d functions on heavy atoms.

3.3.5 Diffuse Functions

Diffuse functions are large-size versions of s- and p-type functions (as opposed to the standard valence-size functions). They allow orbitals to occupy a larger region of space. Basis sets with diffuse functions are important for systems [11] that need electron density relatively far from the nucleus: molecules with lone pairs, anions and other systems with significant negative charge, systems in their excited states, systems with low ionization potentials, descriptions of absolute acidities, and so on.

The 6-31+G(d) basis set is the 6-31G(d) basis set with diffuse functions added to heavy atoms. The double plus version, 6-31++G(d), adds diffuse functions to the hydrogen atoms as well. Diffuse functions on hydrogen atoms seldom make a significant difference in accuracy [11].

3.4 How the Programs Work

The basic steps involved in performing a typical ab initio calculation are very similar and can be treated together. The first task is to determine the type of calculation required. The programs are usually controlled by specific keywords, which request given types of calculations. In nonstandard calculations a more detailed specification of steps to be taken by the program must be applied. If keywords are used, the program converts them to internal parameters, which then control the execution.

The next step is to read in the title for the job (used only for information, and printed out exactly as it is read in), the molecular charge, and the required multiplicity (singlet, doublet, triplet, etc.). The molecular geometry is then read in, usually in the form of a Z-matrix (Figure 7) of atomic number, bond lengths, bond angles, and dihedral angles. Note that the Z-matrix is only a geometrical means of defining the positions of the atoms. It is not meant to tell the program where to put bonds or to represent a given electronic state. The program will (almost) always give the electronic configuration that is most stable for the geometrical arrangement of atoms defined by the Z-matrix. The Z-matrix for the structure shown in Figure 7 can now be built up, one line per atom using the numbering shown below:

First atom. The first atom is always placed at the origin of the coordinate system, and therefore only its atomic number code need be given. A dummy atom is given the symbol X in Gaussian to indicate a dummy atom, (which is an atom with no orbitals).

Second atom. The second atom, the carbon in Figure 7 must now be defined. Because the second atom is always placed on a predetermined axis, only the distance from atom 1 need be defined. Figure 7 shows the methylene Z-matrix for GAUSSIAN 98. The second line indicates that a carbon atom C is bound to atom 1 at a distance of CX Angstroms.

Third atom. The third atom, H_3 in Figure 7 is defined using the distance from the carbon atom and the dummy-carbon-hydrogen angle. The program automatically places this atom in a predetermined Cartesian plane, so that no further definition is required. The third line in Figure 7 indicates that a hydrogen atom, H is bound to the carbon atom number 2, at a distance of CH

(a)

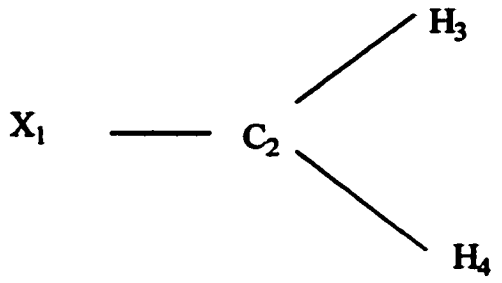

(b)

```
X
C     1     CX
H     2     CH    1     HCX
H     2     CH    1     HCX   3     180.0
CX=1.0
CH=1.09
HCX=122.0
```

Figure 7: A Z-matrix definition for the methylene structure shown in (a)

Angstroms and that it makes an angle with the dummy atom, number 1, of HCX.

Fourth Atom. The fourth atom (H_4) is defined exactly as the third, except that an extra parameter is needed to specify its position uniquely. The distance from C_2 and the dummy-carbon-hydrogen angle together define a circle on which atom 4 must lie. The exact position is defined using a dihedral angle to H_3. Imagine a Newman projection along the C_2— bond. The dihedral angle is simply the angle between the two relevant bonds in this projection. Thus the fourth line in Figure 7 defines a hydrogen atom H, bound to the carbon number 2 at a distance CH, making an angle of HCX with the dummy atom number 1 and a dihedral angle is obtained by imagining a Newman projection along the bond between the atom to which the current atom is bonded and that with reference to which angle is defined (the first two numbered atoms in the current card). The direction used for the dihedral angle is not important, as long as it is consistent throughout the Z-matrix. The variables are then listed separated by a blank line.

The information from the Z-matrix is used to calculate the Cartesian (x,y,z) coordinates of the atoms and, in conjunction with the charge, atomic numbers, and multiplicity, to work out the total number of electrons and the orbital occupancies. At this stage the nuclear repulsion energy may be calculated. Because this number depends only on the atomic numbers and the molecular geometry, it should be the same in different calculations on the same structure. This constancy can be used to check that ab initio calculations with different basis sets have been performed on exactly the same geometry. Ab initio programs may use an internally stored standard set of coefficients and exponents that define the orbitals (the basis set), or these may be read in with the

input for a nonstandard basis. The p-orbitals are always oriented in the x, y, and z directions, although any set of mutually perpendicular axes would give identical results. Ab initio programs next calculate the various one- and two-electron integrals (often hundreds of thousands of them) required later in the calculation. The integrals are identified by indices that are assigned to them and with which they are written to files for later use.

The program must then produce an initial guess, a trial set of molecular orbitals used as a starting point for the SCF calculations. There are several possibilities for the initial guess. The usual form of initial guess for ab initio programs is that obtained from an extended Huckel calculation on the molecule in question (i.e., the initial guess overlay is actually a simple extended Huckel program). The set of orbitals obtained may then be "projected" to give a good approximation of the orbitals expected for the orbitals for the basis set to be used in the ab initio calculation. At this stage the electronic configuration required may also be chosen, although the configuration given by the initial guess is usually the ground state.

The program uses the initial guess as the starting point for an iterative SCF calculation, the part of the program that actually delivers the results required. The solution to the SCF equations is improved cycle by cycle until the electronic energy is at a minimum and the density matrix does not change. At this stage the calculation is said to be converged, or to have reached self consistency, and the program proceeds to the next step. In some cases the SCF does not converge, but either oscillates between two possible solutions or diverges rapidly. Various techniques are used for methods to overcome this [12].

The next stage of the calculation depends on the type of job to be performed. For single point energy calculations, the program may either move directly to the population analysis, which calculates the atomic charges, overlaps, dipole moment, and so forth, or perform some sort of post-SCF correlation energy calculation (by a perturbational, configuration interaction, or density-functional method).

For a geometry optimization the atomic forces are then determined analytically and used to estimate the minimum-energy geometry for the molecular species being calculated. The above process is repeated for each new geometry until the atomic forces are close to zero and the total energy does not change significantly from cycle to cycle. At this stage the optimization is complete and the program moves on to a population analysis of the optimized species. The procedures used to convert the atomic forces into changes in the geometry vary from program to program, and there may even be several options in one program, but the principles outlined above apply to them all [12].

3.5 Frequency Calculations

Molecular vibrational frequencies depend on the second derivative of the energy with respect to the nuclear positions. Analytic second derivatives in the GAUSSIAN program are available for the Hartree-Fock (HF keyword), Density Functional Theory (the B3-LYP keyword) and second-order Mφller-Plesset theory (MP2 keyword) [11].

Because of the nature of the computations involved, frequency calculations are valid only at stationary points on the potential energy surface. Thus, frequency calculations must be performed on optimized structures. For this reason, it is necessary to run a geometry optimization prior to doing a frequency calculation. The most convenient way of ensuring this is to include both Opt and Freq in the route section of the job, which requests a geometry optimization followed immediately by a frequency calculation. A frequency job must use the same theoretical model and basis set as produced in the optimized geometry [11].

A frequency job begins by computing the energy of the structure. It then goes on to compute the frequencies at that structure. GAUSSIAN predicts the frequencies, intensities, and Raman depolarization ratios and scattering activities for each spectral line. Raw frequency values computed at the Hartree-Fock level contain known systemic errors due to the neglect of electron correlation, resulting in overestimates of about 10%-12% [11]. Therefore, it is usual to scale frequencies predicted at the Hartree-Fock level by an empirical factor of 0.8929 [13]. Use of this factor has been demonstrated to produce very good agreement with experiment for a wide range of systems.

Frequencies computed with methods other than Hartree-Fock are also scaled to eliminate known systemic errors in calculated frequencies. Table 3 lists the recommended scale factors for frequencies and for zero-point energies and for use in computing thermal energy corrections. It is shown from Table 3 that, the optimal scaling factors for the frequencies themselves and for zero-point energies and for use in computing thermal energy corrections are slightly different [13]. However, it is also common practice to use the same factor for both of them (0.8929 in the

case of Hartree-Fock). For example, the G2 high accuracy energy method scales computed HF/6-31G(d) zero-point energy corrections by 0.8929 [13].

Another use of frequency calculations is to determine the nature of a stationary point found by a geometry optimization. Geometry optimizations converge to a structure on the potential energy surface where the forces on the system are essentially zero. The final structure may correspond to a minimum on the potential energy surface, or it may represent a saddle point, which is a minimum with respect to some directions on the surface and a maximum in one or more others. First order saddle points which are a maximum in exactly one degree of freedom and a minimum in all other orthogonal degree of freedom correspond to transition state structures linking two minima. There are two pieces of information from the output which are critical to characterizing a stationary point:

- The number of imaginary frequencies
- The normal mode corresponding to the imaginary frequency.

Imaginary frequencies are listed in the output of a frequency calculation as negative numbers. By definition, a structure which has n imaginary frequencies is an n^{th} order saddle point. Thus, ordinary transition structures are usually characterized by one imaginary frequency since they are first-order saddle points.

Table 3: Recommended scale factors for frequencies and for zero-point energies [13]

	Scale Factor	
Method	Frequency	ZPE/Thermal
HF/3-21G	0.9085	0.9409
HF/6-31G(d)	0.8929	0.9135
MP2(Full)/6-31G(d)	0.9427	0.9646
MP2(FC)/6-31G(d)	0.9434	0.9676
SVWN/6-31G(d)	0.9833	1.0079
B-LYP/6-31G(d)	0.994	1.0119
B3-LYP/6-31G(d)	0.9613	0.9804

3.6 Intrinsic Reaction Coordinate (IRC) Calculation

An IRC calculation examines the reaction path leading down from a transition structure on a potential energy surface. Such a calculation starts at the saddle point and follows the path in both directions from the transition state, optimizing the geometry of the molecular system at each point along the path. In this way, an IRC calculation definitely connects two minima on the potential energy surface by a path which passes through the transition state between them [11].

In GAUSSIAN, a reaction path calculation is requested with the IRC keyword in the route section. Prior to running the calculation on GAUSSIAN, certain requirements must be met. An IRC calculation begins at a transition structure and steps along the reaction path a fixed number of times, the default being 6 in the direction toward the two minima that it connects. However, in most cases, it will not step all the way to the minimum on either side of the path. To optimize the transition structure, the Opt=(TS, CalcFc) keyword in the route section is used requesting an optimization to a transition state. The CalcFc option is used to compute the initial force constants, a technique which is generally helpful for transition state optimizations. The Freq keyword is included so that a frequency calculation will automatically be run at the optimized geometry [11].

3.7 Composite Methods

The G2 procedure [14] was introduced by Pople and co-workers for the purpose of making

reliable theoretical thermochemical predictions. G2 procedures have also been successfully applied to the prediction of heats of formation G2 and its more economical variants G2(MP2) [15] and G2(MP2,SVP) are found to consistently predict atomization energies, electron and proton affinities, and ionization energies to within 10 kJ mol^{-1}. G2(MP2,SVP) approximates the QCISD(T)/6-311+G(3df,2p) single-point energy by two additive corrections to a base MP2/6-31G(d) energy. The first is a basis set correction relative to the MP2/6-311+G(3df,2p) energy, and the second is an electron-correlation correction relative to QCISD(T)/6-31G(d). This final total energy is then corrected further with an empirical higher-level correction which attempts to account for residual basis set deficiencies in the above total energy, and also with the zero-point vibrational energy (ZPE). The ZPE used in G2(MP2,SVP) is the HF/6-31G(d) value scaled by 0.8929. Thermal corrections to the data are carried out using MP2/6-31+G(d) vibrational frequencies (scaled by 0.9434) [13]. Theoretical heats of formation ($\Delta_f H°$) are derived by the atomization method employing experimental heats of formation of the constituent atoms [16].

References

[1] W. J. Hehre, L. Radom, P. v. R. Schleyer and J. A. Pople, Ab Initio Molecular Orbital Theory Editor (Ed.) Wiley, New York, 1986.

[2] M. Born and J. R. Oppenheimer, Ann. Physik. 84 (1927) 457.

[3] E. Schrodinger, Ann. Physik 79 (1926) 361.

[4] E. C. Kemble, Fundamental Principles of Quantum Mechanics (Ed.) McGraw Hill, New York, 1965.

[5] I. N. Levine, Quantum Chemistry 3 Editor (Ed.) Allyn and Bacon, Boston, 1985.

[6] C. C. J. Roothan, Rev. Mod. 23 (1951) 69.

[7] G. G. Hall Proc. Roy. Soc.: London, 1951; Vol. A205, pp 541.

[8] J. A. Pople and R. K. Nesbet, J. Chem. Phys. 22 (1954) 571.

[9] C. Moller and M. S. Plesset, Phys. Rev. 46 (1934) 618.

[10] E. Hylleraas, Zeitschrift fur Physik 65 (1930) 209.

[11] J. B. Foresman and *AE*.Frisch, ed. Exploring Chemistry with Electronic Structure .

[12] T. Clark, A Handbook of Computational Chemistry Editor (Ed.) Wiley, Chichester, 1985.

[13] A. P. Scott and L. Radom, J. Phys. Chem. 100 (1996) 16502.

[14] L.A. Curtis, K. Raghavachari, G.W. Trucks, J. A. Pople, J. Chem. Phys. 94 (1991) 7221.

[15] L.A. Curtis, K. Raghavachari, J. A. Pople, J. Chem. Phys. 98 (1993) 1293.

[16] S. G. Lias, J. E. Bartmess, J. F. Liebman, J. L. Holmes, R. D. Levine, W.G. Mallard, J. Phys. Chem. Ref. Data 17 (1998) (suppl.1).

CHAPTER 4

THE MASS SPECTROMETER

4.1 History

Many advances in chemistry may be considered to be directly linked with the invention and technological improvements of instrumentation. A typical example is in the field of mass spectrometry. The knowledge obtained from this analytical technique has been influenced by improvements in such areas as vacuum and electronics technology as well as the computer. The chronological order of the history of mass spectrometry is dealt here encompassing a few of the major turning points in the development of mass spectrometry.

Goldstein [1] in 1886 discovered positive charged gaseous entities. By 1902, W. Wien had shown that these rays of positively electrical charge could be deflected in a magnetic field [2]. Upon the introduction of polyatomic molecules into the discharge tube of a parabolic mass spectograph which incorporated a magnetic field, J. J. Thomson observed the formation of many parabolas, revealing the formation of a variety of positively charged fragments [3]. These parabolas were recorded on a photographic plate, but due to differing sensitivities for various ions, quantitative measurements were not possible. Thomson, then replaced his plate with a Wilson tilted electroscope and Faraday cylinder. By changing the magnetic field, Thomson was able to obtain a plot of the ion current as a function of mass-to- charge (m/z) ratio. C. T. Knipp, in 1911, and later A. J. Dempster reported the construction of an electron bombardment ion source mass spectrometer [4], suitable, not for precise mass measurements, but for measuring the

relative abundances of the ionic species and for studying electron impact processes in gases. Although the technique of mass spectrometry had its beginnings in Thomson's vacuum tube, it was not until 1920 that F. W. Ashton first introduced the term "mass spectrum" when he built the first mass spectrometer capable of separating and enriching the isotopes of a given element. This technique was later used to produce enriched uranium samples for use in the Manhattan Project. Among the results obtained with these first mass spectrometers was the discovery of stable isotopes, leading to the realization that the chemical properties of an element are determined by the atomic number rather than the atomic weight [5].

The next major development leading to the technique of tandem mass spectrometry occurred in 1945 when J. A. Hipple and E. U. Condon [6] observed and explained the presence of metastable ions in a mass spectrum. This was the beginning of the required fundamental studies on the use of metastable ions as a source of chemical and physical information. In the early 1960's the first tandem mass spectrometry experiments were performed in which instruments were used in unconventional modes to study the metastable decompositions of ions. The first development [7] was the introduction of the accelerating-voltage scan on sector instruments. The next development [8-9] was the discovery of the enhancement of the magnitude and quantity of peaks upon the introduction of a collision gas into a localized region of the mass spectrometer. At the time of the initial experiments using a collision gas, the focus of the studies was very narrow, and directed primarily toward exploration of physical aspects of the phenomenon. It was in the 1970's, marked by the publication of the book Metastable Ions [10], that tandem mass spectrometry entered its modern era, a period in which instruments would be designed expressly

for tandem mass spectrometry experiments. The next mile-stone of modern tandem mass spectrometry was the development of the Neutralization-Reionization technique [11-13] which extended the use of mass spectrometry to study the neutral counterparts of ions. The drive to improve mass resolution led to the use of more homogeneous magnetic fields, the introduction of a kinetic energy focusing device, the electrostatic analyzer (ESA), and the increase of the ions' kinetic energy by the use of large ion accelerating voltages. The further development of mass spectrometer design involved the improvement of ion detection systems, which ultimately led to the electron multipliers in use today.

4.2 The Modified VG ZAB-2HF Mass Spectrometer

4.2.1 Introduction

Several years ago, a mass spectrometer was said to function as a complete chemical laboratory [14]. Inside the mass spectrometer, ions are prepared (ion source), the ions of interest are separated (magnetic sector), and are allowed to react spontaneously or under collisional activation (field free region), and the reaction products are analyzed (electric sector). A modified VG ZAB-2HF was used for all the cluster ions studied in this thesis.

The VG ZAB-2HF [15] mass spectrometer is a double focussing instrument of reverse geometry. The term double focussing is used because the beam of ions is submitted to the focussing action of both a magnetic and an electric sector, while the term, reverse geometry is used since the magnetic sector precedes the electric sector. Over the past 15 years, it has been

extensively modified to allow novel experiments to be performed. The last major modification in 1992, was the addition of a third field free region and hence a second electric sector, thus giving the instrument a triple focussing capability. A schematic diagram of the instrument is shown in Figure 8. The individual components of the ZAB are described in the following sections.

4.2.2 The ion source

Ions are generated by either electron impact or chemical ionization. The ion source, is as the rest of the interior of the mass spectrometer, is kept at a high vacuum < 10^{-7} torr. A sample can be introduced into the ion source via an appropriate inlet system at a constant rate, resulting in a stable sample pressure of ≤ 10^{-6} torr. A schematic diagram of the ion source is shown in Figure 9.

If electron impact (EI) is the choice of ionization, electrons are generated from a heated helical filament (2.5 to 3.0 A of current are needed to increase the temperature of the filament (>2000^{0}C) high enough for the emission of electrons). The efficiency of electron emission from the filament is measured by an electrode placed behind the filament. The current induced by the electrons hitting this plate is of the order of 0.3 mA. The electrons are accelerated into the ionization chamber by a potential energy difference between the filament and the electron exit slit which is generally of the order of 70 eV. The electrons that cross the ionization chamber are accelerated

towards the trap which sits at slightly positive potential with respect to the block. The current at the trap is measured to be approximately 20 μA. In order to keep the electrons on their path, two small magnets are placed in parallel with the electrons' path. Due to the heating of the filament, the source temperature is usually maintained at 150^{0}C.

If chemical ionization (CI) is the choice of ionization method used, molecules in the gas-phase are ionized in an ion/molecule reaction where a positively charged ion that has been formed as a result of electron ionization. The most common reaction studied is proton transfer to form a protonated molecule. The protonated molecule is usually a prominent ion in the chemical ionization mass spectrum. Fragmentation occurs to a degree influenced by exothermicity of the ion/molecule reaction, i.e., the amount of internal energy resident in the ion initially formed, and can be controlled by discrete choice of the chemical reagent gas [16].

Samples may be introduced in the vapour phase via three different types of sample inlets. One is the liquid septum inlet, in which a liquid is volatilized in a reservoir and the vapour leaked into the source via a small capillary. The second is the Granville-Philips inlet which is a variable leak valve used for low boiling point liquids or solids which have an appreciable vapour pressure at room temperature. Lastly the solids probe is also a variable temperature inlet, the tip of which contains the solid sample held in a capillary tube. The measured pressure in the ion source sample chamber, read with an ionization gauge situated above the ion diffusion pump is typically between 10^{-7} and 10^{-6} Torr. The actual pressure in the ion source itself is approximately two orders of magnitude higher.

Once the sample is ionized, the ions formed are pushed out of the ionization chamber by the repeller electrode which has a slight positive potential with respect to the source block. These ions exit the block through the CI/EI slit which is set in accordance with the ionization method being used. For an effective ion/molecule reaction, it is necessary to maintain a relatively high pressure (i.e., measured pressure 10^{-5} to 10^{-4} Torr). The CI slit is thus narrower than the EI slit in order to obtain this pressure.

The source block is at 8 kV with respect to the grounded source exit slit. All ions generated in the ion source will fall through a potential gradient (the accelerating voltage, V_{acc}, typically 8 kV) as they leave the ion source, so all ions with mass m and charge ze (where z represents the number of charges and e is the fundamental charge on an electron) generated inside the ion source will leave carrying z x 8 keV of kinetic energy.

$$\frac{mv^2}{2} = zeV_{acc} \qquad (4.1)$$

Hence, all ions of the same charge acquire the same kinetic energy, irrespective of their mass. The beam of ions having the full accelerating voltage is referred to as the main beam. The ion beam then passes through the source slit (Figure 8,2) and through an assembly of focusing lenses. The lens assembly consists of a series of shaped plates onto which electric potentials are applied in order to collimate the ion beam in both the y and z directional axes (the x axis being the trajectory direction) in order to maximize both the shape and the transmission efficiency of the ion beam. The name of the instrument, ZAB, comes from these lenses that should, in principle, produce an ion beam with Zero Aberration.

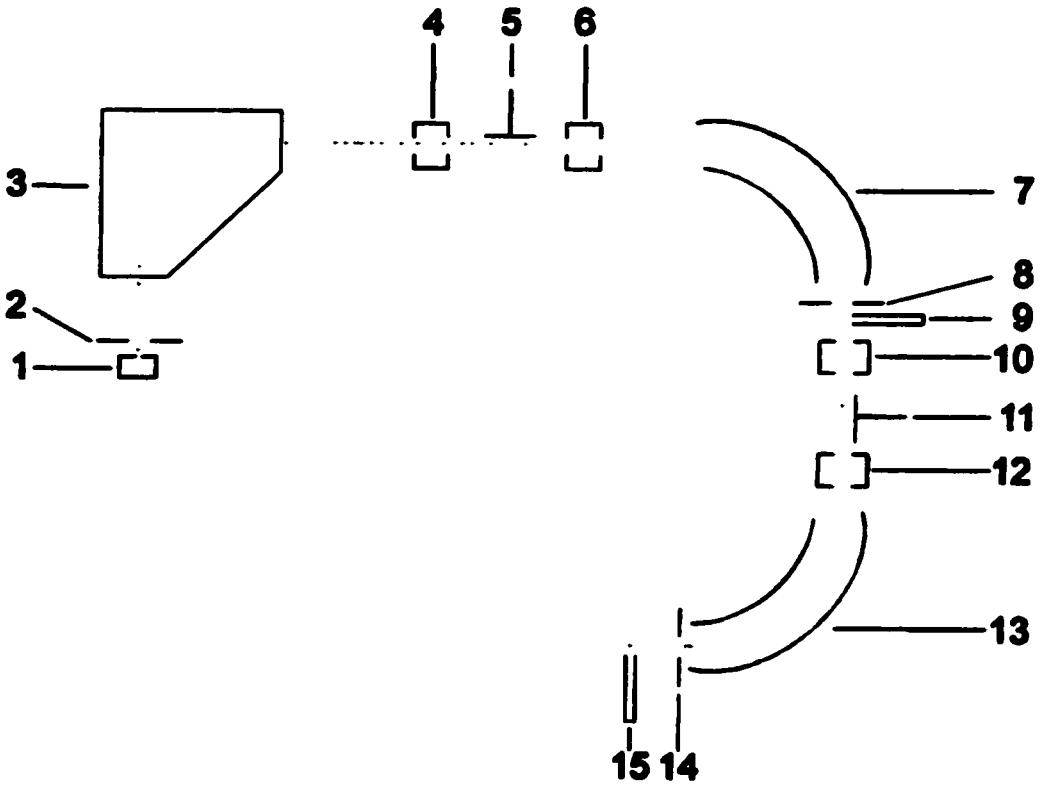

Figure 8: Schematic diagram of the modified VG ZAB-2HF: 1: source 2: slit, 3: magnetic sector, 4: collision cell 1, 5: deflector electrode, 6: collision cell 2, 7: electric sector 1, 8: collector slit, 9: detector, 10: collision cell 3, 11: deflector electrode, 12: collision cell 4, 13: electric sector 2, 14: collector slit and 15: detector.

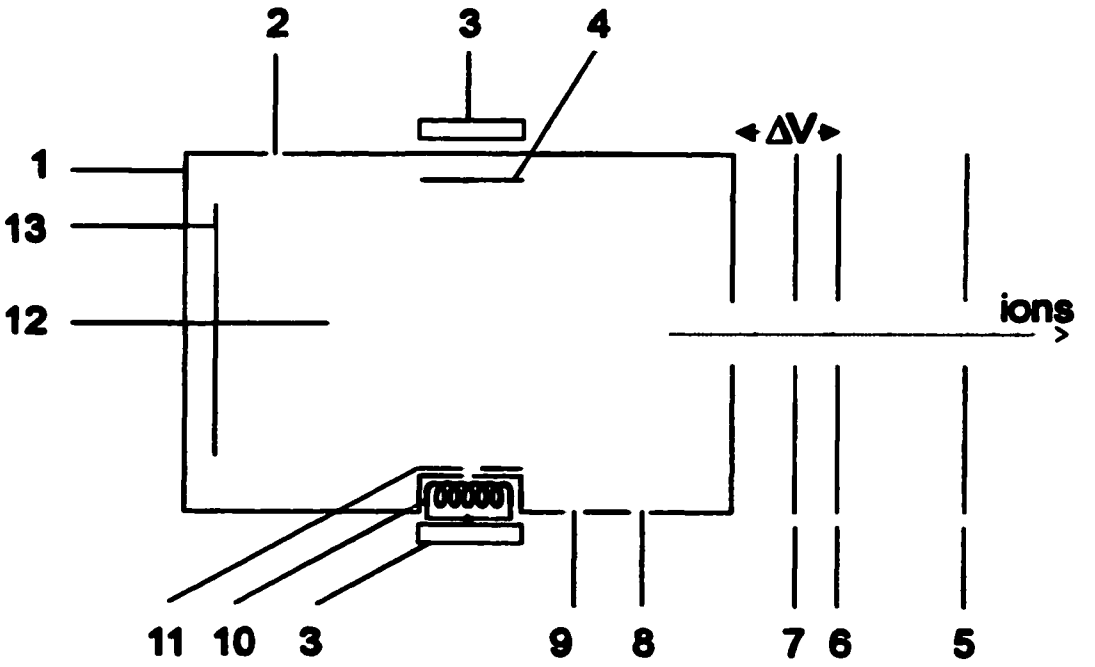

Figure 9:Schematic diagram of ion source in the modified VG ZAB-2F: 1: block, 2: direct liquid inlet, 3: magnet, 4: trap, 5: slit, 6: grounded plate, 7: CI/EI slit, 8: gas inlet, 9: solids probe inlet, 10: filament, 11: electron slit, 12: ionization chamber and 13: repeller.

4.2.3 The Magnetic Analyzer

The source generated ions pass through a magnetic field (B), produced by an electromagnet. They will follow a circular path with a radius (r) through the magnet given by Eq. 4.4 (Figure 10),

$$\frac{mv^2}{r} = BzV$$

$$or \qquad (4.2)$$

$$B = \frac{mv}{zr}$$

Thus, the magnet is a momentum analyzer. For the source generated ions, if we substitute Eq. 4.1 into Eq. 4.2 we obtain:

$$\frac{m}{z} = \frac{B^2r^2}{2V_{acc}} \qquad (4.3)$$

It follows that, by varying B, ions can be selected according to their mass-to-charge ratio, m/z, since r and V_{acc} are constant. If the ions are detected after the magnet, scanning the magnet current will analyze the composition of the ion mixture generated in the ion source and produce the single focusing mass spectrum of the sample.

4.2.4 The Electrostatic Analyzer (ESA)

The ESA consists of two curved plates, being a section of a circle, with radius r, between which an electric field E can be generated by applying a potential to them (Figure 11). Transmission through the ESA will take place when the centrifugal force on the ion equals the electric field force:

$$\frac{mv^2}{r} = zE \qquad (4.4)$$

Hence, the electric sector is a kinetic energy analyzer. For ion source generated ions, if we substitute Eq. 4.1 into 4.4, we obtain

$$E = \frac{2V_{acc}}{r} \qquad (4.5)$$

Setting E to match V_{acc} will ensure that any mass selected, source generated ion will be transmitted through the electric sector. If ions are now detected after the electric sector, scanning the magnetic field will produce the double focusing mass spectrum of the sample. In double focusing mode, greater mass resolution can be obtained, because the ESA focuses the small spread in kinetic energies of the ions. The resolution of the magnet and ESA can be increased (at the cost of ion transmission) by narrowing the slits following them, by analogy with aperture settings in optics.

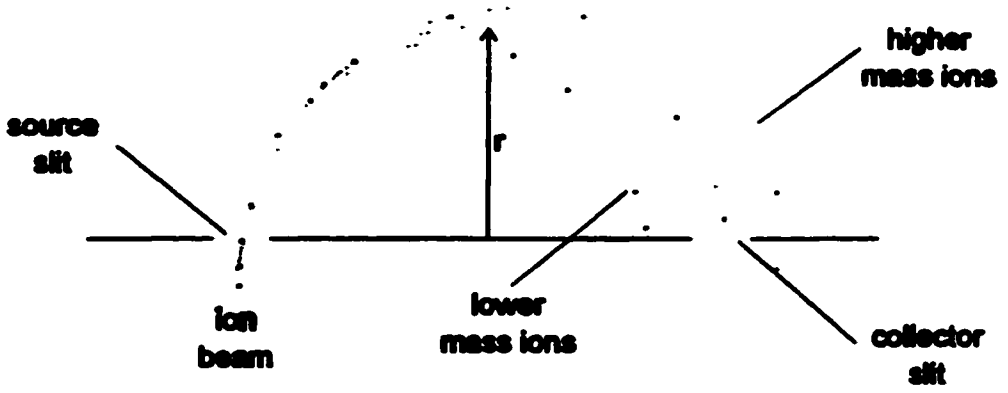

Figure 10: Focusing action of magnetic sector.

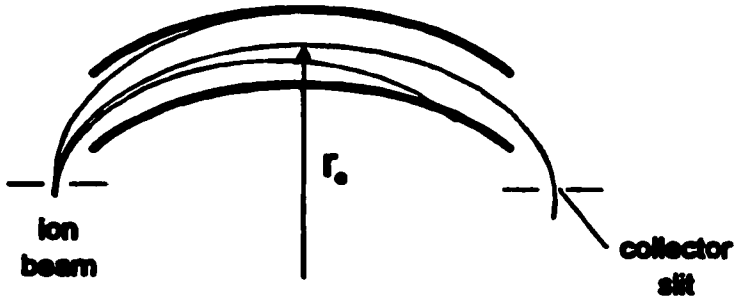

Figure 11: Focusing action of electric sector.

4.2.5 Field Free Regions

Between the source and the magnet, the magnet and ESA1, and the two ESA's are the first, second and third field free regions (FFR's) of the instrument. In these regions ions may dissociate spontaneously or may dissociate following collisional activation. The second and third FFR house the four collision cells (Figure 8). The cells consist of 2-3 cm long blocks of steel through which a 2mm groove is cut. Gas lines are connected to each of the collision cells. The pressure in the cells is monitored by ionization gauges placed in close proximity. The differential pumping in these regions produces a pressure gradient between the cells and their surroundings, preventing the gas from spreading throughout the flight tube. Cell 1 and cell 2 are 10 cm apart while the distance between cell 3 and cell 4 is variable, but is usually set to 6 cm. An assembly of focusing lenses follows cell 2. Half way between each pair of cells is placed a deflector electrode allowing the ions to be expelled from the beam if a negative or a positive potential is placed on it. This enables the study of the neutral species co-generated in the FFR.

4.2.6 Detectors

The detectors are off axis photo multipliers (Figure 12). The detectors are made up of two parts. On one side of the ion beam, is placed a conversion dynode onto which a high negative potential is applied (~20 kV). The positive ions are attracted towards the dynode, impinge on the central portion of the conversion dynode, and secondary electrons are emitted. These electrons are

accelerated towards a CaF_2 scintillator. The scintillations produced are detected by an optically coupled photomultiplier and the signal is amplified. The detector used in the ZAB allows for both the detection of positive and negative ions. Due to this flexibility, a restriction on the maximum possible potential applied to the dynode may result in mass discrimination. The ions with low translational kinetic energy (i.e., low mass fragment ions) may be discriminated against.

4.3 Experiments Performed on the VG ZAB-2HF

4.3.1 Mass-Analyzed Ion Kinetic Energy Spectrometry (MIKES)

Ions accelerated out of the ion source with keV translational kinetic energies (m/z selected with the magnetic sector) will arrive in the FFR of the instrument in several microseconds [16]. Ions dissociating on this timescale (with unimolecular decay rate constants between 10^2 and $10^5 s^{-1}$, depending on the physical geometry of the instrument) are known as "metastable ions" [10]. In the FFR of the mass spectrometer, the unimolecular decomposition fragments, A^+ and B, of the mass selected metastable ion AB^+ will by conservation of energy and momentum have lower translational kinetic energy, T, than their precursor:

$$zT_{A+} = \frac{1}{2} m_{A+} v^2; zT_{B+} = \frac{1}{2} m_{B\bullet} v^2; zT_{AB+\bullet} = \frac{1}{2} m_{AB+\bullet} v^2; \quad (4.6)$$

Thus we find $$T_{A+} = \frac{m_{A+}}{m_{AB+}} T_{AB+\bullet} \qquad (4.7)$$

By scanning the ESA to pass ions with lower translational energies, the fragment ions will sequentially pass through to the detector (ms/ms or ms^2). The final ion abundance versus kinetic energy spectrum (Figure 13) is converted to an ion abundance versus fragment m/z spectrum by the above relationship. The MIKES spectrum is the end result of all low energy unimolecular processes of the selected ions, including isomerization. Hence, isomeric ions which interconvert on the microsecond timescale often have closely related or identical MIKES spectra [17]. There are several characteristic peak shapes expected in a MIKES spectrum that are summarized in Figure 14 and will be discussed further in section 4.3.3.

4.3.2 Collision-Induced Dissociation (CID) Mass Spectrometry

A collision-induced dissociation (CID) mass spectrum [18,19] of mass selected ions is obtained by introducing a target gas (usually He) into a collision cell in one of the field-free regions to achieve 10% reduction in the flux (i.e., single collision conditions). The resulting high energy (keV) CID mass spectrum, contains peaks due to ions formed in virtually all possible unimolecular dissociation processes of the precursor ion. The timescale of the CID fragmentation reactions is quite different from the MIKES experiment, ranging from the time of the collision event ($t \approx 10^{-15}$ s) to the time the ions leave the field-free region. As a result, isomerization

reactions tend not to play a significant part in collision-induced reactions, and thus the CID mass spectra are often characteristic of ion connectivity. It is generally accepted that only the metastable reaction channels may depend upon the initial internal energy [20] distribution of the precursor molecules. All other "high critical energy" dissociation channels should be independent of the initial internal energies. Consequently, identical ions generated from a variety of precursor molecules should have indistinguishable CID mass spectra, whereas isomeric ions, in general, will have distinctive CID characteristics. The effect of internal energy may be best observed when comparing CID mass spectra of both source and metastably generated ions. The two CID mass spectra will be indistinguishable if the structure of the ions is independent of their internal energy content.

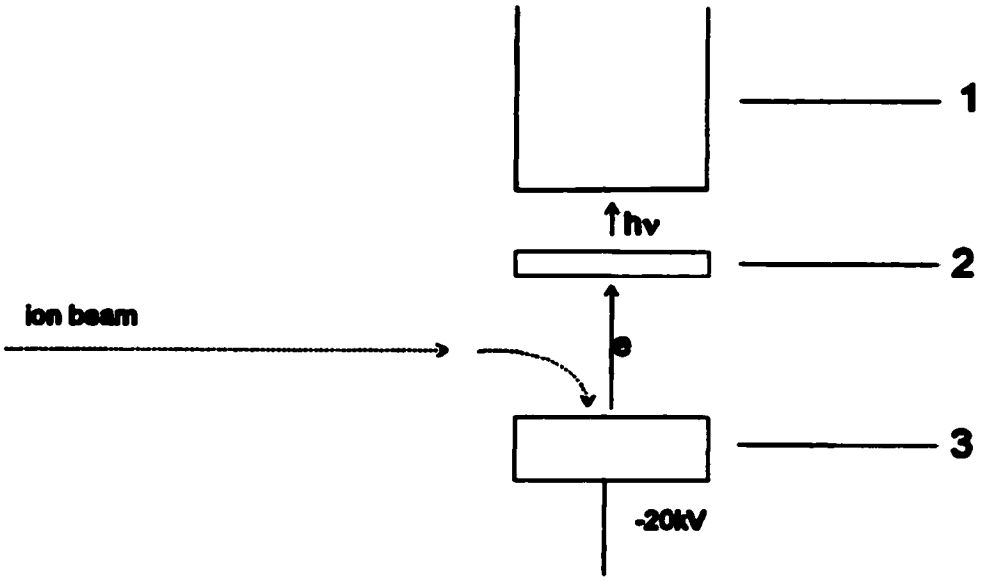

Figure 12: Photo detector: 1: conversion dynode, 2: CaF_2 scintillator and 3: photomultiplier tube.

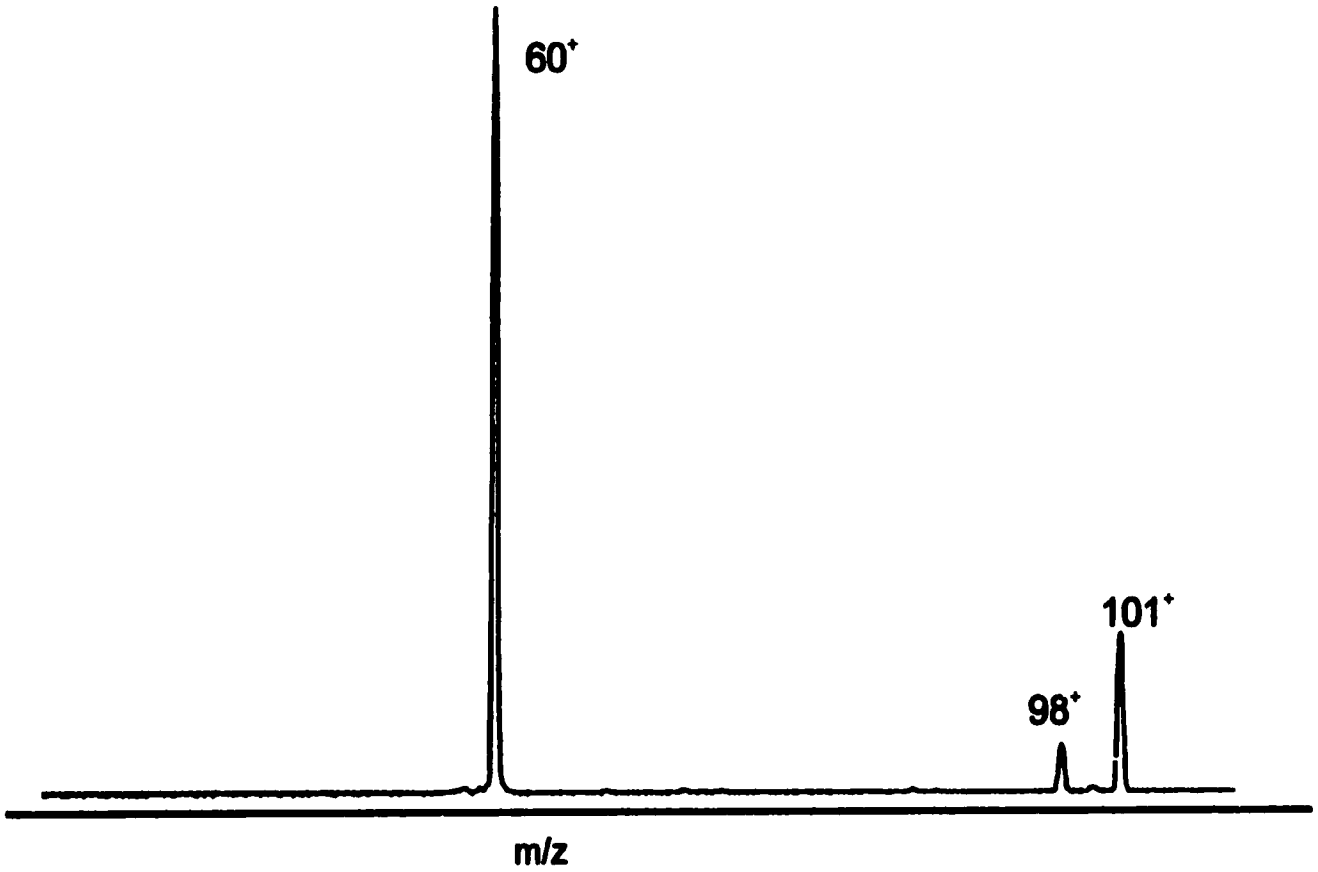

Figure 13:A MIKES of the acetonitrile/ t-butanol proton-bound dimer (m/z 136) Main beam excluded because it is off scale

4.3.3 Kinetic Energy Release (KER) Measurements

In a unimolecular dissociation, excess product energy is typically distributed among the translational, rotational and vibrational modes of the products in a statistical fashion. The experimentally observed phenomenon is the distribution of translational kinetic energies of the departing fragment ions (the kinetic energy release, KER) [10]. In magnetic sector instruments, the result of x-axial (i.e., along the beam path) KER is the observation of fragment ion peaks in the MIKES or CID spectra which have broader kinetic energy distribution than the precursor ion peak. In a CID, however, this spread is complicated by collisional scattering and so KER is most often discussed for peaks in MIKES spectra. The kinetic energy release (KER) associated with a given fragmentation is commonly expressed as the value at half height of the fragment ion peak, $T_{0.5}$, and is calculated according to the equation [10]:

$$T_{0.5}(eV) = \frac{{m_1}^{+^2}}{16 m_2^+ m_3 8000}(W^2_{0.5(fragment)} - W^2_{0.5(mainbeam)}) \qquad (4.8)$$

where m_1^+, m_2^+ and m_3 are the masses of the precursor molecule, the ionic and the neutral fragments, respectively, and $W_{0.5}$ are the width at half-height of the fragment ion and the main beam. The experiment is carried out at high resolution, which is obtained by narrowing down the y-axis beam collimating slits in the instrument so that the width at half-height of the fragment ion

peaks are indicative of the kinetic energy released. It is important to note that since knowledge of the internal energy distribution of the dissociating ions is lacking, the relationship between $T_{0.5}$ and the average KER is strictly qualitative, i.e., a large $T_{0.5}$ indicates a large KER value. How statistical the distribution of product excess energies are will depend on the dynamics of the dissociation [19].

The most commonly observed metastable peak shape is a Gaussian shape (Figure 14a) . These peaks are associated with relatively small kinetic energy releases. As the kinetic energy released increases, flat and eventually dish-shaped metastable peaks are observed (Figure 14b). The dish-shaped top observed in some peaks has no physical or chemical meaning but results from instrumental discrimination. If fragment ions receive large kinetic energy components along the z-axis (that is along the plane of the long axis of the resolving slits); the result is a dish-topped peak because these ions do not pass through the ESA. Metastable peaks which are characterized by marked discontinuities in their profile are referred to as composite metastable peaks. They can be seen to consist of a Gaussian type peak atop a dish-shaped peak or a pair of superimposed dished-shaped peaks (Figure 14c) or a pair of superimposed Gaussians. These peaks may arise [17] when two isomeric precursor ions decompose by loss of a common neutral fragment to yield one or two fragment ion structures or, when a single precursor ion structure fragments to yield a pair of isomeric fragments via different reacting configurations. Because the KER associated with the fragmentation of a given metastable ion is characteristic of the reacting configuration of the ion, this information is used when distinguishing isomeric ions.

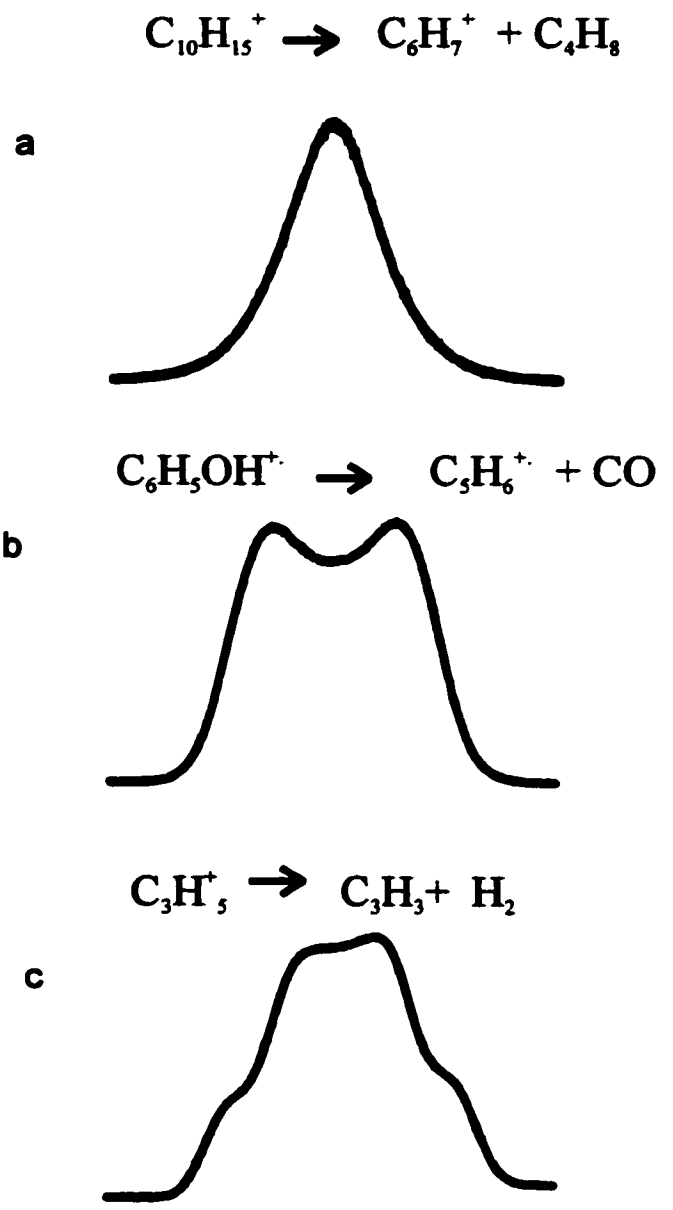

Figure 14: Metastable peak shapes: a) Gaussian b) Dished-topped and c) Composite [18]

4.3.4 Collision Induced Dissociation Ionization (CIDI)

The neutrals co-generated in metastable dissociations may also be investigated. The identification of these neutral species is achieved by collisional ionization. By applying a potential of several hundred volts on the deflector electrode situated in front of a collision cell (Figure 15), all ions are deflected from the beam. The neutrals are unaffected by this potential and they continue their trajectory and enter the collision cell. When kilovolt neutral projectiles encounter a target gas, the collision may produce an ion which contains sufficient internal energy to fragment. This technique is referred to as collision induced dissociation ionization (CIDI) [21] and produces a mass spectrum which can be used to characterize the structure of neutral species co-generated in the metastable decomposition of the precursor molecule. Such information is vital if the thermochemistry of the process is to be investigated and also provides ancillary information that may prove useful when identifying the nature of the ionic species produced.

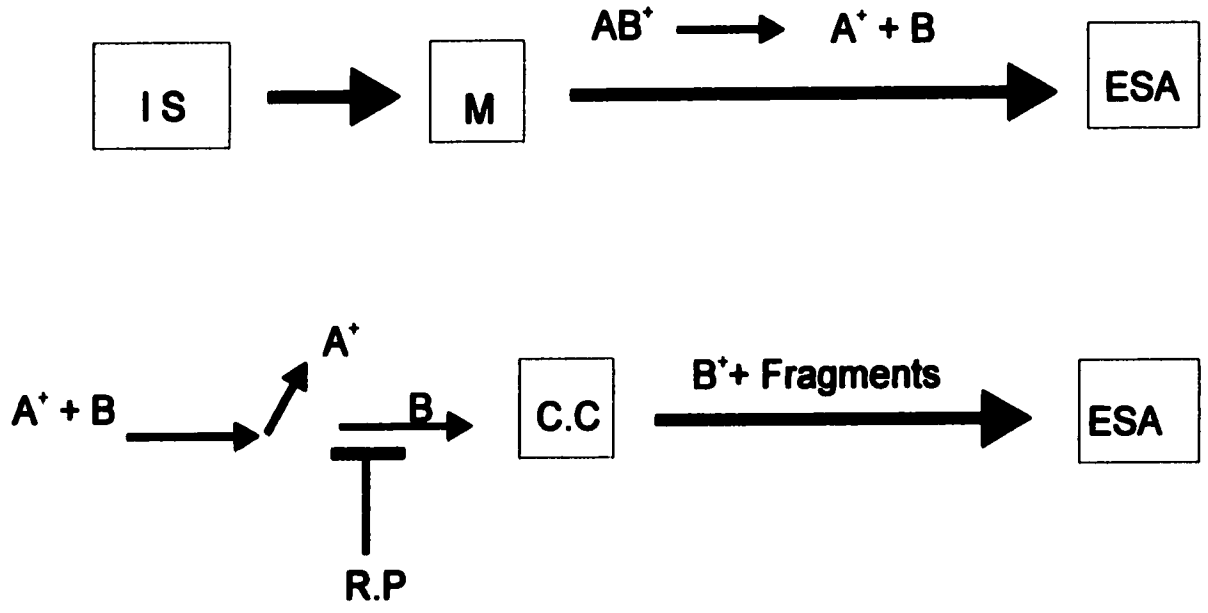

Figure 15:A schematic diagram of a CIDI experiment, IS: Ion source, M: Magnet, R.P: Repeller, C.C: Collision cell, ESA: Electrostatic Analyzer

References

[1] E. Goldstein, Berl. Ber. 39 (1886) 691.

[2] W. Wien, Wied. Ann 65 (1898) 440.

[3] J. J. Thomson, Phil. Mag. 24 (1912) 668.

[4] A. J. Dempster, Phys. Rev. 11 (1918) 316.

[5] J. J. Thomson, Rays of Positive Electricity, ed. (London, Longmans Green and Co., 1913).

[6] J. A. Hipple and E. U. Condon, Phys. Rev. 68 (1945) 54.

[7] M. Barber and R. M. Elliot, ASTM E-14 Conference on Mass Spectrometry, Montreal, 1964.

[8] W. F. Haddon and F. W. McLafferty, J. Am. Chem. Soc. 90 (1968) 4745.

[9] K. R. Jennings, Int. J. Mass Spectrom. Ion Proc. 1 (1968) 227.

[10] R. G. Cooks, J. H. Beynon, R. M. Caprioli and G. R. Lester, Metastable Ions, ed. (Amsterdam, Elsevier Sci. Pub. Co., 1973).

[11] P. M. Curtis, B. W. Williams and R. F. Porter, Chem. Phys. Lett. 65 (1979) 296.

[12] F. W. McLafferty, P. J. Todd, D. C. McGilvery and M. A. Baldwin, J. Am. Chem. Soc. 102 (1980) 3360.

[13] P. O. Danis, C. Wesdemiotis and F. W. McLafferty, J. Am. Chem. Soc. 105 (1983) 7454.

[14] C. J. Porter, J. H. Beynon and T. Ast, Org. Mass Spectrom. 16 (1981) 101.

[15] R. P. Morgan, J. H. Beynon, R. H. Bateman and B. N. Green, Int. J. Mass Spectrom. Ion Phys. 28 (1978) 1978.

[16] K. L. Busch, G. L. Glish and S. A. McLuckey, Mass Spectrometry/Mass Spectrometry Editor, ed. (New York, VCH Publishers, 1988).

[17] H. M. Rosenstock, M. B. Wallenstein, A. L. Wahrhafit and H. Eyring , 1952; Vol. 38, pp 667.

[18] J. L. Holmes, and Terlouw, J. K., Org. Mass Spectrom. 15 (1980) 383.

[19] R. G. Cooks, Collision Spectroscopy, ed. (New York, Plenum Press, 1978).

[20] J. L. Holmes, Org. Mass Spectrom. 20 (1985) 169.

[21] P. C. Burgers, J. L. Holmes, A. A. Mommers and J. K. Terlouw, Chem. Phys. Lett. 102 (1983) 1.

CHAPTER 5

An Experimental and Theoretical Study of the Unimolecular Reactions of Proton-Bound Dimers of CH_3CN and Alcohols

5.1 Introduction

Cluster ions can range in size from simple dimers such as $(He)_2^+$ to large poly-molecular species such as water hydrates, $H_3O^+(H_2O)_n$. Interest in their chemistry stems from their occurrence in earth's atmosphere and in the study of the early stages of the effects of solvation. A central issue when studying the chemistry of gaseous ions is their propensity for rearrangement prior to reaction. Over the years, a variety of thermodynamically stable structures have been discovered including distonic ions [1], ion/neutral complexes [2,3], and bridged ions [4]. These ion structures are ubiquitous to ion dissociation mechanisms, and indeed, the isomerization of gas-phase organic ions appears to be a common occurrence [5-9]. However, the isomerization reactions of cluster ions have not been extensively studied, for examples, see[10-12].

We began studying proton-bound dimers in order to identify possible rearrangements that occur in the course of their unimolecular reactions. The family of proton-bound mixed dimers consisting of nitriles and alcohols all have at least one common feature: they exhibit in their unimolecular decomposition chemistry the competition between simple-bond dissociations and dehydration reactions. In this respect they are similar to many proton-bound alcohol dimers [13-18]. A family of proton-bound dimers that share this propensity for rearrangement are those consisting of CH_3CN and the alcohols methanol, ethanol, n– and i-propanol and the four butanol

isomers (n-, s-, i- and t-butanol). All of these ions exhibit a dehydration reaction that competes on the microsecond timescale with the dissociation of the hydrogen bond in the dimer. Work done in the laboratory [19] before the joined the group showed that the metastable proton-bound dimer of acetonitrile and methanol, $(CH_3CN)(CH_3OH)H^+$, undergoes two unimolecular reactions on the microsecond timescale, a simple bond cleavage reaction to form CH_3CNH^+ and CH_3OH, and the loss of water to form $CH_3CNCH_3^+$. The water loss channel is preceded by rearrangement of the proton-bound dimer to a second isomer, $(CH_3CNCH_3)(H_2O)^+$. The potential energy reaction surface derived for this reaction system is reproduced in Figure 16a. The other alcohol-acetonitrile clusters also exhibit this competition of simple bond cleavage reactions and dehydration reactions, but to varying extents. The competition between the two channels means that there is a fine balancing of the thresholds for dissociation and for isomerization. The present study concerns itself with the other members of this family of proton-bound dimers, those between acetonitrile and the propanols, $(CH_3CN)(CH_3CH_2CH_2OH)H^+$ and $(CH_3CN)((CH_3)_2CHOH)H^+$, and between acetonitrile and the butanols, (n-C_4H_9OH, s-C_4H_9OH, i-C_4H_9OH and t-C_4H_9OH) and to determine the energies of the transition states shown in Figure 16a.

Mass spectrometry is used to identify the key features of the potential energy surfaces, while theoretical calculations on the three dimer systems $(CH_3CN)(CH_3CH_2OH)H^+$, $(CH_3CN)(CH_3CH_2CH_2OH)H^+$ and $(CH_3CN)((CH_3)_2CHOH)H^+$ allow us to compare the key transition states governing the rearrangement process in this family of dimers. In these we identify the key features of the potential energy surfaces using mass spectrometry and ab initio theory and compare the surfaces to its methanol homologue.

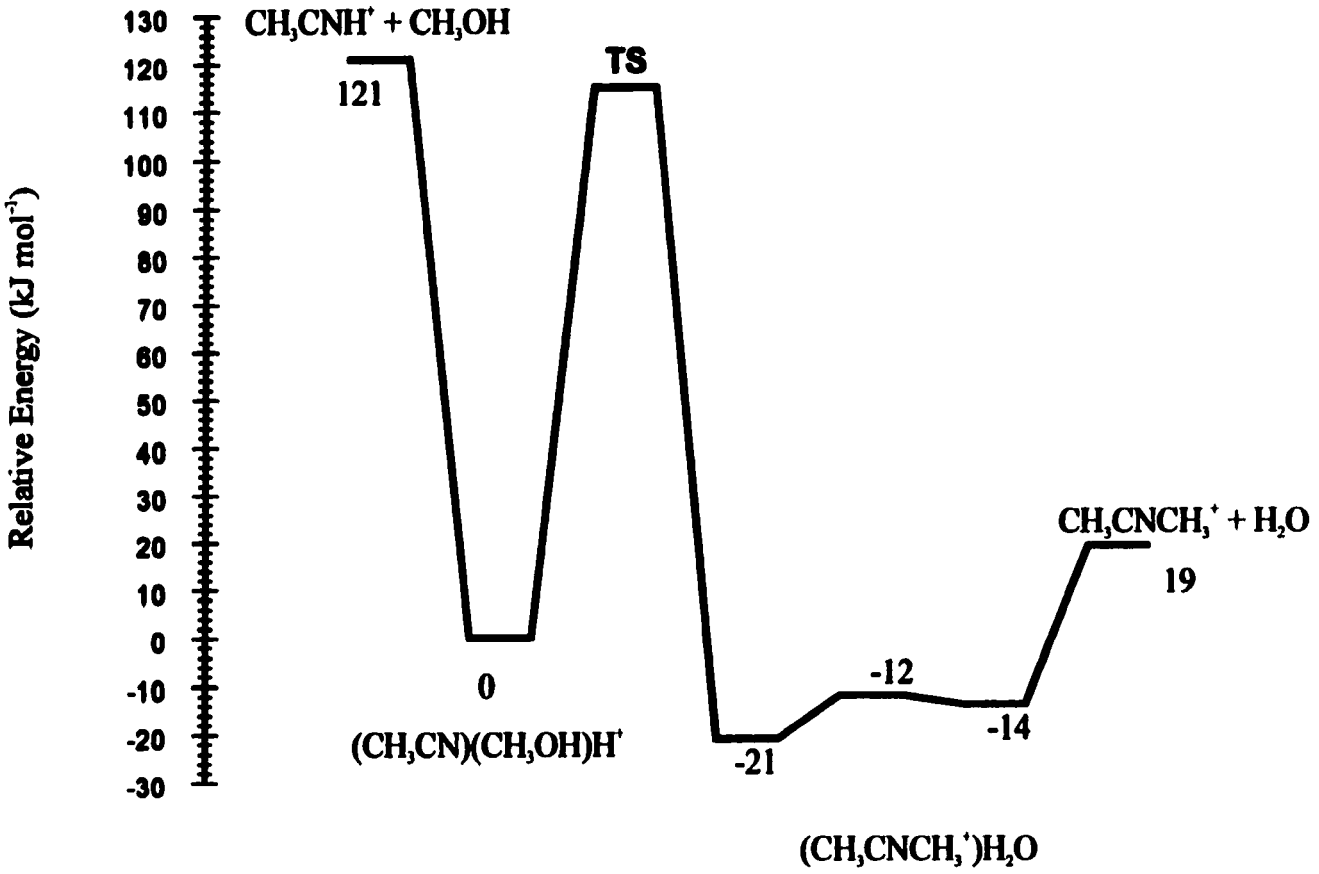

Figure 16a:Potential energy surface for the unimolecular dissociations of the proton-bound dimer $(CH_3CN)(CH_3OH)H^+$ [11]. All values in kJ mol^{-1}

5.2 Experimental Procedures

The experiments were performed on a modified triple sector VG ZAB-2HF mass spectrometer [20] incorporating a magnetic sector followed by two electrostatic sectors (BEE geometry). Protonated cluster ions were generated in the chemical ionization ion source of the instrument. The pressures in the ion source chamber, read with an ionization gauge located above the ion source diffusion pump, were typically between 10^{-5} and 10^{-4} Torr (the pressure in the ion source itself being approximately two orders of magnitude higher). Cluster ions were not observed when the pressure was below 10^{-5} Torr, and there was no evidence of higher order clusters at any of the pressures used in these experiments. Metastable ion (MI) and collision-induced dissociation (CID) mass spectra were recorded in the usual manner in both the second and third field-free regions (2FFR and 3FFR respectively) of the instrument [21]. Helium collision gas was used in all CID experiments and was introduced into the collision cells to achieve 10% reduction in the ion flux (i.e., single collision conditions). All chemicals were commercially obtained and used without further purification. Isotopically labelled compounds (MSD Isotope Ltd) were of 99% purity.

5.3 Computational Procedures

Standard ab initio molecular orbital calculations [22] were performed using the GAUSSIAN 94 [23] and the GAUSSIAN 98 [24] suites of programs. Geometries were optimized, and harmonic

vibrational frequencies were calculated, at both the HF/6-31G(d) and MP2/6-31+G(d) levels of theory. Two recent assessments of theoretical procedures for calculating the properties of proton-bound dimers involving HCN and CH_3CN with a variety of first-row hydrides have shown that geometries optimized at the MP2/6-31+G(d) level of theory provide an adequate foundation for high level single-point energy calculations [25,26]. Relative energies have also been found to be reasonably estimated at this level [27].

For the acetonitrile-methanol proton-bound dimer ion, geometry optimizations were carried out at the HF/6-31G(d), MP2/6-31G(d), and MP2/6-31+G(d) levels of theory. Vibrational frequencies were calculated at the HF/6-31G(d) and MP2/6-31+G(d) levels of theory. Transition states were confirmed by the intrinsic reaction coordinate procedure in GAUSSIAN 98. Single-point energies on the MP2/6-31+G(d) geometries were obtained at the G2, [28] G2(MP2), [29], G2(MP2,SVP) [30] and G2(ZPE=MP2) [31] levels of theory. Scaling factors for the zero-point energies (ZPE) used in these high level treatments were those recommended for the individual procedures (i.e., HF/6-31G(d) ZPE's scaled by 0.8929 for G2, G2(MP2) and G2(MP2,SVP), and MP2/6-31G(d) ZPE's scaled by 0.9646 for G2(ZPE=MP2). Thermal corrections to the data were uniformly carried out using the HF/6-31G(d) vibrational frequencies (scaled by 0.8929). Experimental $\Delta_f H^0$ data reported in the literature for 298 K were converted to 0 K values using the above theoretical corrections. Theoretical heats of formation at 0 K were derived by the atomization method, [32] together with experimental heats of formation of the constituent atoms [33]. A variety of levels of theory were employed to determine the relative energies and thus assess their performance relative to standard G2 theory. The three G2 methods G2, G2(MP2)

and G2(MP2,SVP) all give comparable relative energies, with G2(MP2) deviating from G2 theory by less than 1 kJ mol^{-1} and G2(MP2,SVP) deviating by less than 3.1 kJ mol^{-1}.

For the acetonitrile-ethanol proton-bound dimer ion, single-point energies on the MP2/6-31+G(d) geometries were obtained at the G2(MP2,SVP)[22]level of theory. Previous assessments [25,26]showed that reasonable cluster binding energies and heats of formation can be calculated at this level of theory. G2(MP2,SVP) approximates the QCISD(T)/6-311+G(3df,2p) single-point energy by two additive corrections to a base MP2/6-31G(d) energy. The first is a basis set correction relative to the MP2/6-311+G(3df,2p) energy, and the second is an electron-correlation correction relative to QCISD(T)/6-31G(d). This final total energy is then corrected further with an empirical higher-level correction which attempts to account for residual basis set deficiencies in the above total energy, and also with the zero-point vibrational energy (ZPE). The ZPE used in G2(MP2,SVP) is the HF/6-31G(d) value scaled by 0.8929. Thermal corrections to the data were carried out using MP2/6-31+G(d) vibrational frequencies (scaled by 0.9434) [34]. Theoretical heats of formation ($\Delta_f H°$) were derived by the atomization method employing experimental heats of formation of the constituent atoms [33].

For the acetonitrile-n-propanol and acetonitrile-i-propanol proton-bound dimer ions, standard ab initio molecular orbital calculations were performed using the Gaussian 98 suites of programs. Geometries were optimized, and harmonic vibrational frequencies were calculated, at both the HF/6-31G(d) and MP2/6-31+G(d) levels of theory.

5.4 Results and Discussion

5.4.1 Acetonitrile-Methanol

The G2 surface of the acetonitrile-methanol proton-bound dimer ion is a two-well potential surface (Figure 16b). It shows the proton-bound dimer ion $(CH_3CN)(CH_3OH)H^+$ **1** isomerizes to an intermediate complex **2** (Figure 17) through a transition state, **TS(1-2).** The intermediate complex **2** isomerizes to the isomer **3** through the transition state, **TS(2 -3).** The isomerization of the proton-bound dimer **1** to isomer **3** involves an S_N2 type mechanism. The first step in the process involves the CH_3CN swinging around and the backside attack on the carbon adjacent to the OH_2 group in the protonated methanol to form the complex **2.** The second step involves the stretching of the C — O bond leading to the formation of the thermodynamically stable isomer **3.** The transition state **TS(2 -3)** for the interconversion of the intermediate complex to the isomer **3,** lies 18 kJ mol^{-1} below the simple dissociation products.

5.4.2 Acetonitrile-Ethanol

5.4.2.1 Mass Spectrometry

Metastable $(CH_3CN)(CH_3CH_2OH)H^+$ ions. The 2FFR MI mass spectrum (Figure 18a) of the proton-bound dimer $(CH_3CN)(CH_3CH_2OH)H^+$, (**4**) m/z 88, exhibits three peaks, m/z 70 (-18 amu), m/z 47 (- 41 amu) and m/z 42 (- 46 amu) having relative intensities of 1:0.21:0.27. The loss of 18 amu to form m/z 70 can only be attributed to water loss, while the other two reactions

can be attributed to the loss of acetonitrile (to form protonated ethanol) and ethanol (to form protonated acetonitrile), respectively. The identities of the metastably generated m/z 42 and m/z 47 ions were confirmed by transmitting them into the 3FFR and obtaining their CID mass spectra. These spectra were found to be identical to those of CH_3CNH^+ and $CH_3CH_2OH_2^+$ generated in the ion source by self-protonation. These two ions are likely generated from the proton-bound dimer by simple-bond cleavage reactions.

In the MI mass spectrum, the m/z 42 peak is only slightly more intense than the m/z 47 peak (1.3:1), which is consistent with the relative proton affinities (PA) of acetonitrile and ethanol. The most recent critically evaluated compendium lists the PA of CH_3CN to be 779.2 kJ mol^{-1} and that of CH_3CH_2OH to be 776.4 kJ mol^{-1}.[35] The difference in intensities is more pronounced in the MI mass spectrum of the dimer obtained in the 3FFR (and hence at a longer timescale) where the relative intensities of m/z 70, 47 and 42 are 1:0.11:0.24. Introduction of a trace amount of collision gas into a collision cell results in a dramatic increase in the intensities of m/z 42 and m/z 47 relative to m/z 70, the latter being largely unaffected. This suggests that the dissociation channel leading to m/z 70 involves a rearrangement of the initially generated proton-bound dimer. In this respect the results are analogous to those of the methanol-acetonitrile proton-bound dimer ion [19]. The kinetic energy release (KER) values for the competing processes (dissociation and rearrangement, reported from the full-width at half-height of the three peaks, $T_{0.5}$) are 18 meV (m/z 42), 11 meV (m/z 47) and 26 meV (m/z 70). The first two values are typical values for simple bond dissociation reactions, while the latter is consistent with the dissociation of a weakly bound species (and is similar to that observed for the methanol-acetonitrile dimer) [19].

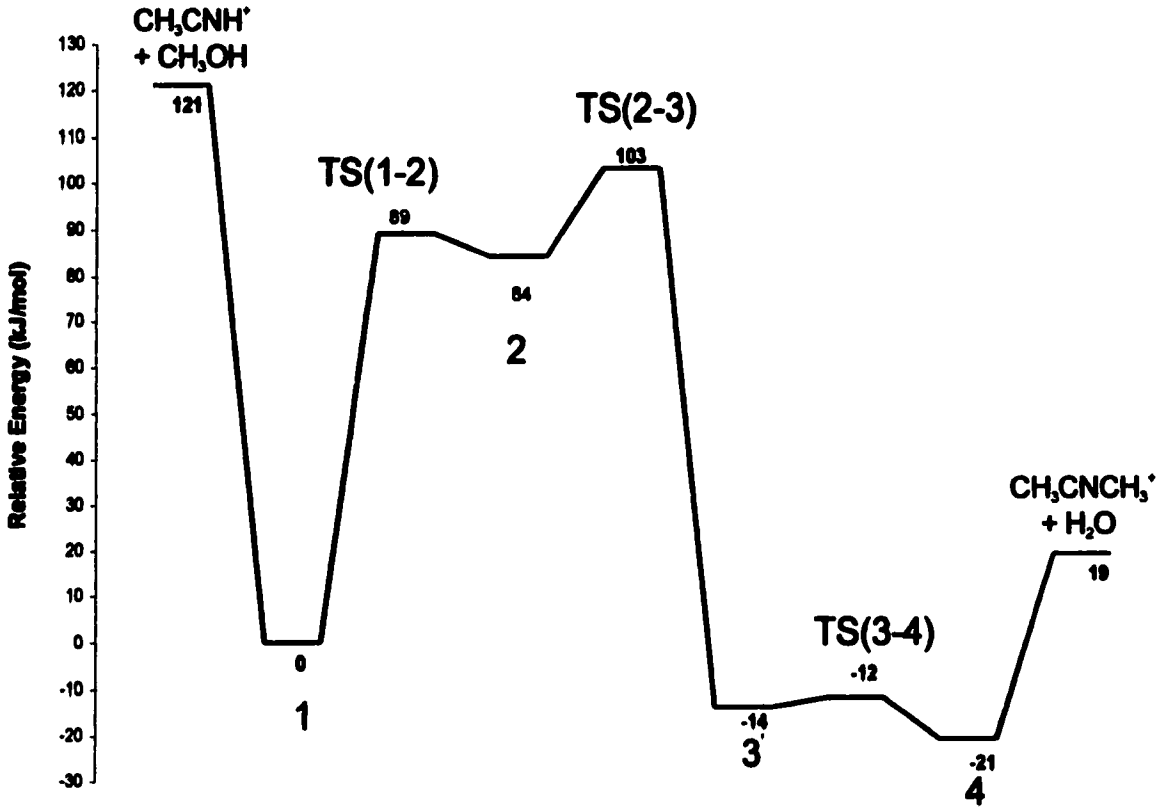

Figure 16b; A G2 Potential energy surface for the unimolecular dissociations of the proton-bound dimer $(CH_3CN)(CH_3OH)H^+$. All values in kJ mol^{-1}.

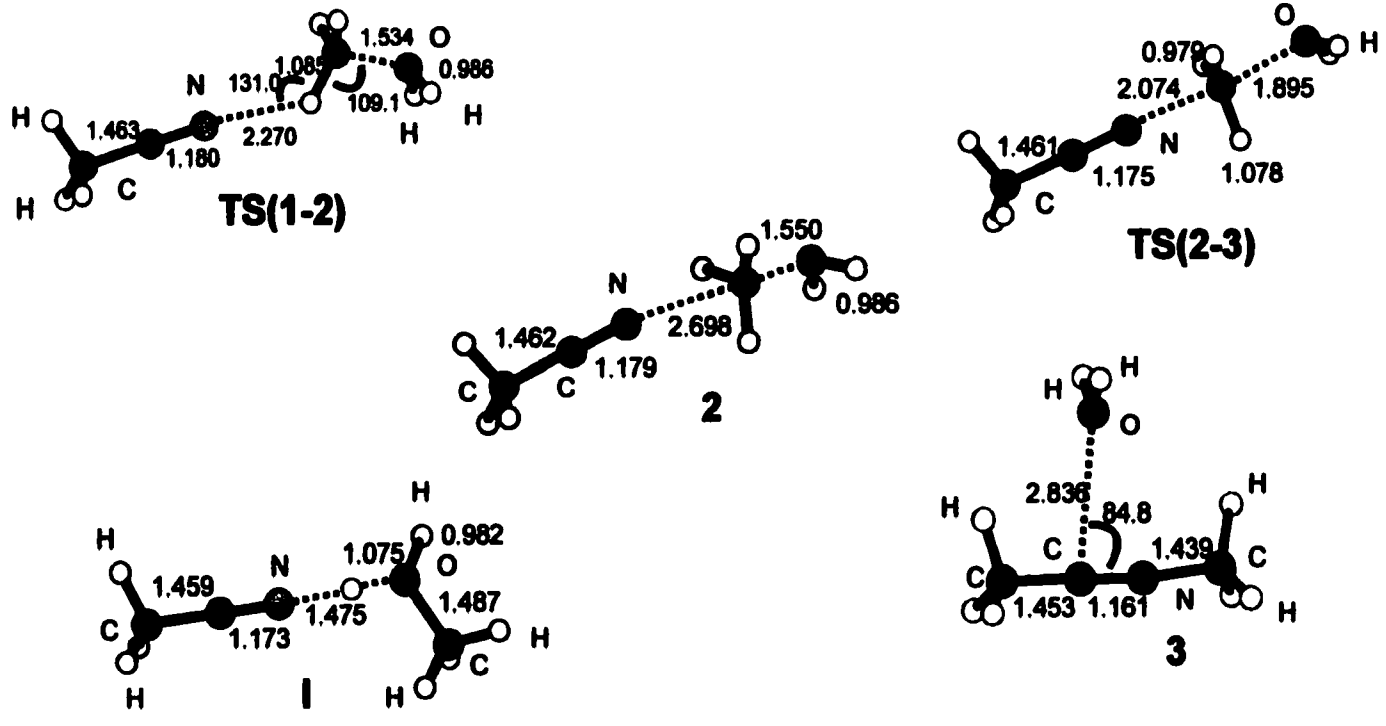

Figure 17:The proton-bound dimer $(CH_3CN)(CH_3OH)H^+$ (1) and isomer (3) and the transition structures TS(1-2) and TS(2-3). All geometries were fully optimized at the MP2/6-31+G(d) level of theory. Bond lengths in angstroms0 angles in degrees.

Collisionally Excited $(CH_3CN)(CH_3CH_2OH)H^+$ ions. The CID mass spectrum of the m/z 88 ions (Figure 18b) shows a substantial increase in the intensities of CH_3CNH^+ and $CH_3CH_2OH_2^+$ (m/z 42 and 47 respectively) relative to m/z 70 (water loss). This is again consistent with the latter channel involving a rearrangement of the initially formed proton-bound dimer. This is because of the relative population of the isomers in the beam. In the time it takes for the ions to react with the collisional gas the population of the original ions (**A** in scheme 1) is larger than that of the rearranged ions (**B** in scheme 1). Upon CID, there is only a small concentration of isomer **B**, in the beam while there is a large population of stable **A** structures. These latter ions will contribute much more to the total observed CID processes than isomer **B**. The relative intensities of the two simple bond cleavage reaction products, however, are inverted in the CID mass spectrum, with m/z 47 being more intense than m/z 42 (Figure 18b). Typically, when a proton-bound dimer dissociates by two competing simple bond cleavage reactions, it is assumed that the two channels are characterized by similar entropies of activation, $\Delta S^{\ddagger}$. The result is that upon collisional activation, the relative intensities of the peaks in the mass spectrum corresponding to the two cleavage reactions become more similar, but do not invert [36]. The present result indicates that these two dissociation channels may be characterized by different entropies of activation (see discussion of RRKM modelling).

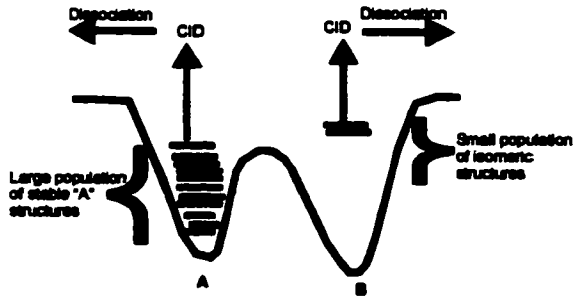

Scheme 1: Ion populations in the ion beam

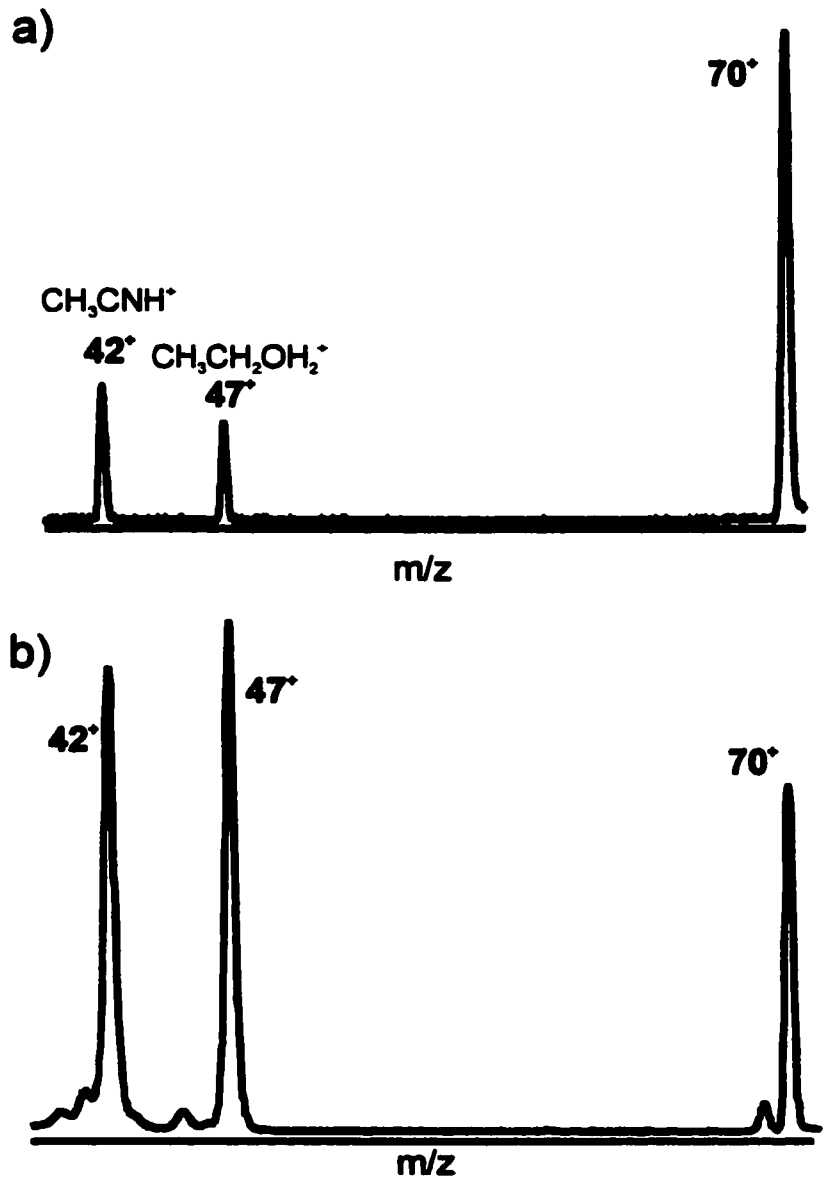

Figure 18. (a) MI mass spectrum of $(CH_3CN)(CH_3CH_2OH)H^+$ obtained in the second field-free region of the VG-ZAB-2HF, (b) CID mass spectrum of $(CH_3CN)(CH_3CH_2OH)H^+$ obtained in the second field-free region of th VG-ZAB-2HF.

5.4.2.2 Identity of m/z 70

The CID mass spectra of source generated m/z 70 and metastably generated m/z 70 were found to be identical (Figure 19). The MI mass spectrum of source generated m/z 70 ions exhibits one peak at m/z 42 which was confirmed to be protonated acetonitrile (Figure 20a). A collision-induced dissociation ionization (CIDI) [37] experiment was performed (Figure 20b) in order to identify the neutral species accompanying this dissociation. The mass spectrum exhibits four consecutive peaks from m/z 25 through m/z 28, indicating that the neutral lost is C_2H_4 and not CO or HCNH. Based on this data, and from analogy to the methanol-acetonitrile dimer ion reaction surface, we propose two possible isomers for m/z 70: $CH_3CNCH_2CH_3^+$ (**7**) and $(CH_3CN)(C_2H_4)H^+$ (**8**).

5.4.2.3 Isotopic Labelling Studies

Isotopically labelled cluster ions were studied to determine the extent of interchange of the hydrogen atoms in the proton-bound dimer. The cluster ions $(CD_3CN)(CH_3CH_2OH)H^+$ (m/z 91), formed by the reaction of CD_3CN with CH_3CH_2OH in the ion source) exhibit three fragment ion peaks in their MI mass spectrum, m/z 73 (- 18 amu), m/z 47 ($CH_3CH_2OH_2^+$) and m/z 45 (CD_3CNH^+), Figure 21a. The identities of these ions were confirmed by their CID mass spectra. These observations indicate that there is no mixing of the methyl hydrogens on acetonitrile with those of the bridging hydrogens (the H^+ bridge and hydroxy hydrogen) or those on the ethyl group.

Ethanol-d_5 was introduced into the ion source and reacted with CH_3CN to form m/z 93 $(CH_3CN)(CD_3CD_2OH)H^+$. The MI mass spectrum contained five peaks, m/z 42 (CH_3CNH^+), m/z 52, ($CD_3CD_2OH_2^+$) and a set of peaks with m/z 73, 74 and 75 (Figure 21b). The latter three peaks represent the loss of D_2O, HOD and H_2O, respectively, in the ratio 0.04: 0.09 : 1.0. These results, coupled with those discussed above, show that a small amount of interchange occurs between the ethyl hydrogens and the bridge hydrogens, but that this mixing occurs only after isomerization of the originally formed proton-bound dimer. The results also show that this mixing is a minor process, with the initially formed isomer ion preferentially dissociating to lose H_2O.

5.4.2.4 Summary of Experimental results

The experimental results are consistent with a two-well reaction surface similar to that proposed for the methanol-acetonitrile proton-bound dimer ion. It is clear from the isotopic labelling experiments that, while there appears to be secondary reactions after isomerization of the proton-bound dimer that result in some hydrogen exchange, these reactions do not compete favourably with dissociation to m/z 70 + H_2O.

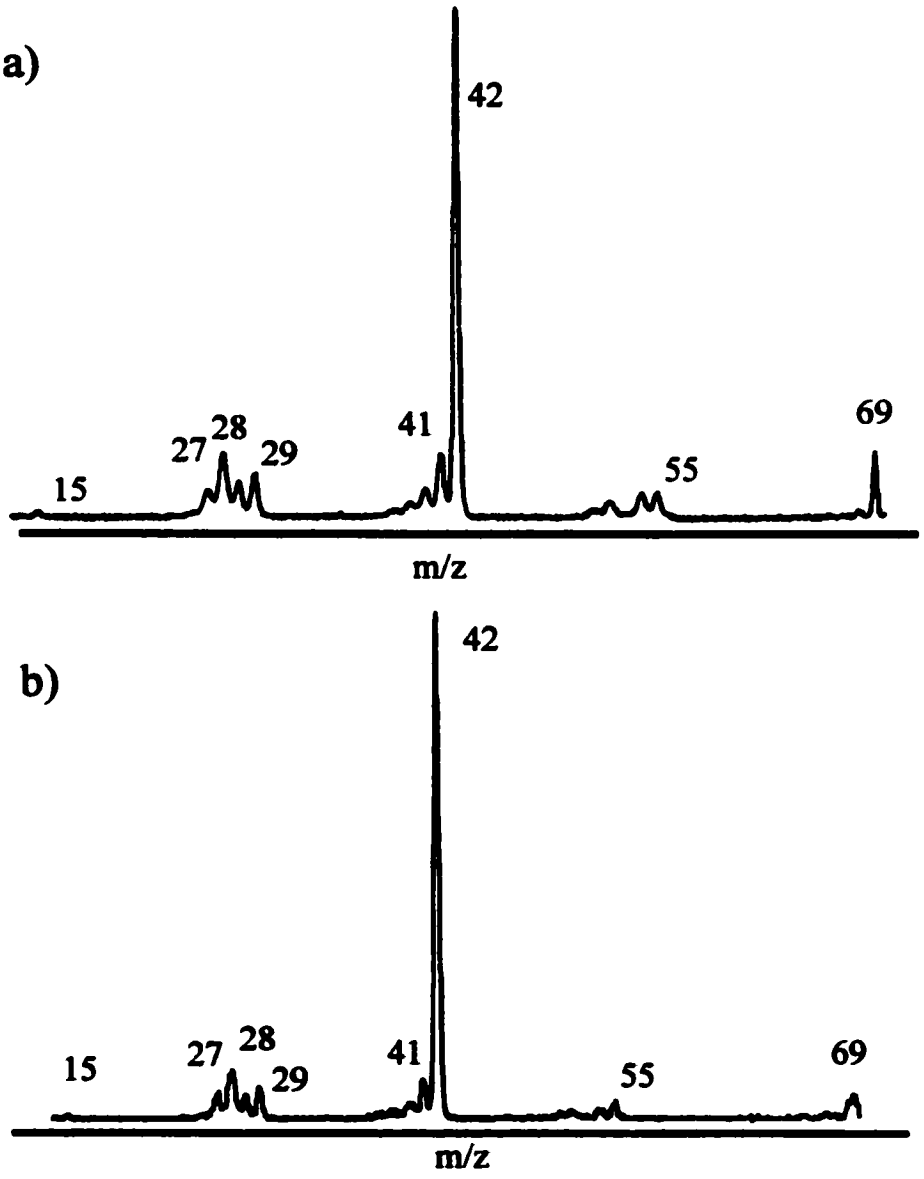

Figure19. (a) CID of source generated m/z 70 (b) CID of metastably generated m/z 70

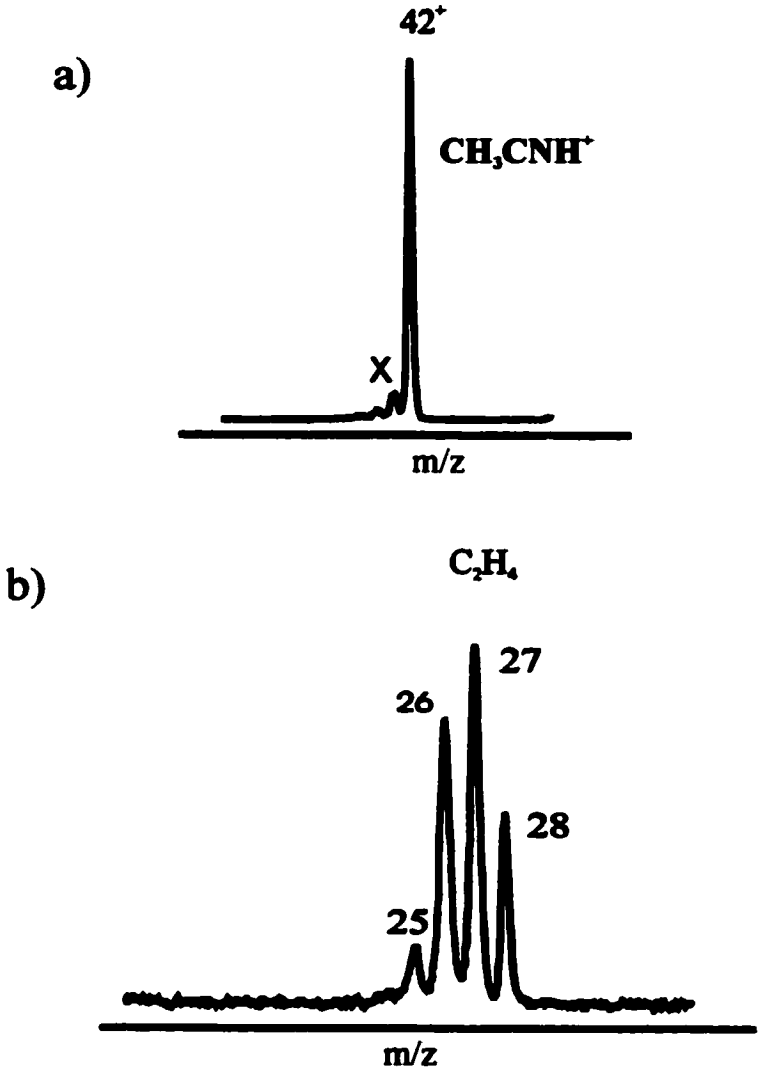

Figure 20. a) MI mass spectrum of source generated m/z 70 b) CIDI mass spectrum to identify neutral species accompanying dissociation of m/z 70 (X) represents an artifact.

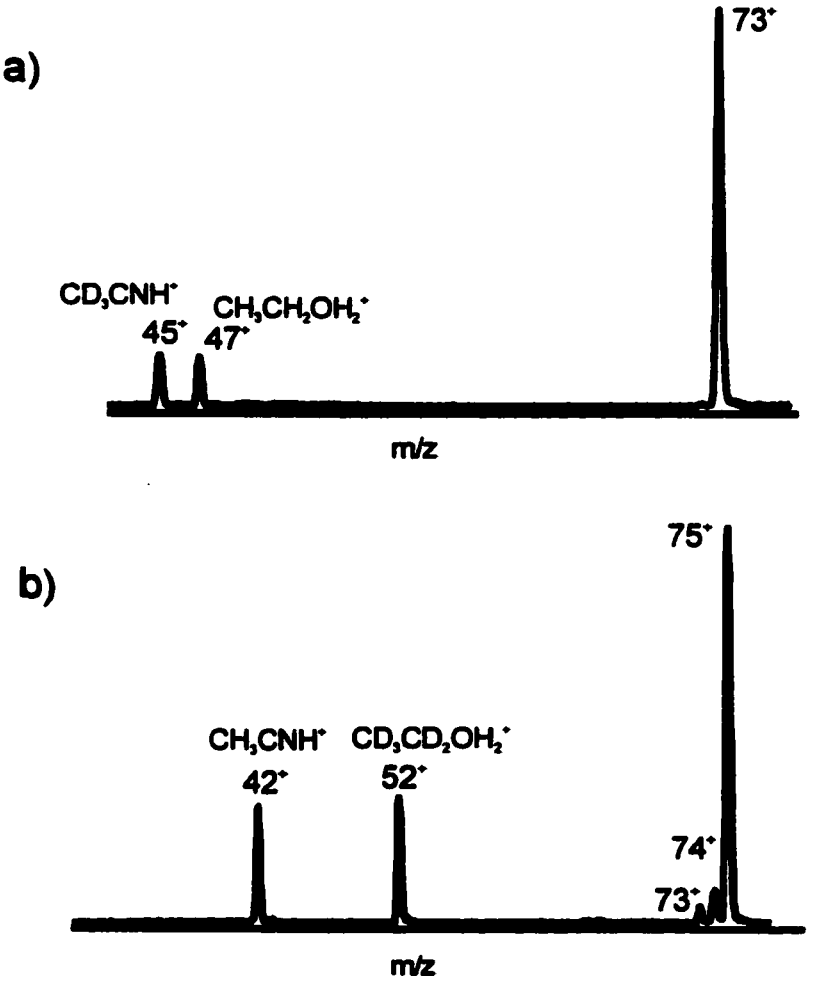

Figure 21. (a) MI mass spectrum of the isotopically labeled ion $(CD_3CN)(CH_3CH_2OH)H^+$ and (b) MI mass spectrum of the isotopically labeled ion $(CH_3CN)(CD_3CD_2OH)H^+$ obtained in the 2FFR of the instrument.

5.4.2.5 Ab initio Calculations

The mass spectrometric results indicate that there is likely to be a thermodynamically stable isomer or a limited number of isomers in the reaction that are responsible for water loss. Ab initio calculations have been used to identify possible structures and model the reaction surface. Structures optimized at the MP2/6-31+G(d) level of theory can be found in Figure 22, and relative energies at this and at the G2(MP2,SVP) level of theory are listed in Table 4, while the potential energy surface is shown in Figure 23. Calculated heats of formation for all equilibrium species are compared to available experimental values in Table 5.

Isomeric forms of m/z 70. Two stable isomers of m/z 70 were located (Figure 22): a covalently bonded structure, **7** , analogous with that found in the previous methanol-acetonitrile study [19], and a proton-bound acetonitrile-ethene dimer, **8**. Ion **7** is calculated to be 99 kJ mol^{-1} lower in energy than ion **8** at the G2(MP2,SVP) level of theory (Table 4). The transition state structure (Figure 22) for the interconversion of the two isomeric m/z 70 ions lies 58 kJ mol^{-1} above ion **8**, and 8 kJ mol^{-1} above the fragmentation products $CH_3CNH^+ + C_2H_4 + H_2O$. The height of this barrier suggests that while **7** may isomerize to **8** prior to metastable dissociation to CH_3CNH^+, the reverse isomerization is unlikely.

5.4.2.6 Isomeric forms of m/z 88

A limited number of isomeric forms of the proton-bound dimer (**4**) were investigated in an attempt to model the reaction surface. Since m/z 70 is formed by the loss of water, a probable

candidates consisted of the above-mentioned m/z 70 isomer **7** with an electrostatically bound water molecule (Figure 22). Structures **6** and **9** are ion-molecule complexes between $CH_3CNCH_2CH_3^+$ and H_2O. Other attempts involving moving the water to other locations all optimized to **6**. The relative energies of these two isomers at the MP2 level of theory showed that **6** and **9** were thermodynamically more stable than the proton-bound dimer, with **6** being slightly lower in energy than **9** (Table 4). G2(MP2,SVP) level calculations put these two isomers slightly higher in energy than **4** (2 and 11 kJ mol^{-1}, respectively). As with the methanol-acetonitrile surface, it is expected that the barrier to interconversion of these two isomers is small. Another possible series of isomers would consist of ion **8** with an electrostatically bound water, $(CH_3CN)(C_2H_4)(H_2O)H^+$ **10** (structure not shown). The energy of **10** relative to **4** is calculated to be 90 kJ mol^{-1} at the G2(MP2,SVP) level of theory. Since the binding energy of a molecule of ethene to $(CH_3CN)(H_2O)H^+$ is small, the formation of the $(CH_3CN)(C_2H_4)(H_2O)H^+$ isomer should be accompanied by the appearance of m/z 60, $(CH_3CN)(H_2O)H^+$ (**11**), in the MI mass spectrum. The absence of m/z 60 in Figure 18 indicates that this isomerization channel is not a significant process.

5.4.2.7 The isomerization mechanism

The isomerization from the proton-bound dimer to isomer **6** likely involves the interconversion of a series of ion/dipole complexes in a mechanism that is similar to the S_N2-type mechanism that has been demonstrated for the proton-bound alcohol dimer ions [38,40] The alcohol dimer mechanism consists of the backside attack of the neutral alcohol on the carbon adjacent to the

OH_2 moeity in the protonated alcohol. Two stable intermediate complexes have been calculated in the case of the methanol dimer, $[CH_3O(H)\cdots CH_3OH_2]^+$ (13) and $[CH_3O(H)CH_3\cdots OH_2]^+$ (14), which ultimately lead to the formation of the proton-bound dimer of dimethyl ether and water [40-42].

An intermediate ion-dipole complex **5** similar to ion **15** above for the methanol dimer, has been located (Figure 22a). This ion is calculated to lie 96 kJ mol^{-1} above the proton-bound dimer at the G2(MP2,SVP) level of theory. So, an S_N2 type mechanism is also feasible for the isomerization of this proton-bound dimer. The dimer first rearranges to the complex **5** (via TS (**4-5**), which then undergoes the shortening of the N — C bond and the elongation of the C—OH_2 (TS (**5-6**)) bond leading to isomers **6** and **9**. This mechanism is also consistent with the isotopic labelling studies that show retention of the labels on the acetonitrile methyl group, the ethanol ethyl group and the bridging hydrogens. The transition state for the interconversion of the intermediate complex to isomer **6** lie 28 kJ mol^{-1} below the dissociation products and 124 kJ mol^{-1} above the proton-bound dimer.

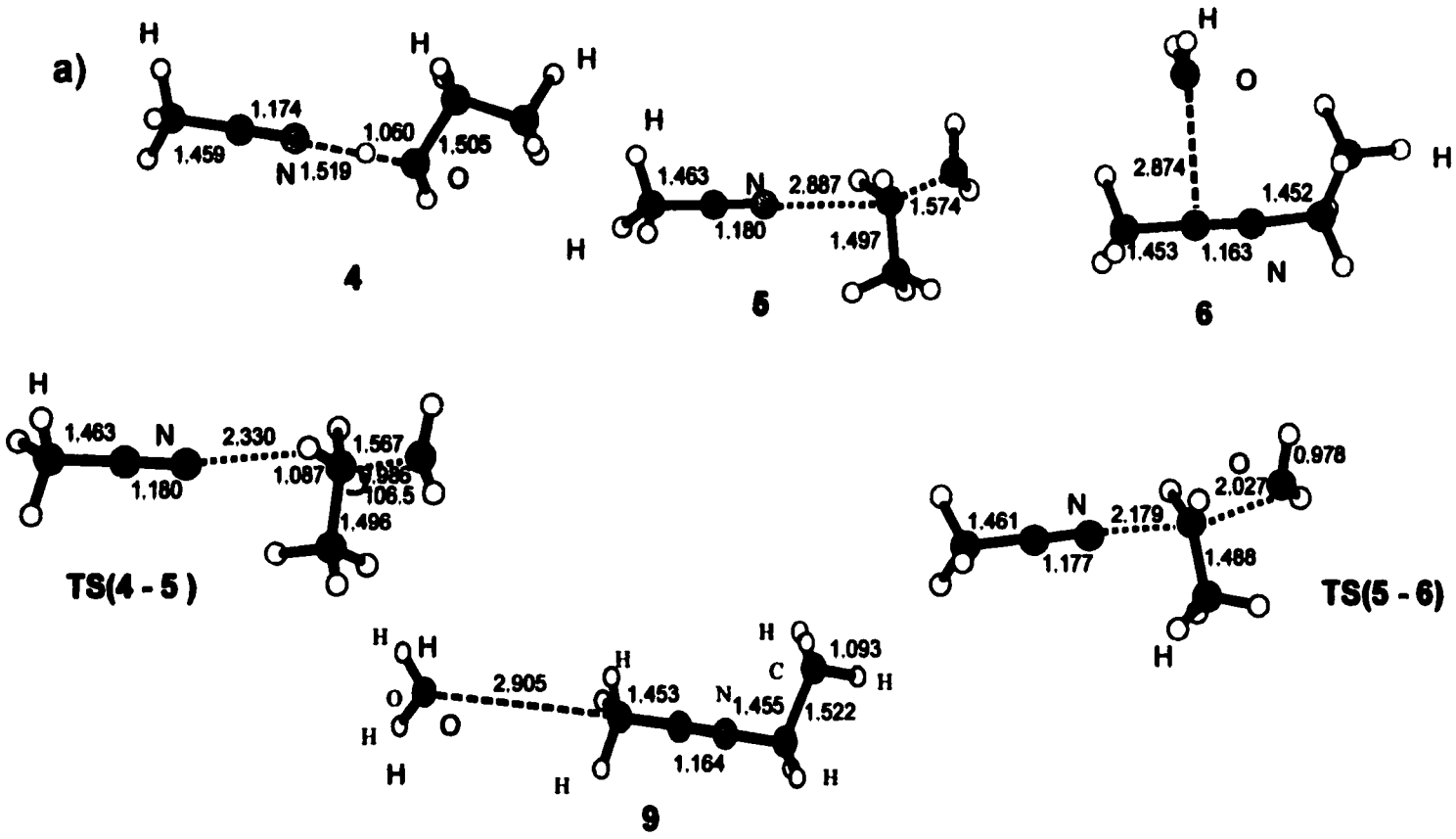

Figure 22(a) : Equilibrium and transition structures for the rearrangement of the proton-bound dimer $(CH_3CN)(CH_3CH_2OH)H^+$.

b)

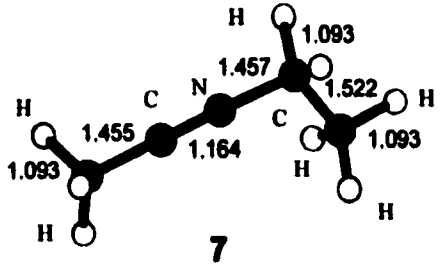

7

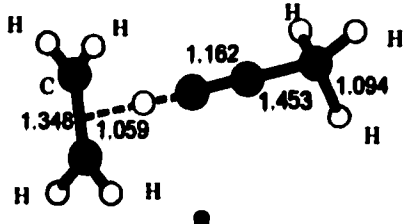

8

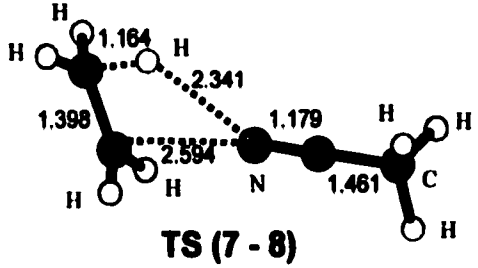

TS (7 - 8)

Figure 22(b). Isomers of m/z 70, 7 and 8, and the transition structure for their interconversion TS(7 - 8). All geometries were fully optimized at the MP/6-31+G(d) level of theory. Bond lengths are in angstroms, bond angles in degrees.

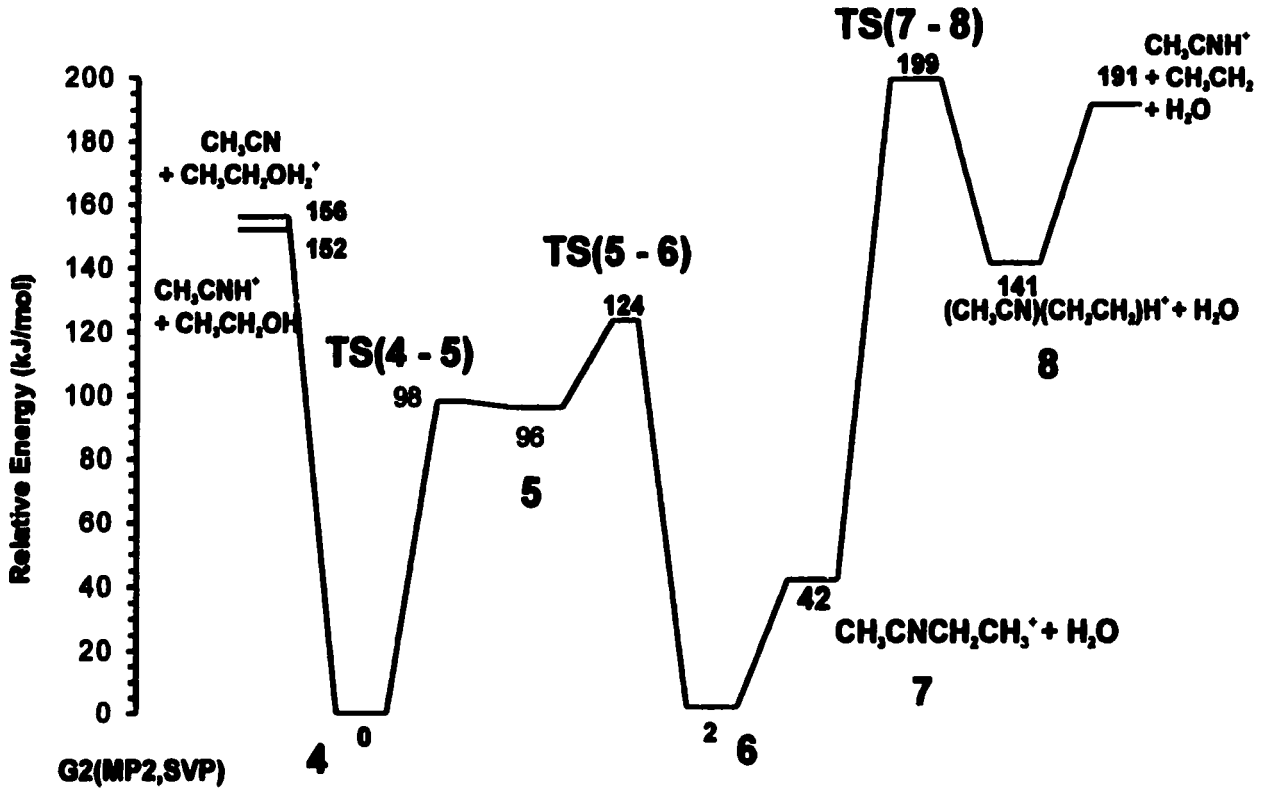

Figure 23:Theoretical reaction profile for $(CH_3CN)(CH_3CH_2OH)H^+$ Relative energies calculated at G2(MP2,SVP). All values are in kJ mol^{-1}.

TABLE 4: Calculated Relative Energies

ion	relative energy[a]	
	MP2/6-31+G(d)	G2(MP2,SVP)
4	0	0
6	-8	2
9	-7	11
5	75	96
7 + H_2O	31	42
8 + H_2O	142	141
TS(4 → 6)	130[b]	130[b]
TS(4 → 5)		98
TS(5 → 6)		124
TS(7 → 8) + H_2O	204	199
CH_3CNH^+ + CH_3CH_2OH	139	152
$CH_3CH_2OH_2^+$ + CH_3CN	134	156
CH_3CNH^+ + C_2H_4 + H_2O	194	191

[a] Values are in kJ mol^{-1} at 0 K. [b] From RRKM modelling (see text).

TABLE 5: Comparison of Calculated G2(MP2,SVP) and Experimental Heats of Formation[a]

species	$\Delta_f H°_0$	$\Delta_f H°_{298}$	LBLHLM[b]	NIST[c]
4	460	433		
7	741	720		
8	841	823		
6	462	438		
9	472	449		
8	556	529		
CH_3CN	79	71	74 ± 1	74.04 ± 0.37
CH_3CNH^+	832	825	817[d]	824.8
CH_3CH_2OH	-220	-238	-234.8 ± 0.2	-235.3 ± 0.5
$CH_3CH_2OH_2^+$	537	516	507[f]	518.3[g]
H_2O	-239	-242	-241.83	-241.826 ± 0.040
C_2H_4	59	50	52.2 ± 1	52.47

[a] Values are in kJ mol^{-1}. [b] Reference 33, 298 K values. [c] Reference 38 , 298 K values.

[d] Based on PA(CH_3CN) = 787 kJ mol^{-1}. [e] Based on PA(CH_3CN) = 779.2 kJ mol^{-1}.

[f] Based on PA(CH_3CH_2OH) = 788 kJ mol^{-1}. [g] Based on PA(CH_3CH_2OH) = 776.4 kJ mol^{-1}.

5.4.2.8 RRKM Estimate of the Isomerization Barrier Height

The reactions in Figure 23 were kinetically modelled with RRKM theory in an attempt to estimate the transition state energy based on the relative intensities of the two reactions in the MI mass spectrum [41]. The microcanonical rate constant, k(E), is a function of the density (ρ) and sum ($N^{\ddagger}$) of states of the reacting ion and transition state, respectively. In its simplest form,

$$k(E) = \frac{\sigma N^{\ddagger}(E - E_0)}{h\rho(E)} \qquad (5.1)$$

where E represents the internal energy of the reacting ion, E_0 is the 0 K activation energy, σ is the symmetry number and h is Planck's constant. The sums and densities of states were calculated using the Beyer-Swinehart direct-count algorithm [41] employing scaled MP2/6-31+G(d) harmonic vibrational frequencies (Table 6). Rate constants were calculated employing the G2(MP2,SVP) 0 K activation energies. The resulting log $k(E)$ vs E curves are presented in Figure 24.

There are six elementary reactions that need to be addressed: the reaction leading from **4** to $CH_3CNH^+ + CH_3CH_2OH$ (k_1), the reaction leading from **4** to $CH_3CH_2OH_2^+ + CH_3CN$ (k_2), the forward isomerization of **4** to **6** (k_3), the dissociation of **6** to **7** + H_2O (k_4), the isomerization of **7** to **8** (k_5) and the dissociation of **8** to $CH_3CNH^+ + C_2H_4 + H_2O$ (k_6). The interconversion of **6** and **9** is expected to be so fast that we have approximated the second potential well with ion **6**. The reverse isomerization of **6** to **4** was not considered because the dissociation of **6** to **7** + H_2O

will be the dominant process for ion **6** (Figure 23). This is consistent with the observation from the isotopic labelling studies that no mixing of the acetonitrile-methyl hydrogens occurs in the labelled clusters. The conversion of **7** to **8** (k_5) was modeled with the ab initio transition structure **TS(7 → 8)**. The $\Delta S^{\ddagger}$(600 K) for this process is -70 J K^{-1} mol^{-1}, and thus the log $k(E)$ vs E curve rises only gradually with increasing internal energy (Figure 24). For the dissociation reaction channels leading from the proton-bound dimer to products, the vibrational frequencies for the transition states were modeled using those of ion **4**, less one mode that most closely matched the dissociation reaction (206 cm^{-1}). In addition, the very small vibrational frequency in ion **4** due to hindered internal rotation about the hydrogen bond (6 cm^{-1}) was not included in the $\rho(E)$ and $N^{\ddagger}(E\text{-}E_0)$ calculations as a distinct vibration, rather it was treated as a hindered internal rotor with a rotational constant of 19.7 GHz. To achieve a suitably loose transition state, the lowest five TS frequencies were scaled to obtain an entropy of activation, $\Delta S^{\ddagger}$(600 K), of 14 J K^{-1} mol^{-1}. This value is typical for simple bond cleavage reactions. It was noted earlier that the two dissociation reactions from ion **4** leading to CH_3CNH^+ and $CH_3CH_2OH_2^+$ may be characterized by different $\Delta S^{\ddagger}$ values. Increasing the $\Delta S^{\ddagger}$(600 K) from +14 to +20 J K^{-1}mol^{-1} for the protonated ethanol channel leads to log $k(E)$ vs E curves that cross in the metastable internal energy window (Figure 24). This modest difference in $\Delta S^{\ddagger}$ may explain the similarity of the two signals in the MI mass spectrum and the inversion in intensity in the CID mass spectrum.

The isomerization of **4** to **6** was modeled in a similar fashion to that discussed above. Without using the ab initio transition structure, the entire S_N2 type reaction was modelled with a single set of frequencies. The transition state, **TS (4 → 6)**, frequencies chosen were those for **4**, less one mode at 1007 cm^{-1} to represent the motion over the col on the reaction surface. In this case, the

low vibrational frequency in **4** of 6 cm^{-1} was included in the $\rho(E)$ of **4** and a scaled value included for the $N^{\ddagger}$ of the transition state. The lowest 5 frequencies were then scaled to achieve a $\Delta S^{\ddagger}$(600 K) value of -12 J K^{-1} mol^{-1}. The unknown quantity in this process is the activation energy. However, since the isomerization competes with the dissociation to $CH_3CH_2OH_2^+ + CH_3CN$ and $CH_3CNH^+ + CH_3CH_2OH$ on the microsecond timescale, (the MI spectrum), the E_0 for the isomerization can be adjusted to produce the desired overlapping log $k(E)$ vs E curves (Figure 24). The estimate that this provides for the activation energy for this reaction is 130 kJ mol^{-1}. It is important to keep in mind the qualitative nature of this modelling. However, it is also important to note that this value is not very far from the activation energy obtained from an ab initio calculation (124 kJ mol^{-1}). Thus where ab initio theory is not available, RRKM calculation will provide adequate information. The segment of the internal energy distribution of the dimer ion responsible for observations in the second-field free region of the mass spectrometer is governed by the timescale of the instrument [42]. However, the estimated frequencies used in the RRKM calculation, and the modelling of the isomerization of **4** to **6** with a single transition state, all lead to uncertainties in this value of the isomerization activation energy. It is still valuable, though, to be able to estimate an approximate value for this process.

5.5 $(CH_3CN)(CH_3CH_2CH_2OH)H^+$ and $(CH_3CN)((CH_3)_2CHOH)H^+$

5.5.1 Mass Spectrometry

The 2FFR MI mass spectrum (Figure 25a) of the proton-bound dimer $(CH_3CN)(CH_3CH_2CH_2OH)H^+$ (**16**), m/z 102, exhibits four peaks, m/z 84 (-18 amu), m/z 61 (-

41 amu), m/z 60 (- 42 amu) and m/z 42 (-60 amu) having relative intensities of 1.0 : 0.93 : 0.06 : 0.03. The loss of 18 amu to form m/z 84 can only be attributed to the loss of water, while the other three reactions can be attributed to the loss of acetonitrile (to form $CH_3CH_2CH_2OH_2^+$), propene (to form m/z 60) and propanol (to form CH_3CNH^+), respectively. The identities of the metastably generated m/z 42 and m/z 61 ions were confirmed by transmitting them into the 3FFR and obtaining their CID mass spectra. These spectra were found to be identical to those of CH_3CNH^+ and $CH_3CH_2CH_2OH_2^+$ generated in the ion source by self-protonation. The 3FFR CID of the metastably generated m/z 60 contained a single peak at m/z 42. Loss of 18 mass units suggests that this ion is $(CH_3CN)(H_2O)H^+$. More evidence for this ion structure will be presented later. Due to their low abundance in the ion source, it was not possible to examine source generated m/z 60 ions.

In the MI mass spectrum, the m/z 61 peak is 30 times more intense than the peak with m/z 42, which is consistent with the relative proton affinities (PA) of propanol and acetonitrile. The most recent critically evaluated compendium lists the PA of $CH_3CH_2CH_2OH$ to be 786.5 kJ mol^{-1} and that of CH_3CN to be 779.2 kJ mol^{-1} [35]. Introduction of a trace amount of collision gas into a collision cell in the 2FFR results in a dramatic increase in the intensities of m/z 61 and m/z 42 relative to m/z 84 and m/z 60, the latter two signals being largely unaffected. This suggests that the fragmentation channels leading to m/z 84 and m/z 60 involve rearrangement of the initially generated proton-bound dimer. In this respect the results are analogous to those of the methanol-acetonitrile and ethanol-acetonitrile proton-bound dimer ions [19,43,44]. The kinetic energy release (KER) values for the competing MI processes (reported from the full-width at half-height of the three peaks, $T_{0.5}$) are 8.3 meV (m/z 42), 12.8 meV (m/z 61) and 34 meV (m/z 84). The

first two values are typical values for simple bond dissociation reactions, while the latter is consistent with the dissociation of a weakly bound species. The 2FFR MI mass spectrum (Figure 25b) of the proton-bound dimer $(CH_3CN)((CH_3)_2CHOH)H^+$ (**21**), m/z 102, exhibits three peaks, m/z 84 ($-H_2O$), m/z 61 ($(CH_3)_2CHOH_2^+$) and m/z 60 having relative intensities of 1.0 : 0.07 : 0.03. The products were identified as describe above. The absence of CH_3CNH^+ is consistent with the PA of acetonitrile being 13.8 kJ mol^{-1} lower than that of i-propanol [23]. The kinetic energy release (KER) values for the competing processes ($T_{0.5}$) are 27 meV (m/z 84) and 18.8 meV (m/z 61) in the MI mass spectrum (m/z 60 being too small to obtain a reliable value). The CID mass spectrum of m/z 102 also contains ions with m/z 42 (CH_3CNH^+), m/z 43 ($C_3H_7^+$) and m/z 45. Propene loss to form m/z 60 also increases in abundance. Both the MI and CID results show that ions **16** and **21** are distinguishable species that do not interconvert on the microsecond time scale of these experiments.

Isotopically labelled cluster ions were studied to determine the extent of interchange of the hydrogen atoms in the two proton-bound dimers. The cluster ions $(CD_3CN)(CH_3CH_2CH_2OH)H^+$ (m/z 105, formed by the reaction of CD_3CN with $CH_3CH_2CH_2OH$ in the ion source) exhibit four fragment ion peaks in their MI mass spectrum, m/z 87 (-18 amu), m/z 63, m/z 61 ($CH_3CH_2CH_2OH_2^+$) and m/z 45 (CD_3CNH^+) (Figure 26a). These observations indicate that there is no mixing of the methyl hydrogens on acetonitrile with the bridging hydrogens (the H^+ bridge and hydroxy hydrogen) or those on the propyl group. The shift of three mass units of m/z 60 to m/z 63, suggests that this ion has an intact acetonitrile group. This supports the assignment of the $(CH_3CN)(H_2O)H^+$ structure to m/z 60. Propanol-d_7 was introduced into the ion source and reacted with CH_3CN to form m/z 109 $(CH_3CN)(CD_3CD_2CD_2OH)H^+$. The MI mass spectrum

contained five peaks, m/z 42 (CH_3CNH^+), m/z 61 (nominally $(CH_3CN)(H_2O)D^+$), m/z 68 $CD_3CD_2CD_2OH_2^+$ and two peaks having m/z 90 and 91 (Figure 26b). These latter two peaks represent the loss of HOD and H_2O, respectively, in the ratio 0.05 : 1.0. These results show that a small amount of interchange occurs between the propyl hydrogens and the bridge hydrogens, but that this mixing occurs only after isomerization of the originally formed proton-bound dimer. The mixing is a minor process, with the rearrangement reaction preferentially resulting in dissociation to H_2O.

The results from the isotopically labelled $(CD_3CN)((CH_3)_2CHOH)H^+$ ions (m/z 105, formed by the reaction of CD_3CN with $(CH_3)_2CHOH$ in the ion source) are similar to the case involving n-propanol in that the acetonitrile methyl hydrogens do not lose their positional identity (Figure 27a). Isopropanol-d_8 was introduced into the ion source and reacted with CH_3CN which resulted in the formation of three cluster ions, m/z 109 $(CH_3CN)((CD_3)_2CDOH)H^+$, m/z 110 $(CH_3CN)((CD_3)_2CDOD)H^+$ and m/z 111 $(CH_3CN)((CD_3)_2CDOD)D^+$. Although the location of the label among the bridging hydrogens cannot be determined, m/z 109 was selected to assure that only H was in the bridge and to avoid contamination of the ion beam with isotopic contribution from a lower mass ion. The MI mass spectrum contained seven peaks, small signals at m/z 42 (CH_3CNH^+), m/z 49 (nominally $(CD_3)_2CH^+$) and m/z 61 (nominally $(CH_3CN)(H_2O)D^+$), and stronger signals at m/z 68 (nominally $(CD_3)CDOH_2^+$), m/z 89, 90 and 91 (Figure 27b). The last three peaks represent the loss of D_2O, HOD and H_2O, respectively, in the ratio 0.19 : 0.36 : 1.0. In contrast to the n-propanol containing dimer ion, there is extensive mixing of the bridging hydrogens with those on the propyl group in the present system. This further distinguishes the proton-bound dimers ions.

TABLE 6: Vibrational Frequencies Used in the RRKM Analysis

species	harmonic vibrational frequencies (cm^{-1})[a]
4	6, 36, 51, 88, 125, 206, 266, 348, 349, 432, 543, 829, 837, 954, 1007,1028, 1074, 1075, 1130, 1227, 1296, 1344, 1452, 1457, 1480, 1503, 1504, 1533, 1543, 1561, 1764, 2273, 2289, 3113, 3120, 3170, 3201, 3222, 3222, 3222, 3257, 3663.
7	19, 114, 156, 255, 295, 369, 480, 675, 820, 985, 1067, 1068, 1084, 1147, 1195, 1331, 1401, 1448, 1473, 1489, 1489, 1527, 1534, 1543, 2387, 3110, 3123, 3148, 3211, 3216, 3216, 3221, 3233.
8	10, 70, 71, 132, 167, 183, 341, 348, 856, 878, 920, 969, 1027, 1052, 1076, 1076, 1084, 1269, 1403, 1448, 1485, 1485, 1515, 1682, 2218, 2946, 3111, 3199, 3210, 3216, 3216, 3291, 3313.
6	25, 58, 63, 118, 134, 167, 193, 268, 285, 304, 364, 375, 482, 683, 822, 987, 1064, 1075, 1097, 1151, 1197, 1333, 1403, 1438, 1470, 1491, 1503, 1530, 1535, 1549, 1716, 2398, 3114, 3124, 3148, 3210, 3216, 3221, 3228, 3237, 3719, 3843.
TS(4 → $CH_3CH_2OH_2^+$) ($DS^{\ddagger}$ = 14 J K^{-1} mol^{-1})	(206)[b] 6, 18, 26, 44, 63, 266, 348, 349, 432, 543, 829, 837, 954, 1007, 1028, 1074, 1075, 1130, 1227, 1296, 1344, 1451, 1457, 1480, 1503, 1504, 1533, 1543, 1561, 1765, 2273, 2289, 3114, 3120, 3170, 3201, 3222, 3222, 3222, 3257, 3663.
TS(4 → CH_3CNH^+) ($DS^{\ddagger}$ = 14 J K^{-1} mol^{-1})	(206)[b] 6, 18, 26, 44, 63, 266, 348, 349, 432, 543, 829, 837, 954, 1007, 1028, 1074, 1075, 1130, 1227, 1296, 1344, 1451, 1457, 1480, 1503, 1504, 1533, 1543, 1561, 1765, 2273, 2289, 3114, 3120, 3170, 3201, 3222, 3222, 3222, 3257, 3663.
TS(4 → 6) ($DS^{\ddagger}$ = -12 J K^{-1} mol^{-1})	(1007)[b], 8, 55, 78, 134, 188, 206, 266, 348, 349, 432, 543, 829, 837, 954, 1028, 1074, 1075, 1130, 1227, 1296, 1344, 1451, 1457, 1480, 1503, 1504, 1533, 1543, 1561, 1765, 2273, 2288, 3114, 3120, 3170, 3201, 3222, 3222, 3222, 3257, 3663.
TS(6 → 7) ($DS^{\ddagger}$ = 14 J K^{-1} mol^{-1})	(118)[b], 11, 27, 30, 56, 64, 193, 268, 285, 304, 364, 375, 482, 683, 822, 987, 1064, 1075, 1097, 1151, 1197, 1333, 1403, 1438, 1470, 1491, 1503, 1530, 1535, 1549, 1716, 2398, 3114, 3124, 3148, 3210, 3216, 3221, 3228, 3237, 3719, 3843.
TS(8 → products) ($DS^{\ddagger}$ = 14 J K^{-1} mol^{-1})	(167)[b], 7, 38, 38, 68, 89, 341, 348, 856, 878, 920, 969, 1027, 1052, 1076, 1076, 1084, 1269, 1403, 1448, 1485, 1485, 1515, 1682, 2218, 2946, 3111, 3199, 3210, 3216, 3216, 3291, 3313.
TS(7 → 8) ($DS^{\ddagger}$ = -70 J K^{-1} mol^{-1})	7, 61, 61, 162, 217, 265, 349, 361, 762, 871, 939, 1077, 1077, 1206, 1248, 1279, 1322, 1386, 1459, 1508, 1508, 1519, 1610, 2231, 2637, 3120, 3203, 3220, 3221, 3238, 3307, 3358.

[a] MP2/6-31+G(d) frequencies scaled by 0.9434 as recommended by Scott and Radom [34].

[b] Corresponds to the vibrational mode that most closely matches the dissociation reaction.

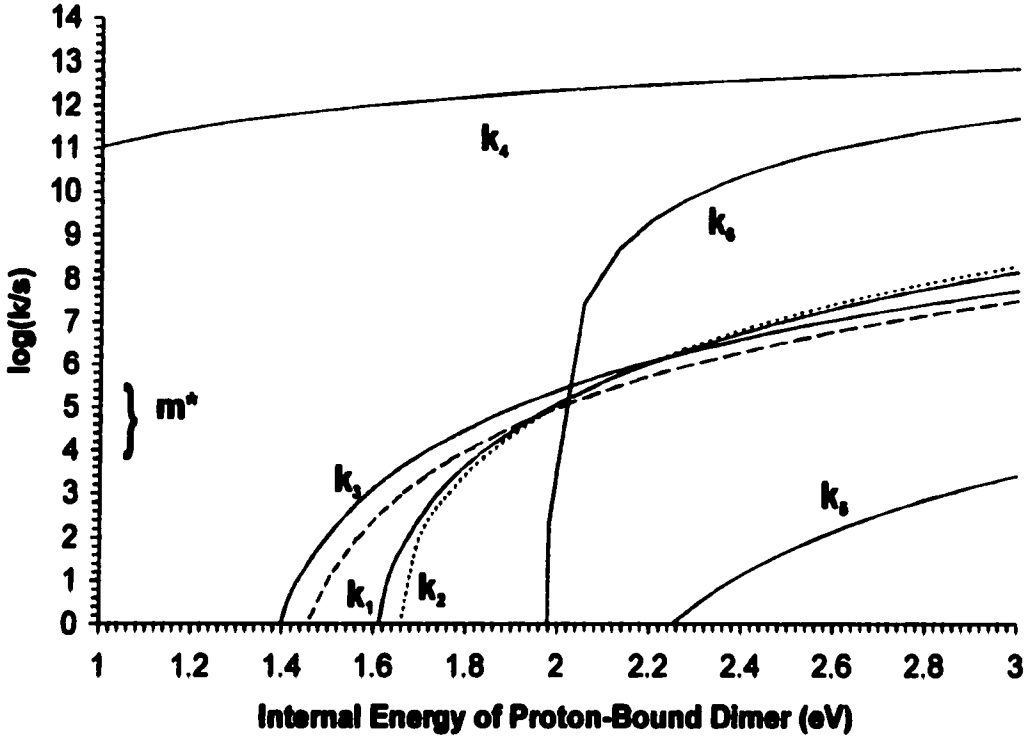

Figure 24. Plot of log k(E) vs ion internal energy curves for the six elementary reactions of $(CH_3CN)(CH_3CH_2OH)H^+$ (all energies are referred to the ground state of the proton-bound dimer): k_1: the reaction leading from 4 to $CH_3CNH^+ + CH_3CH_2OH$; k_2 the reaction leading from 4 to $CH_3CH_2OH_2^+ + CH_3CN$; k_3 the forward isomerization of 4 to 6 employing an E_o of 130 kJ mol^{-1}; k_4: the dissociation of 6 to 7 + H_2O; k_5: the isomerization of 7 to 5; k_6: and the dissociation of 5 to $CH_3CNH^+ + C_2H_4 + H_2O$. A dashed line represents k_3 using an E_o of 135 kJ mol^{-1}. The region m* denotes the range of rate constants responsible for observations in the 2FFR of the instrument.

5.5.2 Identity of m/z 84 in the $(CH_3CN)(CH_3CH_2CH_2OH)H^+$ and $(CH_3CN)((CH_3)_2CHOH)H^+$ systems

Both proton-bound dimers **16** and **21** exhibit water loss to form an ion having m/z 84. The CID mass spectra of the source- and metastably-generated m/z 84 ions starting from **16** are the same, as are the source- and metastably-generated m/z 84 ions originating from **21**. Metastable source-generated m/z 84 ions from both precursors exhibit a single peak, m/z 42, in their MI mass spectra; the measured $T_{0.5}$ values were 34 meV (for the ions originating from **16**) and 27 meV (for the ions originating from **21**). Collision-induced dissociation ionization (CIDI)[37] experiments on the respective source-generated ions result in mass spectra having consecutive peaks from m/z 26 through m/z 28 and m/z 39 through 43, indicating that the neutral lost is C_3H_7 in both cases. From these results it is possible that a common m/z 84 ion is formed upon dissociation of **16** and **21**. However, the He CID mass spectra of the ions formed from **16** and **21** are distinguishable, indicating that a distinct m/z 84 ion is formed from each precursor (Table 7). The differences lie in the intensities of two small peaks, m/z 54 and m/z 55 (nominally loss of C_2H_6 and C_2H_5 respectively). The He CID mass spectrum of m/z 84 ions from **16** exhibits a m/z 55 : 54 : 42 ratio of 0.04 : 0.02 : 1.0 while the ratio in the spectrum of ions generated from **21** is <0.01 : <0.01 : 1.0. Thus, the m/z 84 ions generated from **16** and **21** are distinct species that do not interconvert on the time scale of the experiment. Based on this data, and from analogy to the methanol-acetonitrile and ethanol-acetonitrile dimer ion reaction surfaces, we propose three possible isomers for m/z 84: $CH_3CNCH_2CH_2CH_3^+$ (**19**) and $CH_3CNCH(CH_3)_2^+$ (**24**) and $(CH_3CN)(C_3H_6)H^+$ (**20**). The CID results can be rationalized if ethane and ethyl loss are assumed to be more facile from an ion containing an n-propyl group, **19**. The He CID mass

spectrum of ion **20** (formed by the ion/molecule reaction between CH_3CN and $CH_3CH{=}CH_2$ in the ion source) is also distinguishable from the metastably generated m/z 84 ions from **16** and **21** in that it shows a smaller m/z 43 : 42 ratio (0.07), Table 7. The results for ion **20** are not conclusive as the signal was quite weak and a background source of m/z 84 contaminated the spectrum. This is further indicated by the m/z 43 : 42 ratio which is large considering that the PA values for CH_3CN and propene differ by almost 30 kJ mol^{-1}. Based on these results, tentative assignments of the m/z 84 ions resulting from the dissociation of **16** and **21** can be made to ions **19** and **24**, respectively. This will be discussed in more detail in a later section.

5.5.3 Ab initio calculations

The mass spectrometric results indicate that there is likely to be a thermodynamically stable isomer or isomers in the reactions of **16** and **21** that are responsible for water loss. Ab initio calculations have been used to identify possible structures and model the reaction surface for the propanol containing dimers. Structures and surfaces optimized at the MP2/6-31+G(d) level of theory can be found in Figures 29 and 31 and relative energies are listed in Tables 8 and 9.

5.5.4 Isomeric Forms of m/z 84

The three isomers of m/z 84 discussed previously, $CH_3CNCH_2CH_2CH_3^+$ (**19**), $CH_3CNCH(CH_3)_2^+$ (**24**) and $(CH_3CN)(C_3H_6)H^+$ (**20**) were found to be equilibrium structures on the MP2/6-31+G(d) surface. Ion **19** has two conformers resulting from a cis and trans arrangement of the propyl

group relative to the nitrile functionality. The cis form lies only 1 kJ mol^{-1} lower in energy than the trans configuration (labelled **19'** in Figure 28). The most stable isomer is **24**, which lies 19 kJ mol^{-1} lower in energy than **19** which in turn is 94 kJ mol^{-1} lower in energy than **20**. Isomerization of the n-propyl containing ion **19** to the proton-bound acetonitrile-propene dimer **20** occurs over a high barrier that is predicted to be 69 kJ mol^{-1} above ion **20** and is actually 5 kJ mol^{-1} above the dissociation products $CH_3CNH^+ + C_3H_6$ (Table 8 and Figure 29). The transition structure for the interconversion of **24** and **20** lies 12 kJ mol^{-1} above **20** and 53 kJ mol^{-1} below the dissociation products $CH_3CNH^+ + C_3H_6$ (Table 9 and Figure 30). These results confirm that isomers **19** and **24** do not interconvert prior to loss of propene and are consistent with the experimental observations if the m/z 84 ions from **16** have structure **19** while those from **21** have structure **24**.

5.5.5 Isomeric forms of m/z 102

A number of isomeric forms of the proton-bound dimers **16** and **21** were investigated to model the reaction surface. Since m/z 84 is formed by loss of water, it is highly likely that there are isomeric forms of the proton-bound dimers consisting of the m/z 84 isomers (**19**, **24** and **20**) with an electrostatically bound water molecule (Figure 31). Isomers **18**, **23** (water bound to isomers **19'** and **24**, respectively) and **25** (water bound to isomer **20** not shown) represent ion-water complexes of the three m/z 84 products. At the MP2/6-31+G(d) level of theory, isomers **18** and **23** are both thermodynamically more stable than their respective proton-bound dimers **16** and **21** (Tables 8 and 9). The relative energies of the three ions indicate that **23** is the most stable,

followed by **18** (20 kJ mol^{-1} higher than **23**) and **25** (113 kJ mol^{-1} higher than **23**). Isomer **25** has a very small threshold to dissociation to m/z 60 $(CH_3CN)(H_2O)H^+$ (5 kJ mol^{-1}) and so any isomerization process that leads to **25** will likely proceed directly to m/z 60. Hence, the presence of m/z 60 in the mass spectrum is an indication of the extent to which such a process competes with the alternative path, which is the isomerization of **16** to **18** and **21** to **23**. For the two propanol containing dimers studied here, formation of m/z 60 is a minor process (Figure 25a and b).

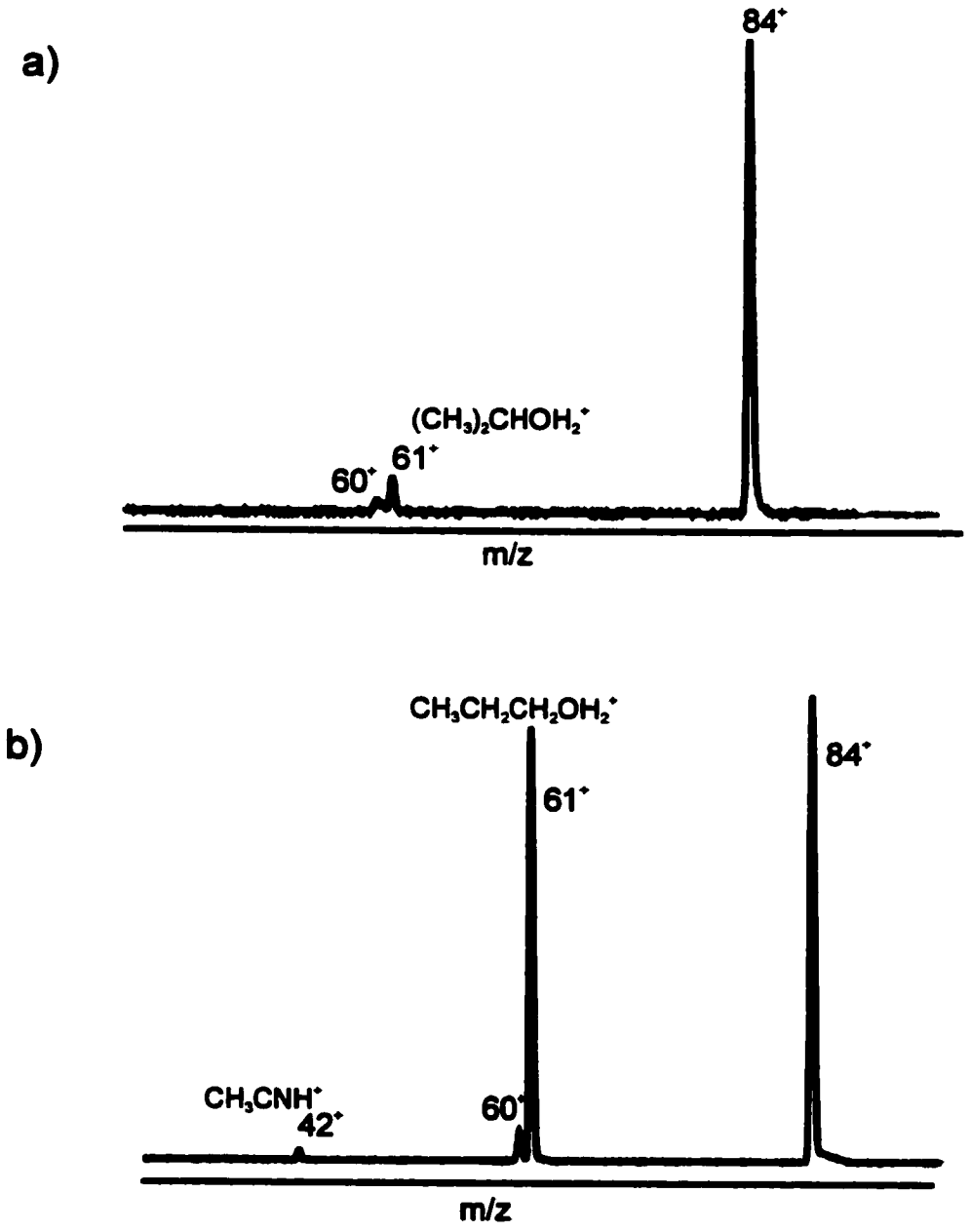

Figure 25. a) MI mass spectrum of $(CH_3CN)((CH_3)_2CHOH)H^+$ obtained in the second field free region of the VG ZAB-2HF, b) MI mass spectrum of $(CH_3CN)((CH_3CH_2CH_2OH)H^+$ obtained in the second field free region of the VG ZAB-2HF.

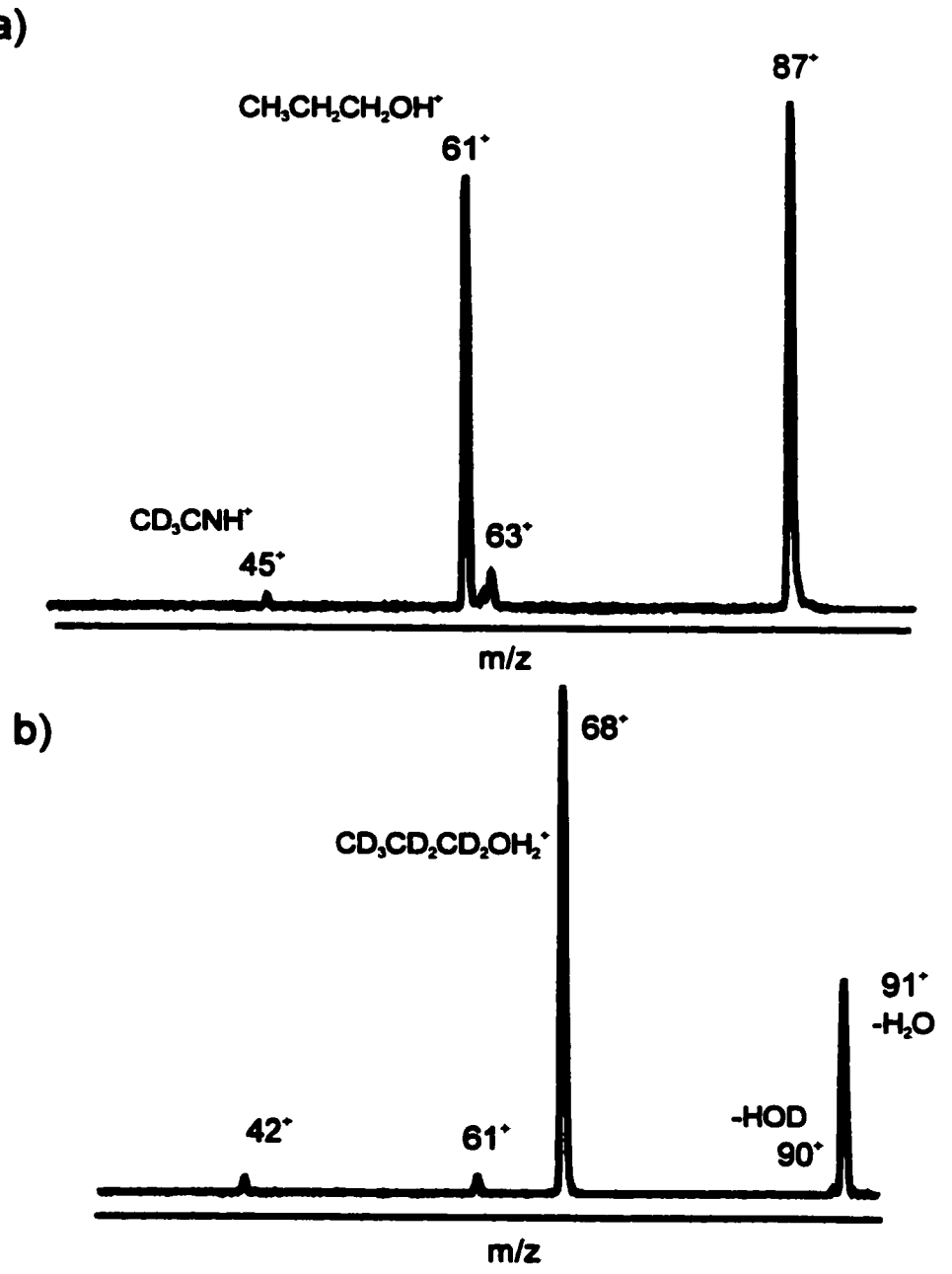

Figure 26. MI mass spectra of isotopic labelled $(CH_3CN)(CH_3CH_2CH_2OH)H^+$ a) $(CD_3CN)(CH_3CH_2CH_2OH)H^+$, b)$(CH_3CN)(CD_3CD_2CD_2OH)H^+$.

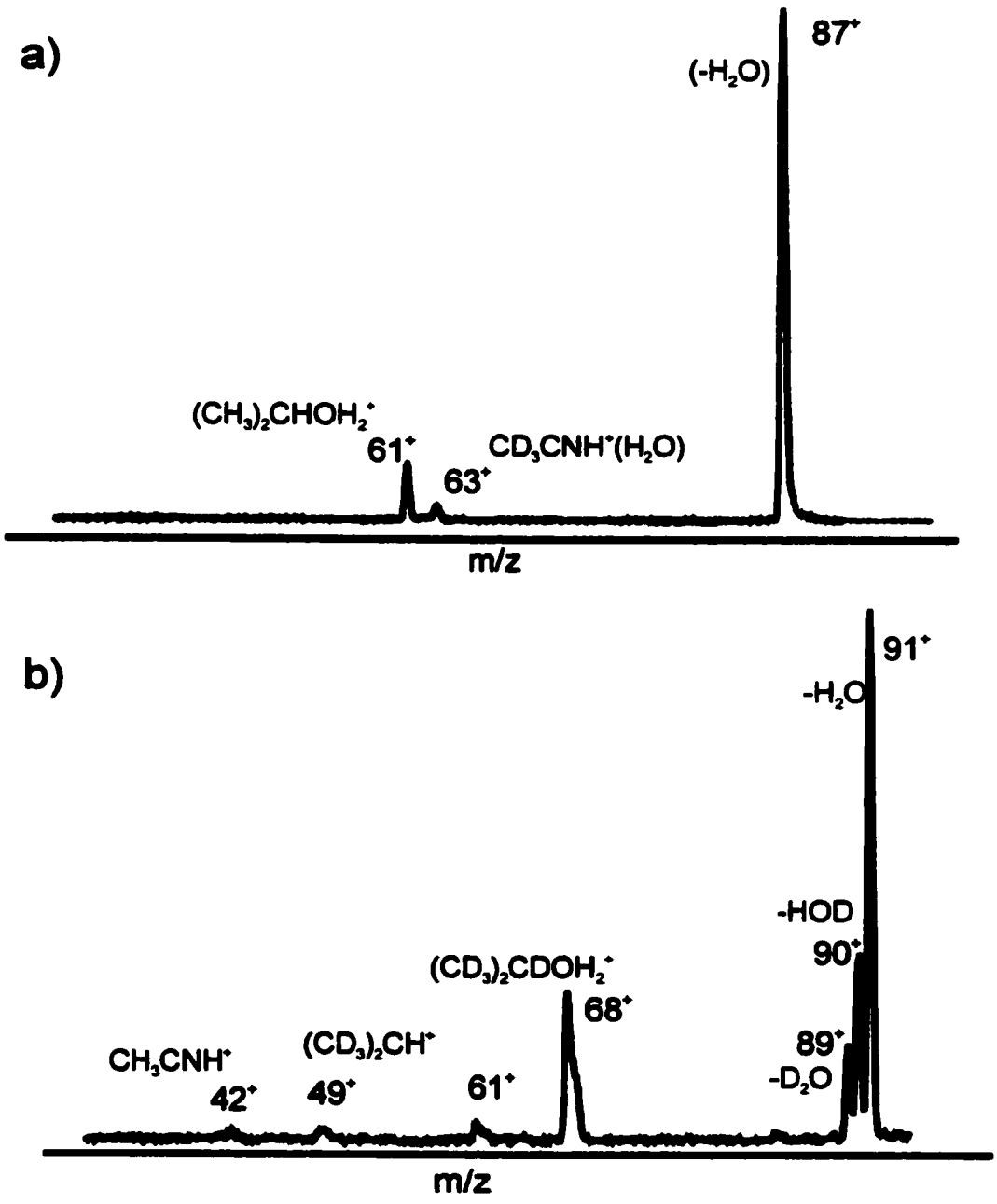

Figure 27. Mass spectra of isotopic labelled (a)$(CD_3CN)((CH_3)_2CHOH)H^+$. (b) $(CH_3CN)((CD_3)_2CDOH)H^+$.

Table 7. Relative Peak Intensities in the He CID Mass Spectra of m/z 84 ions.

Precursor	m/z													
	69	68	56	55	54	43	42	41	40	39	38	28	27	26
$(CH_3CN)(CH_3CH_2CH_2OH)H^{+a}$	0.01	0.01	0.02	0.01	<0.01	0.14	1.0	0.07	0.02	0.04	0.01	0.01	0.03	0.01
$(CH_3CN)(CH_3CH_2CH_2OH)H^{+b}$	0.02	0.02	0.02	0.04	0.02	0.16	1.0	0.13	0.03	0.05	0.02	0.03	0.05	0.02
$(CH_3CN)((CH_2)_2CHOH)H^{+a}$	0.01	0.02	–	–	<0.01	0.12	1.0	0.07	0.03	0.05	0.01	0.01	0.03	0.02
$(CH_3CN)((CH_2)_2CHOH)H^{+b}$	0.02	0.02	–	< 0.01	<0.01	0.15	1.0	0.10	0.03	0.04	0.01	0.02	0.04	0.02
$(CH_3CN)(CH_2{=}CHCH_3)H^{+}$	–	–	–	–	–	0.07	1.0	–	–	–	–	–	–	–

[a] Source generated m/z 84.

[b] Metastably generated m/z 84.

[c] Generated by ion/molecule reaction in the ion source. There was a background signal at m/z 84, and only the fragment ions m/z 43 and 42 were observed to be affected by changes in acetonitrile and propene pressure. However, due to low signal levels, the presence of other fragment ions cannot be discounted.

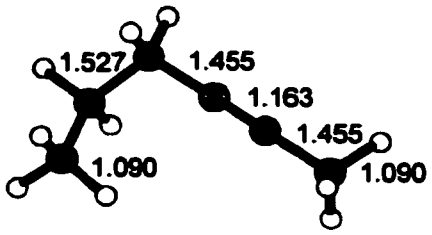

19

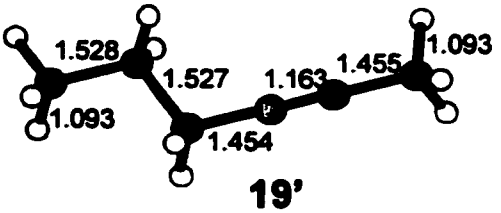

19'

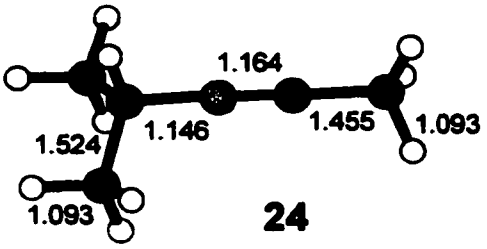

24

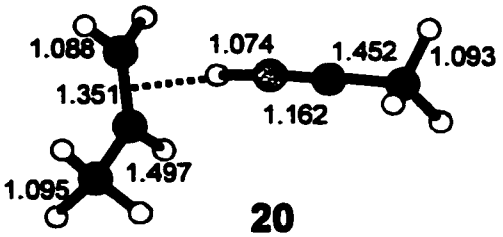

20

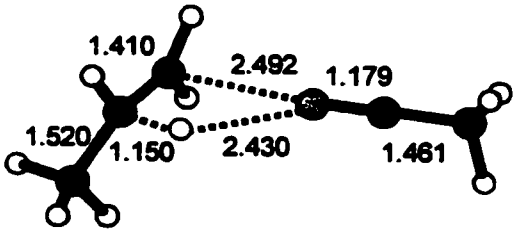

TS(19 - 20)

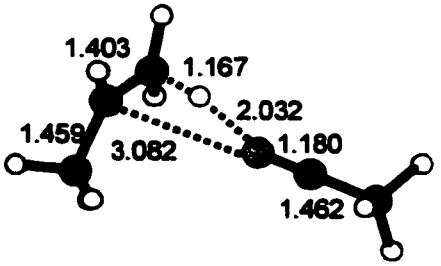

TS(24 -20)

Figure 28. Equilibrium structures for products (m/z 84, isomers 5-7) resulting from water loss from the proton-bound dimers $(CH_3CN)(CH_3CH_2CH_2OH)H^+$ and $(CH_3CN)((CH_3)_2CHOH)H^+$ and the transition structures for their interconversion. All geometries are optimized at the MP2/6-31+G(d) level of theory. Bond lengths are in Angstroms, bond angles in degrees.

Table 8. Calculated Relative Energies For

$(CH_3CN)(CH_3CH_2CH_2OH)H^+$

	E_{rel}[a,b]
16	0
TS(16 - 17)	77
17	76
TS(17 - 18)	106
18	-16
25	77
19 + H_2O	27
19' + H_2O	28
TS (19 - 20) + H_2O	191
20 + H_2O	122
$(CH_3CN)(H_2O)H^+ + C_3H_6$	81
$CH_3CH_2CH_2OH_2^+ + CH_3CN$	132
$CH_3CNH^+ + CH_3CH_2CH_2OH$	144
$CH_3CNH^+ + C_3H_6 + H_2O$	186
$H_3O^+ + CH_3CN + C_3H_6$	292

[a] MP2/6-31+G(d) values incorporating a scaled (by 0.9434)[34] ZPE correction based on MP2/6-31+G(d) vibrational frequencies.

[b] Values are in kJ mol^{-1} at 0 K.

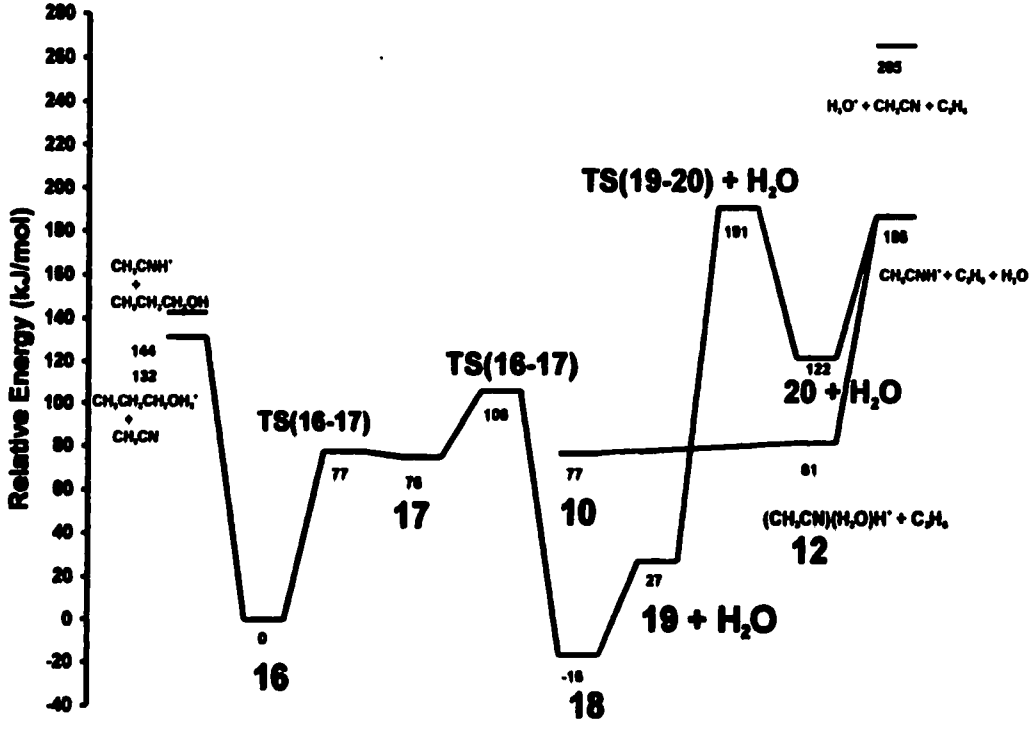

Figure 29:Calculated minimum energy reaction pathway for the unimolecular process of $(CH_3CN)((CH_3CH_2OH)H^+$. All energies were obtained at the MP2/6-31+G(d) level of theory and incorporate an MP2/6-31+G(d) zero-point energy correction scaled (by 0.9534) .

Table 9. Calculated Relative Energies For $(CH_3CN)((CH_3)_2CHOH)H^+$

	E_{rel}[a,b]
21	0
TS(21 - 22)	70
22	69
TS(22 - 23)	97
23	-10
25	103
24 + H_2O	35
TS(24 - 20) + H_2O	160
20 + H_2O	148
$CH_3CN(H_2O)H^+ + C_3H_6$	108
$(CH_3)_2CHOH_2^+ + CH_3CN$	127
$CH_3CNH^+ + (CH_3)_2CHOH$	150
$CH_3CNH^+ + C_3H_6 + H_2O$	213
$H_3O^+ + CH_3CN + C_3H_6$	292

[a] MP2/6-31+G(d) values incorporating a scaled (by 0.9434)[34] ZPE correction based on MP2/6-31+G(d) vibrational frequencies.

[b] Values are in kJ mol^{-1} at 0 K.

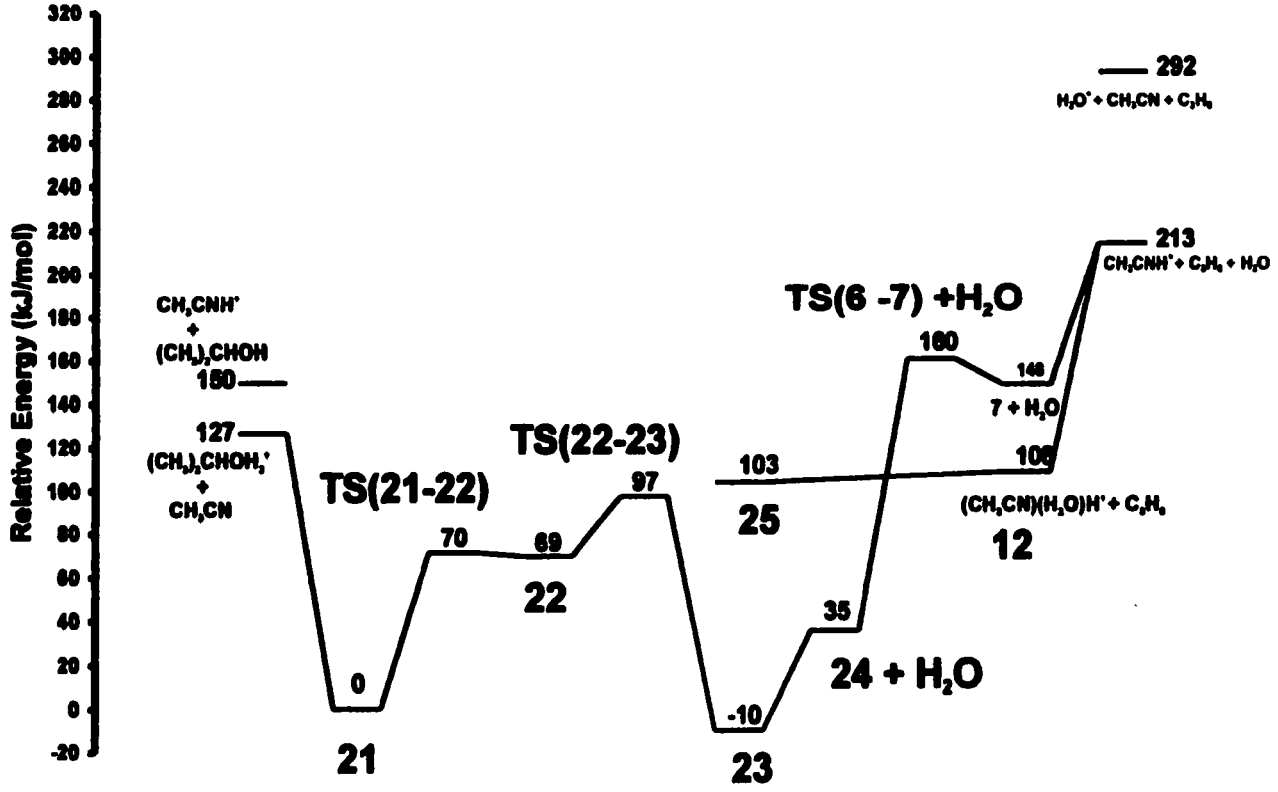

Figure 30:Calculated minimum energy reaction pathway for the unimolecular process of $(CH_3CN)((CH_3)_2CHOH)H^+$ All energies were obtained at the MP2/6-31+G(d) level of theory and incorporate an MP2/6-31+G(d) zero-point energy correction scaled by 0.9534.

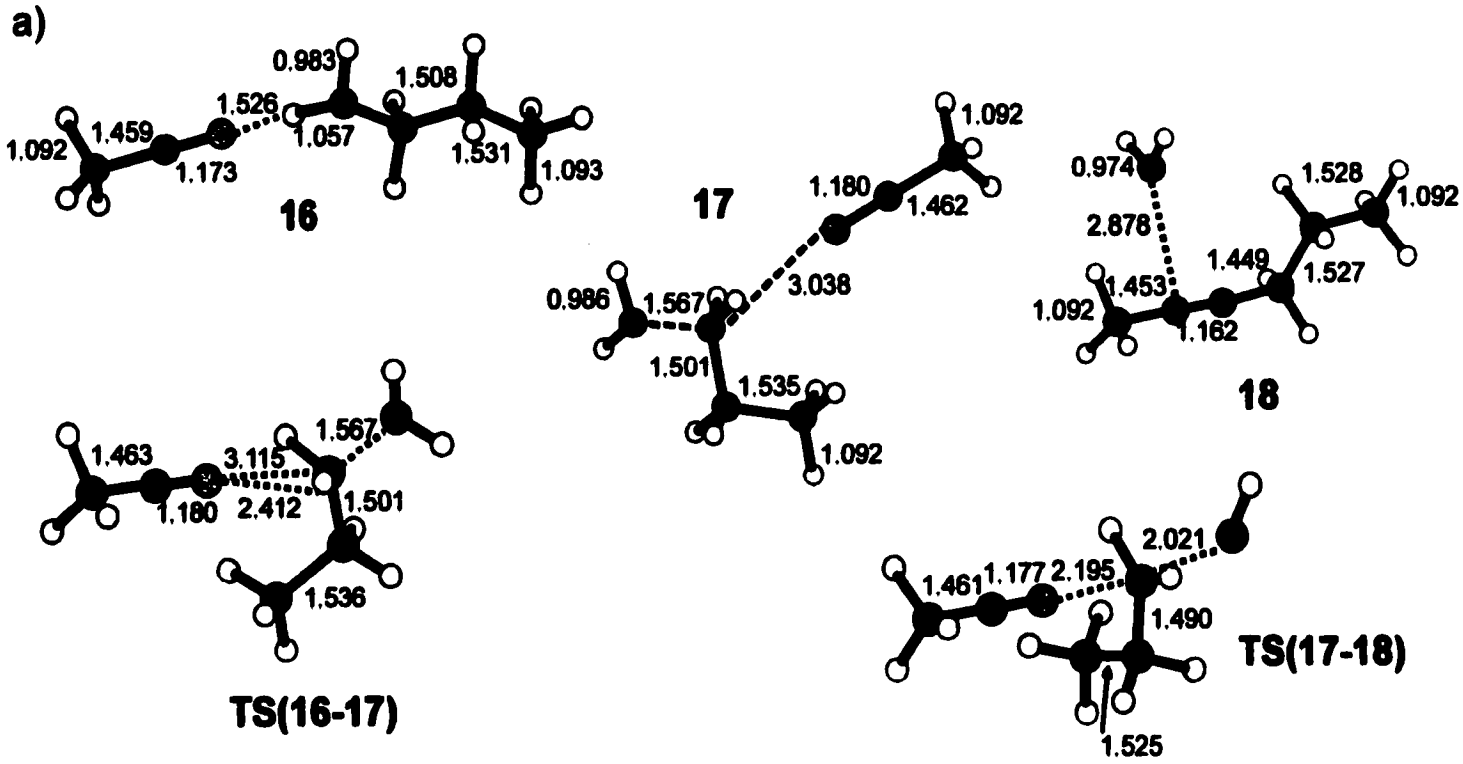

Figure 31(a):Equilibrium and transition structures of the proton-bound dimer $(CH_3CN)(CH_3CH_2CH_2OH)H^+$ to $(CH_3CNR)(H_2O)^+$ where R = $CH_3CH_2CH_2$. All geometries are optimized at the MP2/6-31+G(d) level of theory. Bond lengths are in Angstroms, bond angles in degrees.

b)

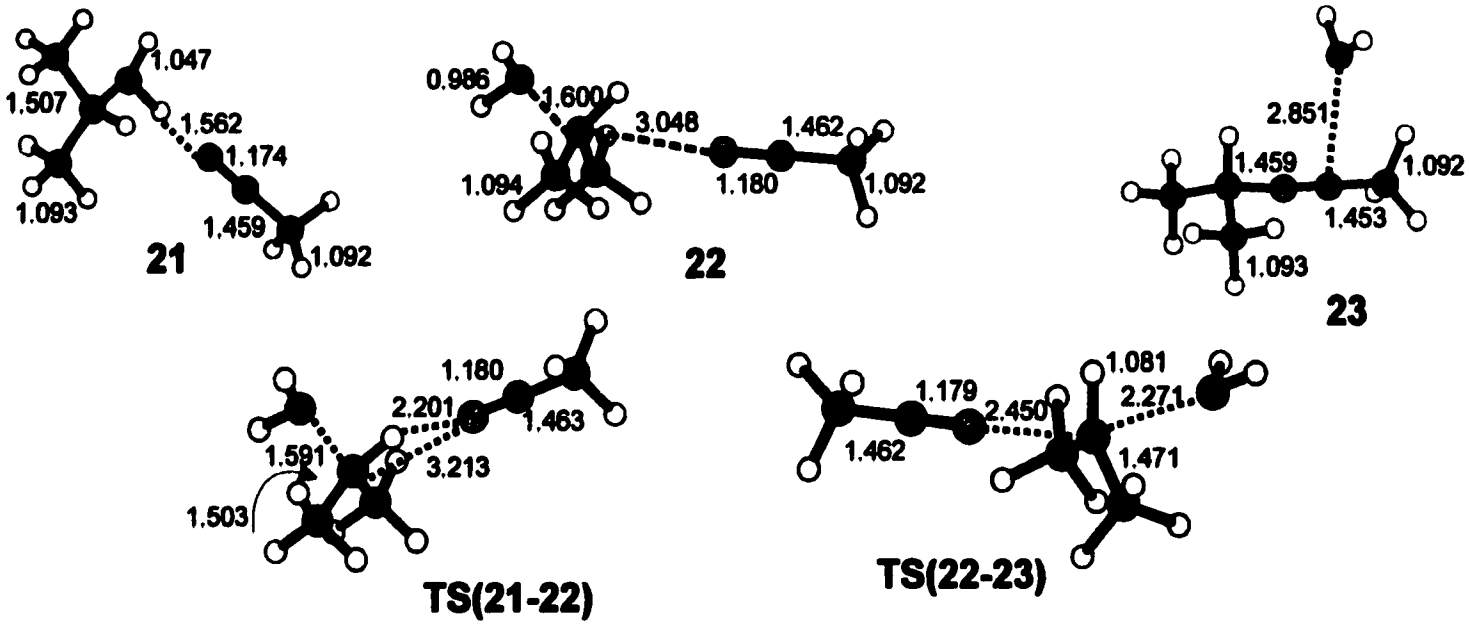

Figure 31(b):Equilibrium and transition structures of the proton-bound dimer $(CH_3CN)((CH_3)_2CHOH)H^+$ to $(CH_3CNR)(H_2O)^+$ where R = $(CH_3)_2CH$. All geometries are optimized at the MP2/6-31+G(d) level of theory. Bond lengths are in Angstroms, bond angles in degrees.

5.6 $(CH_3CN)(ROH)H^+$ (R = n-butyl, s-butyl, i-butyl and t-butyl)

The 2FFR MI mass spectrum (Figure 32a) of the proton-bound dimer $(CH_3CN)(CH_3CH_2CH_2CH_2OH)H^+$ (**26**), m/z 112, exhibits three peaks, a water loss signal at m/z 98, m/z 75 (loss of CH_3CN) and m/z 60 (loss of butene) having relative intensities of 0.54 : 1.0 : 0.06. The lack of a signal at m/z 42 is consistent with the relative proton affinities (PA) of n-butanol and acetonitrile, 789.2 kJ mol^{-1} and 779.2 kJ mol^{-1} respectively.[35] However, the four protonated butanol isomers have very similar CID mass spectra (Table 10), and thus it was not possible to unequivocally identify the protonated butanol being generated in these systems. That the ion is likely generated by simple-bond cleavage in the proton-bound dimer is supported by the fact that the introduction of a trace amount of collision gas into a collision cell results in a significant increase in the intensity of m/z 75 relative to m/z 98 and m/z 60, which remain largely unaffected. In this respect the results are analogous to those of the previous systems. The He CID mass spectrum of the source generated m/z 60 ions exhibited a series of peaks m/z 42, 41, 40, 39, and 28 having relative intensities of 1.0 : 0.14 : 0.05 : 0.02 : 0.02. The CID of source-generated m/z 63 from the $(CD_3CN)(CH_3CH_2CH_2CH_2OH)H^+$ dimer ion exhibits a base peak at m/z 45. The shift in three mass units indicates m/z 60 is likely to be $CH_3CN(H_2O)H^+$ as it loses water to form m/z 42 (CH_3CNH^+).

The 2FFR MI mass spectrum (Figure 32b) of the proton-bound dimer $(CH_3CN)(s\text{-}C_4H_9OH)H^+$ (**27**) exhibits the same three peaks as **26**, but in very different ratios (m/z 98 : 75 : 60 ratios of 0.56 : 1.0 : 0.17). Again the absence of CH_3CNH^+ is consistent with the PA of acetonitrile being

35.8 kJ mol^{-1} lower than that of s-butanol [35]. Introduction of a trace amount of collision gas into a collision cell results in an increase in the intensities of m/z 75 and the appearance of m/z 42 which is consistent if the two channels result from simple bond cleavage in the dimer.

The MI mass spectrum (Figure 28c) of the proton-bound dimer $(CH_3CN)(i\text{-}C_4H_9OH)H^+$ (**28**) exhibits the same three peaks as the above two dimers (m/z 98, 75 and 60) and a fourth signal at m/z 57 (m/z 98 : 75 : 60 : 57 ratios 1.0 : 0.29 : 0.16 : 0.12). The kinetic energy release (KER) values are 6.5 meV (m/z 57), 6.9 meV (m/z 75), 27.2 meV (m/z 60) and 30.1 meV (m/z 98). The CID mass spectrum of m/z 116 shows an increase in the intensities of both m/z 75 and m/z 57 and the appearance of m/z 42 while both m/z 60 and m/z 98 remain unchanged. Both of these results support the assignment of m/z 57 (which is likely due to the consecutive loss of H_2O from m/z 75) and 75 to simple cleavage reactions and m/z 60 and 98 to rearrangement processes. The small kinetic energy release value of the m/z 57 ion in the MI mass spectrum precludes its formation from m/z 98, even though the 3FFR MI mass spectrum of the metastably-generated m/z 98 exhibits a single fragment ion peak at m/z 57 (- CH_3CN), indicating that the m/z 98 fragment ion is itself metastable.

The proton-bound dimer $(CH_3CN)(t\text{-}C_4H_9OH)H^+$ (**29**) has a unique MI mass spectrum (Figure 32d) that contains three peaks at m/z 60, 98 and 101 (-15 amu). The lack of simple dissociation products indicates that the barriers leading to the water and butene loss channels are significantly lower than the dissociation thresholds for the proton-bound dimer.

Isotopically labelled cluster ions were studied to determine the extent of interchange of the hydrogen atoms in the proton-bound dimers **24 - 27**. The cluster ions formed by the reaction of CD_3CN with n-C_4H_9OH, s-C_4H_9OH, i-C_4H_9OH and t-C_4H_9OH in the ion source exhibit no mixing of the methyl hydrogens on acetonitrile with those of the bridging hydrogens or those on the butyl group. The butanols were not labelled, but from the results of the methanol, ethanol and propanol containing dimer ions, there may be secondary reactions after isomerization of the proton-bound dimer ions resulting in some exchange of hydrogens.

5.6.1 Identity of m/z 98 in the $(CH_3CN)(ROH)H^+$ (R = n-butyl, s-butyl, i-butyl and t-butyl) systems

The He CID mass spectra of the metastably-generated m/z 98 ions are summarized in Table 11, along with the corresponding source-generated ions. Unlike the propyl-containing systems, the mass spectra for source- and metastably-generated ions from corresponding precursors are rarely the same; the only case that an argument can be made for them being the same is for the m/z 98 ions generated from $(CH_3CN)(CH_3CH_2CH(CH_3)OH)H^+$ (Table 11). Each of the metastably-generated m/z 98 ions has, however, a unique CID mass spectrum, indicating that a unique structure is formed from each precursor. The m/z 98 ion generated from $(CH_3CN)(CH_3CH_2CH_2CH_2OH)H^+$ is characterized by an intense peak at m/z 70 which is due to loss of 28. This can only be due to loss of ethane, which may be more likely from a precursor containing the n-butyl moiety, perhaps $CH_3CNCH_2CH_2CH_2CH_3^+$. Also, simple bond dissociation

in such an ion would lead to the unfavorable primary cation, $CH_3CH_2CH_2CH_2^+$,explaining the lack of a prominent m/z 75 in the CID mass spectrum (Table 11). The ion generated from $(CH_3CN)(CH_3CH_2CH(CH_3)OH)H^+$ has a weaker, but significant m/z 70 peak in its CID mass spectrum and is dominated by m/z 56. A possible structure of $CH_3CNCH(CH_3)CH_2CH_3^+$ includes the ethyl group that can lead to ethane loss. The CID mass spectra of the m/z 98 ions generated from $(CH_3CN)((CH_3)_2CHCH_2OH)H^+$ and $(CH_3CN)((CH_3)_3COH)H^+$ are dominated by m/z 57, presumably the t-butyl cation. However, they differ in that the ions generated from $(CH_3CN)((CH_3)_3COH)H^+$ also exhibit significant peaks at m/z 42, 41 and 39. The He CID mass spectra of the $(CH_3CN)(butene)H^+$ ions, generated by the reaction of acetonitrile and the butene isomers 1-butene, trans-2-butene and isobutene are also presented in Table 11 for comparison. The spectra of these three ions are dominated by m/z 57, but are distinguishable based on the intensities of m/z 83, 70 and 42 (Table 11). Based on the results in Table 11, it is possible that the m/z 98 ion generated from metastable $(CH_3CN)((CH_3)_2CHCH_2OH)H^+$ precursor ions has the $(CH_3CN)((CH_3)_2C{=}CH_2)H^+$ structure.

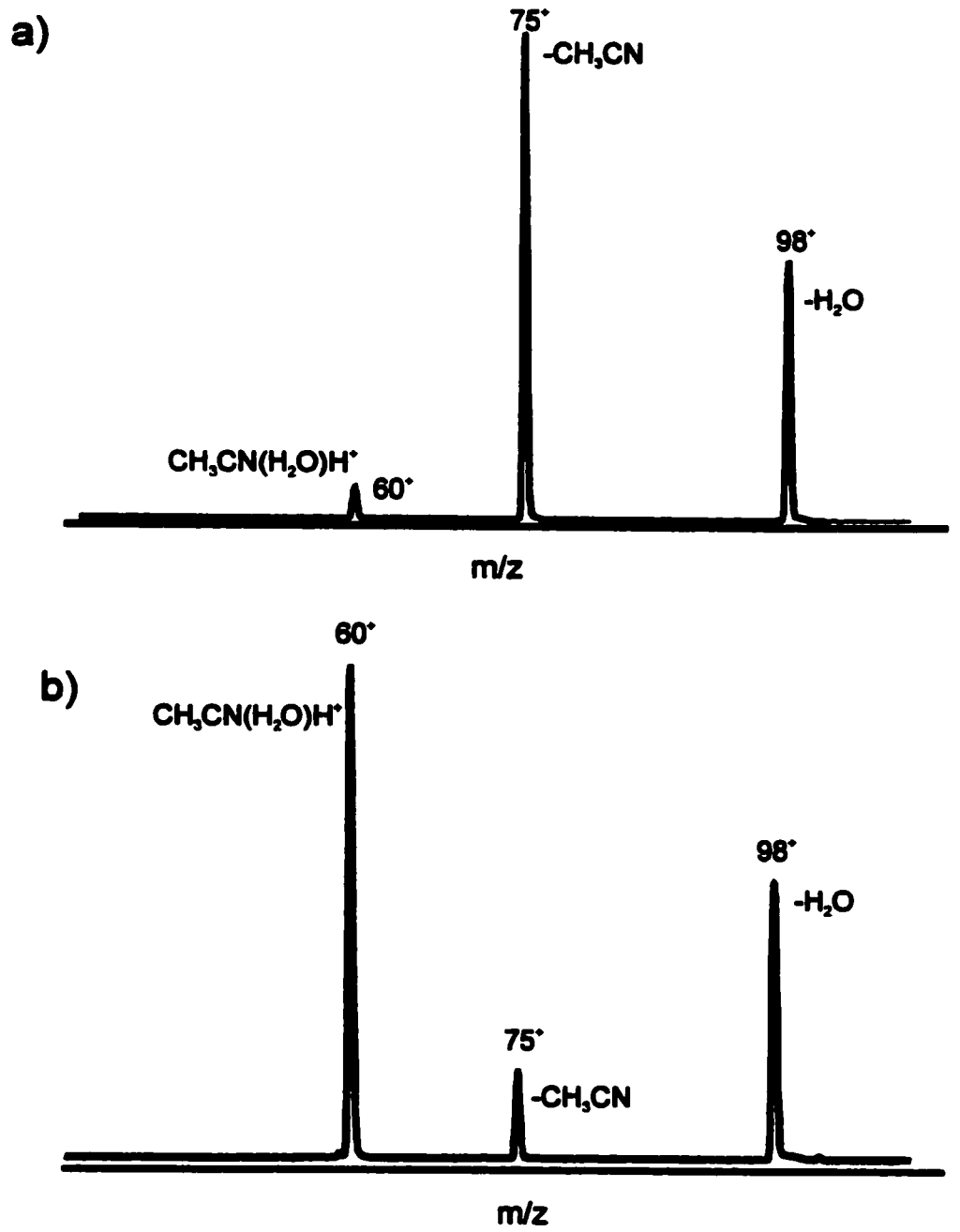

Figure 32: MI mass spectra (a) $(CH_3CN)(n\text{-}C_4H_9OH)H^+$ (b) $(CH_3CN)(s\text{-}C_4H_9OH)H^+$.

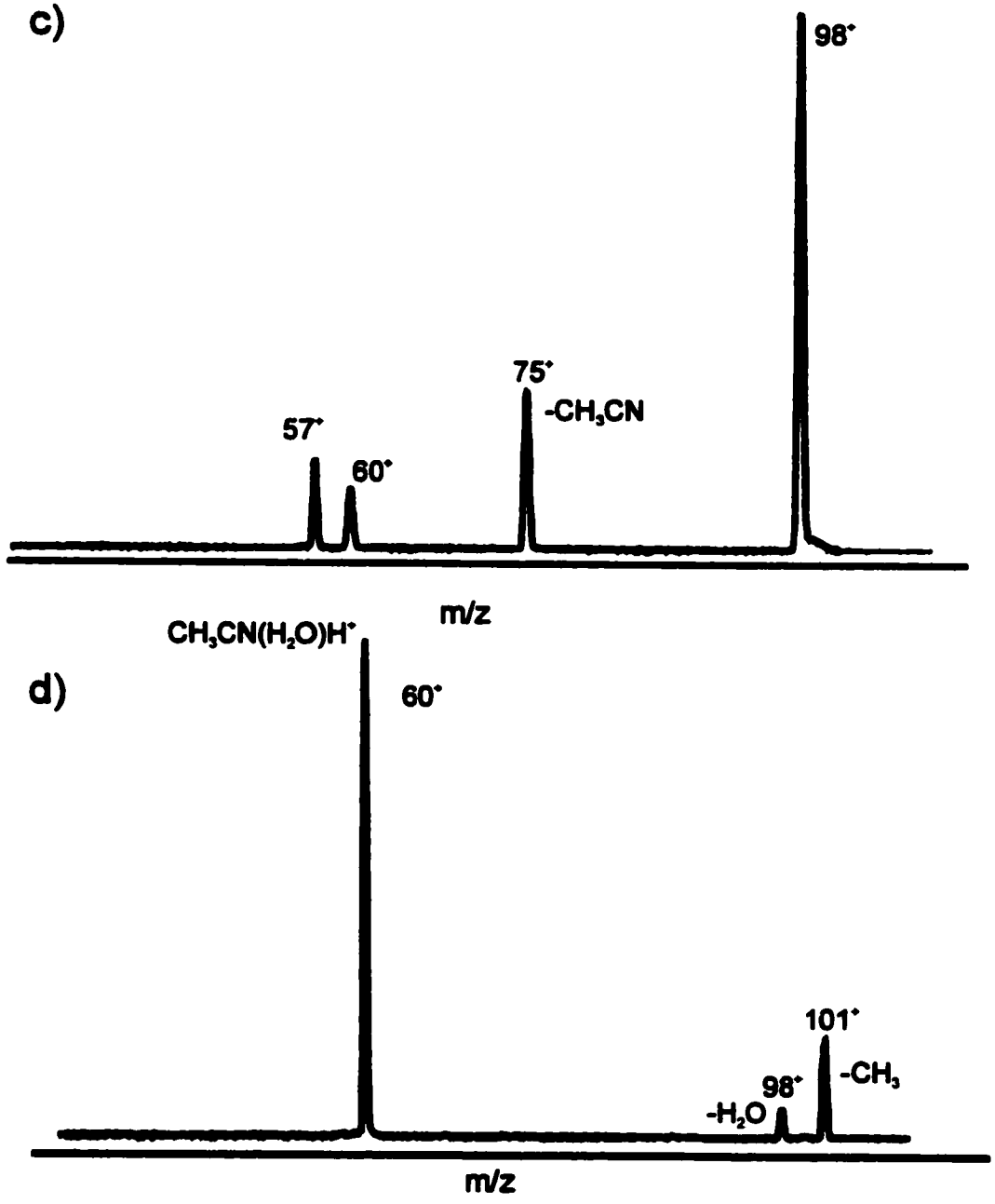

Figure 32. MI mass spectra of (c $(CH_3CN)(i\text{-}C_4H_9OH)H^+$ (d) $(CH_3CN)(t\text{-}C_4H_9OH)H^+$.

Table 10. Relative Peak Intensities in the He CID Mass Spectra of m/z 75 ions.

Precursor	m/z											
	57	56	52	45	43	42	41	39	38	31	29	27
$CH_3CH_2CH_2CH_2OH_2^{+a}$	1.0	0.04	–	–	<0.01	–	0.02	<0.01	–	<0.01	<0.01	0.01
$CH_3CH_2CH(CH_3)OH_2^{+a}$	1.0	0.03	–	0.02	<0.01	–	0.05	0.03	–	<0.01	0.03	0.02
$(CH_3)_2CHCH_2OH_2^{+a}$	1.0	0.01	–	–	<0.01	<0.01	0.02	0.01	–	<0.01	0.01	<0.01
$(CH_3)_3COH_2^{+a}$	1.0	0.03	–	–	–	–	0.06	0.05	–	<0.01	0.03	0.02
$(CH_3CN)(CH_3CH_2CH_2CH_2OH)H^{+b}$	1.0	0.03	–	–	<0.01	0.02	0.08	0.02	–	0.02	0.02	0.02
$(CH_3CN)(CH_3CH_2CH(CH_3)OH)H^{+b}$	1.0	0.06	0.11	0.06	0.06	–	0.07	–	0.08	–	0.06	0.02
$(CH_3CN)((CH_3)_2CHCH_2OH)H^{+b}$	1.0	–	–	–	–	–	–	–	–	–	–	–

[a] m/z 75 generated when only the butyl alcohol was present in the ion source.
[b] Metastably generated m/z 75.

Table 11. Relative Peak Intensities in the He CID Mass Spectra of m/z 98 ions.

Precursor	m/z													
	83	70	69	68	58	57	56	43	42	41	39	29	28	27
$(CH_3CN)(CH_3CH_2CH_2CH_2OH)H^{+a}$	0.01	0.02	0.04	0.02	–	0.45	0.03	–	1.0	0.03	0.01	0.01	<0.01	0.02
$(CH_3CN)(CH_3CH_2CH_2CH_2OH)H^{+b}$	0.02	0.86	0.05	0.1	–	0.2	1.0	–	0.36	0.06	–	–	–	–
$(CH_3CN)(CH_3CH_2CH(CH_3)OH)H^{+a}$	0.13	0.27	0.05	0.02	16	0.2	1.0	0.03	0.08	<0.01	0.04	0.02	0.02	0.02
$(CH_3CN)(CH_3CH_2CH(CH_3)OH)H^{+b}$	0.1	0.13	0.06	0.1	0	0.10	1.0	0.04	0.25	0.16	0.12	0.05	0.03	0.05
$(CH_3CN)((CH_3)_2CHCH_2OH)H^{+a}$	<0.01	–	–	0.04	–	1.0	0.09	–	0.88	0.09	0.05	0.05	–	0.04
$(CH_3CN)((CH_3)_2CHCH_2OH)H^{+b}$	–	–	–	–	–	1.0	–	–	0.09	0.03	0.01	0.01	–	–
$(CH_3CN)((CH_3)_3COH)H^{+a}$	1.0	0.18	0.11	0.04	0.9	0.29	0.61	0.07	0.08	0.35	–	0.06	0.02	0.05
$(CH_3CN)((CH_3)_3COH)H^{+b}$	–	–	–	–	–	1.0	–	–	0.13	0.15	0.12	–	–	–
$(CH_3CN)(CH_3CH_2CH=CH_2)H^{+a}$	0.03	0.03	0.02	–	0	1.0	0.07	0.04	0.14	0.05	0.03	0.03	0.04	0.02
$(CH_3CN)(t\text{-}CH_3CH=CHCH_3)H^{+a}$	0.12	0.12	0.03	<0.01	0	1.0	0.61	<0.01	0.07	0.07	0.03	0.02	0.01	0.02
$(CH_3CN)((CH_3)_2CH=CH_2)H^{+a}$	<0.01	<0.01	–	–	–	1.0	0.05	–	0.04	0.04	0.03	0.01	–	0.01

[a] Source generated m/z 98.

[b] Metastably generated m/z 98.

5.7 Isomerization Mechanism of Nitrile-Alcohol Proton-Bound Dimers

The isomerization from the proton-bound dimers incorporating CH_3CN and the alcohols methanol, [34] ethanol, n-propanol and i-propanol involves an S_N2 type mechanism. The first step in the process consists of the backside attack of CH_3CN on the carbon adjacent to the OH_2 group in the protonated alcohol to form an intermediate complex $(CH_3CN{\bullet\bullet\bullet}ROH_2)^+$ (R = CH_3 **2**, $CH_2(CH_3)$ **5**, $CH_2(CH_2CH_3)$ **17** and $CH(CH_3)_2$ **22**). The second step involves the stretching of the C—O bond in the protonated alcohol moiety and the shortening of the N—C bond, $[CH_3CN—R—OH]^{+\ddagger}$, followed by the formation of the thermodynamically stable isomer(s) $(CH_3CNR)(H_2O)^+$. Equilibrium structures corresponding to intermediate ion-dipole complexes **2, 5, 17** and **22** have been located at the MP2/6-31+G(d) level of theory (Figures 31). Transition structures have been found for the interconversion of the proton-bound dimers **1, 4, 16** and **21** and the complexes **2, 5, 17** and **22**, as well as the transition states for the second step of the isomerization from **2, 5, 17** and **22** to $(CH_3CNCH_3)(H_2O)^+$ **3**, $(CH_3CNCH_2CH_3)(H_2O)^+$ **6, 18** and **23**. A summary of the relative energies for the four isomerization processes are listed in Table12 [19,43,44].

In each of the four dimer systems presented in Table 12, the key transition state governing the isomerization to $(CH_3CNR)(H_2O)^+$ is that which connects this isomer to the intermediate complex $(CH_3CN{\bullet\bullet\bullet}ROH_2)^+$. This transition state involves the shortening of the N—C bond and lengthening of the C—O bond in the complex. In effect, it also sets the bond dissociation threshold for the intermediate complex. Examination of the relative energies in Table 12

(comparing values at the MP2 level of theory for the four systems), the dissociation energy of $(CH_3CN{\bullet\bullet\bullet}ROH_2)^+$ changes from 24 kJ mol^{-1} for the methanol system to 35 kJ mol^{-1} for the ethanol system and then drops back to 30 and 28 kJ mol^{-1} for the two propanol containing ions. So, the C—O bond strength changes significantly, but not dramatically, upon alkyl substitution of the central methyl group in the intermediate complex. The overall relative barrier height (i.e., the relative energy of TS(complex - isomer)) is fairly consistent at the MP2 level of theory: 107, 110, 106 and 97 kJ mol^{-1} going across Table 12. The most notable value is that for the i-propyl containing system. Dimethyl substitution of the central methyl group in the complex results in the lowest transition state energy (by ~ 10 kJ mol^{-1}) of the four species studied here. This also accounts for the predominance of m/z 84 in the MI mass spectrum of $(CH_3CN)((CH_2)_2CHOH)H^+$.

5.8 Conclusion

The proton-bound dimers of acetonitrile with the alcohols methanol, ethanol, – and i- propanol, n-, i- , s- and t- butanol all exhibit a competition between isomerization and dissociation in their MI mass spectra. Mass spectrometry and ab initio theory have been used to elucidate the unimolecular reaction pathways of these systems. The main isomerization channel is an internal S_N2 reaction that involves the formation of an intermediate complex $(CH_3CN{\bullet\bullet\bullet}ROH_2)^+$ prior to the loss of water to form $(CH_3CNR)^+$. Methyl substitution of the carbon atom adjacent to the OH_2 moiety lowers the energy of the intermediate complex and hence, the barrier to isomerization.

Table 12. Comparison of the relative energies of the isomerization process for $(CH_3CN)(ROH)H^+$ (R = CH_3, CH_3CH_2, $CH_3CH_2CH_2$ and $(CH_3)_2CH$).[a]

	R = CH_3[b]		CH_3CH_2[c]		$CH_3CH_2CH_2$	$(CH_3)_2CH$
	G2	MP2/6-31+G(d)	G2(MP2,SVP)	MP2/6-31+G(d)	MP2/6-31+G(d)	MP2/6-31+G(d)
$(CH_3CN)(ROH)H^+$	0	0	0	0	0	0
TS (dimer - complex)	89	87	98	77	77	70
$(CH_3CN\bullet\bullet\bullet ROH_2)^+$	84	83	96	75	76	69
TS (complex - isomer)	103	107	124	110	106	97
$(CH_3CNR)(H_2O)^+$	-21	-22	2	-14	-16	-10
Dimer → products[d]	121	129	152	139	132	127
Isomer → products[e]	19	25	42	31	27	35

[a] Values in kJ mol^{-1} at 0 K.

[b] A portion of this data has been previously published in Reference [19]. The results are similar to MP2/6-311G(d,p) values obtained by Fridgen et al [44].

References

[1] B. F. Yates, W. J. Bouma and L. Radom, Tetrahedron 22 (1986) 6225.

[2] D. Harnish and J. L. Holmes, J. Am. Chem. Soc. 113 (199) 9729.

[3] T. H. Morton, Org. Mass Spectrom. 26 (1991) 18.

[4] N. Heinrich and H. Schwartz, Role of ion-molecule complexes in the reaction of gaseous ions in Ion and Cluster Ions Spectroscopy (Amsterdam, Elsevier, 1989).

[5] G. Schaftener, R. Postma, P. J. A. Ruttnik, P.C. Burgers, G.A. McGibbon and J. K. Terlouw, Int. J. Mass Spectrom. Ion Proc. 100 (1990) 521.

[6] J. L. Holmes C. E. C. A. Hop and J. K. Terlouw, Org. Mass Spectrom. 21 (1986) 776.

[7] J.A. Booze, T. Baer, J. Phys. Chem. 96 (1992) 5715.

[8] P.M. Mayer and T. Baer, J. Phys. Chem. 100 (1996) 5715.

[9] O.A. Mazyar, P.M. Mayer and T. Baer, Int. J. Mass Spectrom. And Ion Processes 167/167 (1997) 389.

[10] J.E. Szulejko and T.B. McMahon, Org. Mass Spectrom. 28 (1993) 1009.

[11] V. Aviyente, M. Iraqi, T. Peres, and C. Liftshitz, J. Am. Soc.. Mass Spectrom. 2 (1991) 113.

[12] H.E. Audier, C. Monteiro, P. Mourgues and D. Robin, Rapid Commun. Mass Spectrom. 3 (1989) 84.

[13] J.L. Beauchamp and M.C. Caserio, J. Am. Chem. Soc. 94 (1972) 2638.

[14] J.L. Beauchamp, M.C. Caserio and T.B. McMahon, J. Am. Chem. Soc. 96 (1974) 6243.

[15] F. Mafune, J. Kohno and T. Kondow, J. Phys. Chem. 100 (1996) 10041.

[16] X. Zang,X. Yang and A.W. Castleman, Chem. Phys. Lett. 185 (1991) 298.

[17] W.Y. Feng, M. Iraqi and C. Liftshitz, J. Phys. Chem. 97 (1993) 3510.

[18] E.Y. Feng and C. Liftshitz, Int. J. Mass Spectrom. Ion Processes 149/150 (1995) 13.

[19] P.M.. Mayer, J. Phys. Chem. A 103 (1999) 3687.

[20] J.L. Holmes, and P.M. Mayer, J. Phys. Chem. 99 (1995) 1366.

[21] K.L. Busch, G.L. Glish and S.A. McLuckey, Mass Spectrometry/Mass Spectrometry, VCH Publishers: New York, 1988.

[22] W.J. Hehre, L. radom, P.v.R. Schleyer, J.A. Pople, Ab initio Molecular Orbital Theory; Wiley: New York, (1986).

[23] M.J. Frisch, G.W. Trucks, H.B. Schegel, P.M.W. Gill, B.G. Johnson, M.A. Robb, J.R. Cheeseman, T. Keith, A. Peterson, A. Montgomery, K. Raghavachari, M.A. Al-Laham, V.G. Zakrweski, J.V. Ortiz, J.B. Foresman, J. Cioslowski, B.B. Stefanov, A. Nanayakkara, M. Challacombe, C.Y. Peng, P.Y. Ayala, W. Chen, M.W. Wong, A.L. Andres, E.S. Replogle, R. Gomperts,R.L. Martin, D.J. Fox, J.S. Blinkley, D.J. Defrees, J. Baker, J.P. Stewart, M. Head-Gordon, C. Gonzalez, J.A. Pople, *GAUSSIAN 94* (Rev. E.1); Gaussian, Inc.: Pittsburgh, (1995).

[24] M.J. Frisch, G.W. Trucks, H.B. Schegel, G.E Scuseria, G.E. Robb, M.A. Robb, J.R. Cheeseman, V.G. Zakrweski, A. Montgomery, R.E. Stratmann, J.C. Burant, S. Dapprich, J.M. Millam, A.D. Daniels, K.N. Kudin, M..C. Strain, O. Farkas, J. Tomasi, V. Barone, M. Cossi, R. Cammi, B. Mennucci, C. Pomelli, C. Adamo, S. Clifford, J. Ochterski, A. Peterson, P.Y. Ayala, Q. Cui, K. Morokuma, D.K. Maliek, A.D. Rabuck, K. Raghavachari, J.V. Ortiz, J.B. Foresman, J. Cioslowski, B.B. Stefanov, A. Nanayakkara, M. Challacombe, C.Y. Peng, P.Y. Ayala, W. Chen, M.W. Wong, M. Head-

Gordon, C. Gonzalez, J.L Andres, E.S. Replogle, J.A. Pople, *GAUSSIAN 98* (Rev. A.7); Gaussian, Inc.: Pittsburgh, (1998).

[25] P.M. Mayer J. Chem. Phys. 110 (1999) 7779.

[26] P.M. Mayer, J. Phys. Chem. A. 103 (1999) 5905.

[27] P.M. Mayer, Chem. Phys. Lett. 314 (1999) 311.

[28] L.A. Curtiss, K. Raghavachari, G.W. Trucks, and J. Pople, J. Chem. Phys. 94 (1991) 7221.

[29] L.A. Curtiss, K. Raghavachari, and J. Pople, J. Chem. Phys. 98 (1993) 1293.

[30] L.A. Curtiss, P.C. Redfern, B.J. Smith, and L. Radom, J. Chem. Phys. 104 (1996) 5148.

[31] L.A. Curtiss, K. Raghavachari, and J. Pople, J. Chem. Phys. 103 (1995) 4192.

[32] A. Nicolaides, A. Ruak, M.N. Glukhovtsev, and L. Radom, J. Phys. Chem. 100 (1996) 17460.

[33] S.G. Lias, J.E. Bartmess, J.F. Liebman, J.L. Holmes, R.D. Levine, and W.G. Mallard, J. Phys. Chem. Ref. Data 17 (1988) (suppl. 1).

[34] A.P. Scott, L. Radom, J. Phys. Chem. 100 (1996) 16502.

[35] E.P. Hunter, and S.G. Lias, J. Phys. Chem. Ref. Data 17 (1988) (Suppl. 1).

[36] J.L. Holmes, C. Aubry, and P.M. Mayer, J. Phys. Chem. A. 103 (1999) 705.

[37] P.C. Burgers, and J.L. Holmes, Int. J. Mass Spectrom. Ion Processes 54 (1984) 15.

[38] K. Raghavachari, J. Chandrasekhar, and R.C. Burnier, J. Am. Chem. Soc. 106 (1984) 3124.

[39] J.C. Sheldon, G.J. Currie, and J.H. Bowie, J. Chem. Soc.. Perkin Trans. 2 (1986) 941.

[40] G. Bouchoux, and N. Choret, Rapid Commun. Mass Spectrom. 11 (1997) 1799.

[41] T. Baer, and W.L. Hase, Unimolecular Reaction Dynamics, Theory and Experiments; Oxford University Press: New York, (1996).

[42] J.L. Holmes, C. Aubry, and P.M. Mayer, J. Phys. Chem. 103 (1999) 705.

[43] R.A. Ochran, A. Annamalai, and P.M. Mayer, J. Phys. Chem. A 104 (2000) 8505.

[44] T.D. Fridgen, J.D. Keller, and T.B. McMahon, J.Phys. Chem. A 105 (2001) 3816.

CHAPTER 6

How Does Chlorine Substitution on Acetonitrile affect the Internal S_N2 Isomerization of Proton-Bound Dimers $(ClCH_2CN)(ROH)H^+$ [R=CH_3, C_2H_5, C_3H_7] ?

6.1 Introduction

In three recent publications [1-3] mass spectrometry and ab initio calculations were employed to investigate the unimolecular decomposition of proton-bound pairs consisting of acetonitrile and the alcohols methanol, ethanol, n-propanol, iso-propanol, n-butanol, s-butanol, iso-butanol and t-butanol. Common to the chemistry of these pairs (on the microsecond timescale) was the competition between simple hydrogen-bound cleavage and dehydration reactions. The latter reaction channel involves an S_N2-type rearrangement with the initial isomerization of $(CH_3CN)(ROH)H^+$ [R = alkyl] to an intermediate $(CH_3CN{\bullet\bullet\bullet}R{\bullet\bullet\bullet}OH_2)^+$ ion (via TSa) followed by the stretching of the C—O bond in this ion to form a thermodynamically stable isomer $(CH_3CNR)(H_2O)^+$ (via TSb) [2-4]:

The competition between dissociation and isomerization is a result of the similar barrier energies for the two processes. One question which arises is how universal such a competition will be

$$(CH_3CN)(ROH)H^+ \xrightarrow{TSa} (CH_3CN{\bullet\bullet\bullet}R{\bullet\bullet\bullet}OH_2)^+ \xrightarrow{TSb} (CH_3CNR)(H_2O)^+$$

when the monomeric units in the pair are modified by functional groups. If a moiety is used that affects the energetics of the simple dissociation products, what will be the effect on the transition state leading to the S_N2 isomerization products? The previous work examined the methyl-

substitution effects on the central carbon in the $(CH_3CN{\bullet\bullet\bullet}R{\bullet\bullet\bullet}OH_2)^+$ ion. Sequential methyl substitution stabilized this ion and TSa, but only dimethyl-substitution lowered the relative energy of the rate limiting TSb [3]. To further examine this aspect of the competition in nitrile-alcohol clusters, we have studied the unimolecular decomposition of proton-bound pairs consisting of chloroacetonitrile and the alcohols methanol, ethanol, n– and i-propanol. Detailed calculations have been included for the $(ClCH_2CN)(CH_3OH)H^+$ system for comparison to the $(CH_3CN)(CH_3OH)H^+$ ion. The proton affinity (PA) of chloroacetonitrile is significantly lower than that of acetonitrile which will affect the relative energies of the possible simple-dissociation products and thus the degree to which it competes with the isomerization reaction. Not as obvious is the effect of chloro-substitution on the transition state leading to the S_N2 isomerization products.

6.2 Experimental Details

The experiments were performed on a modified triple sector VG ZAB-2HF mass spectrometer [5] incorporating a magnetic sector followed by two electrostatic sectors (BEE geometry). Protonated cluster ions were generated in the chemical ionization ion source of the instrument. The pressures in the ion source chamber, read with an ionization gauge located above the ion source diffusion pump, were typically between 10^{-5} and 10^{-4} Torr (the pressure in the ion source itself being approximately two orders of magnitude higher). Cluster ions were not observed when the pressure was below 10^{-5} Torr, and there was no evidence of higher order clusters at any

of the pressures used in these experiments. Metastable ion (MI) and collision-induced dissociation (CID) mass spectra were recorded in the usual manner in both the second and third field-free regions (2FFR and 3FFR respectively) of the instrument [6]. Helium collision gas was used in all CID experiments and was introduced into the collision cells to achieve 10% reduction in the ion flux (i.e., single collision conditions). All chemicals were commercially obtained and used without further purification.

6.3 Computational Details

Standard ab initio molecular orbital calculations [7] were performed using the Gaussian 98 [8] suite of programs. Geometries were optimized, and harmonic vibrational frequencies were calculated at the MP2/6-31+G(d) level of theory. Our previous work has shown that relative energies on these reaction surfaces are adequately described at this level of theory [1-3,9]. Transition states were confirmed by the intrinsic reaction coordinate method in Gaussian 98. Unimolecular reaction rate constants were estimated using the standard RRKM expression [10]:

$$k(E) = \frac{\sigma N^{\ddagger}(E - E_0)}{h\rho(E)} \qquad (1)$$

where $N^{\ddagger}(E-E_0)$ is the transition state sum-of-states above the activation energy E_0 and $\rho(E)$ is the density of states of the reactant ion at an internal energy E. The sums and densities of states

were obtained via the direct count algorithm of Beyer and Swinehart [11]. For isomerization reactions the vibrational frequencies and relative energies of the reactant ions and the transition state structures were obtained from the ab initio calculations (vibrational frequencies were scaled by 0.9434 prior to use [12]). The only unknowns are the vibrational frequencies for the effective transition states for the simple-bond cleavage reactions. Since the RRKM calculations are being used for a qualitative understanding of the relative kinetics on the reaction surface, the transition state vibrational frequencies for simple cleavage reactions were estimated by employing the vibrational frequencies of the reactant ions and scaling the lowest five modes to achieve an entropy of activation, $\Delta S^{\ddagger}(600K)$, of +12 J K^{-1} mol^{-1}. In addition, the vibration due to rotation about the hydrogen bond in the proton-bound pair was removed from both the reactant ion and the approximated transition state and instead was treated as a hindered internal rotation [12].

6.4 Results and discussion

The 2FFR MI mass spectra of each ion, $(ClCH_2CN)(CH_3OH)H^+$, $(ClCH_2CN)(CH_3CH_2OH)H^+$, $(ClCH_2CN)(CH_3CH_2CH_2OH)H^+$ and $(ClCH_2CN)((CH_3)_2CHOH)H^+$ are shown in Figure 33. In each case the isotopically pure ^{35}Cl containing ions were selected.

6.4.1 $(ClCH_2CN)(CH_3OH)H^+$

The chloroacetonitrile-methanol proton-bound ion (Figure 33a) $(ClCH_2CN)(CH_3OH)H^+$ (**30**), *m/z* 108, exhibits two peaks, *m/z* 90 (-18 amu) and *m/z* 33 (-75 amu). The loss of 18 amu is attributed to the loss of water while the other peak is due to the loss of $ClCH_2CN$ to form $CH_3OH_2^+$. The absence of a peak due to protonated chloroacetonitrile (*m/z* 76) is consistent with the relative proton affinities (PA) of methanol (754.3 kJ mol^{-1}) and chloroacetonitrile (745.7 kJ mol^{-1}) [13].

Ab initio calculations were employed to map out the minimum energy reaction pathways for the $(ClCH_2CN)(CH_3OH)H^+$ ion at the MP2/6-31+G(d) level of theory. Optimized structures for equilibrium and transition states are shown in Figure 34 and relative energies are listed in Table 13. The reaction leading to water loss was assumed to proceed via an S_N2-type reaction similar to that observed for the acetonitrile-containing pairs. The first step in the process involves a backside attack of $ClCH_2CN$ on the carbon adjacent to the OH_2 group in the protonated alcohol to form an intermediate complex **31** $(ClCH_2CN\bullet\bullet\bullet CH_3\bullet\bullet\bullet OH_2)^+$ (via **TS(30-31)**, TSa). The second step involves the stretching of the C—O bond in the protonated alcohol and the shortening of the N—C bond (**TS(31-32)**, TSb), followed by the formation of the thermodynamically stable isomer **32** $(ClCH_2CNCH_3)(H_2O)^+$. Ion **32** dissociates to ion **33** plus water. The transition state for the interconversion of the intermediate complex **31** to ion **32**, **TS(31-32)** lies 104 kJ mol^{-1} above **30** and 19 kJ mol^{-1} below the lowest energy simple dissociation products $(CH_3OH_2^+ + ClCH_2CN)$.

Table 13. Calculated relative energies for the proton-bound pair $(ClCH_2CN)(CH_3OH)H^+$, its isomers, transition structures and fragmentation products.

	relative energy[a]
$(ClCH_2CN)(CH_3OH)H^+$ **(30)**	0
$(ClCH_2CN\bullet\bullet\bullet CH_3\bullet\bullet\bullet OH_2)^+$ **(31)**	72
$(ClCH_2CNCH_3)(H_2O)^+$ **(32)**	-6
TS(30-31)	76
TS(31-32)	104
$ClCH_2CNCH_3^+$ **(33)** + H_2O	34
$ClCH_2CNH^+ + CH_3OH$	144
$CH_3OH_2^+ + ClCH_2CN$	123

[a]Values calculated at the MP2/6-31+G(d) level of theory incorporating scaled (by 0.9434) MP2/6-31+G(d) zero-point vibrational energies (in kJ mol^{-1} at 0 K).

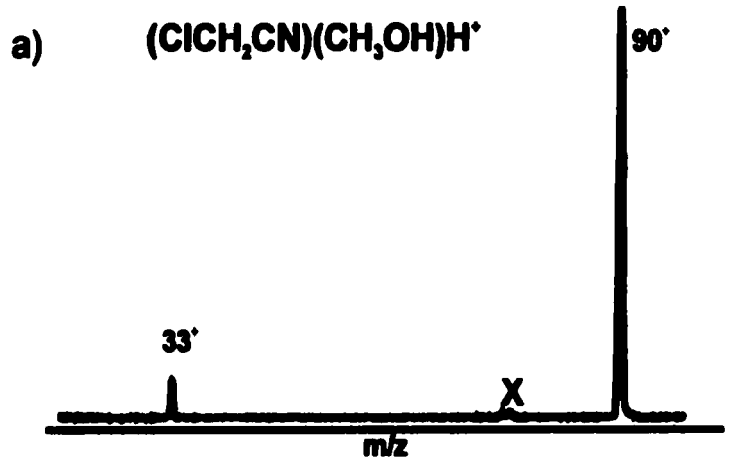

Figure 33: MI mass spectrum in the 2FFR of the VG ZAB-2HF of $(ClCH_2CN)(CH_3OH)H^+$. Artifacts, denoted with an (X), are due to the ^{13}C contribution of a peak in the mass spectrum one unit lower in mass.

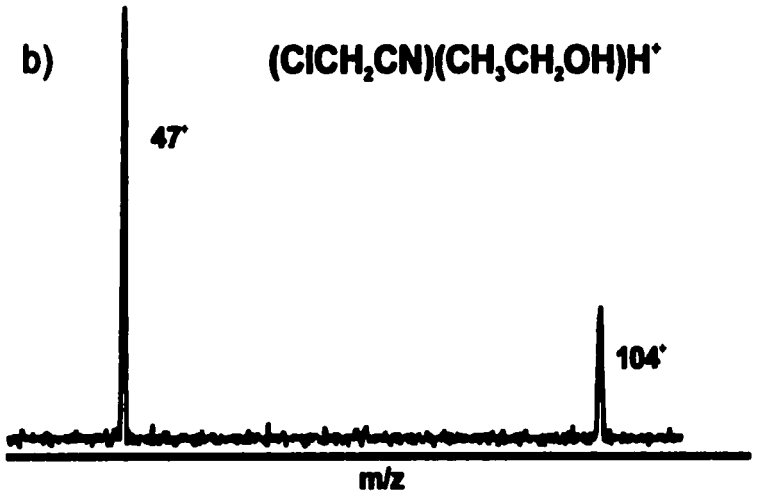

Figure 33: MI mass spectrum in the 2FFR of the VG ZAB-2HF of $(ClCH_2CN)(CH_3CH_2OH)H^+$.

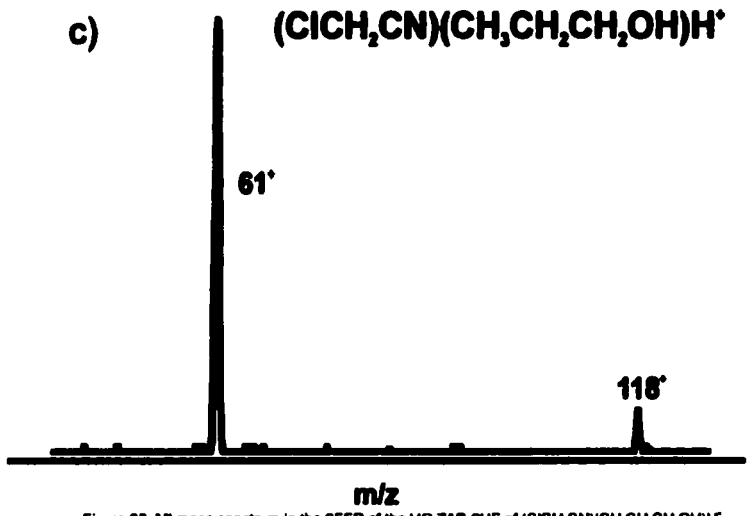

Figure 33: MI mass spectrum in the 2FFR of the VG ZAB-2HF of $(ClCH_2CN)(CH_3CH_2CH_2OH)H^+$.

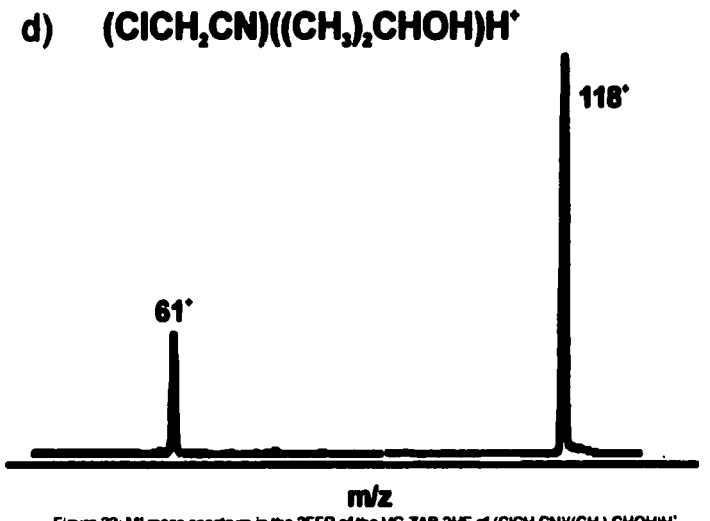

Figure 33: MI mass spectrum in the 2FFR of the VG ZAB-2HF of $(ClCH_2CN)((CH_3)_2CHOH)H^+$.

The reaction pathways for the two proton-bound pairs $(ClCH_2CN)(CH_3OH)H^+$ and $(CH_3CN)(CH_3OH)H^+$ are compared in Figure 35. Chloro-substitution on the acetonitrile has a small stabilizing effect on TSa and the intermediate ion in the S_N2 mechanism but has no effect on the highest energy transition state leading to the water-loss products (TSb). The lowest energy simple-dissociation products become $CH_3OH_2^+ + ClCH_2CN$, which lie 2 kJ mol^{-1} higher than $CH_3CNH^+ + CH_3OH$ (relative to their respective proton-bound pairs). The calculations predict a difference in energy between the two channels (E_0(dissociation) - E_0(isomerization)) of 19 kJ mol^{-1} in the chloro-substituted system compared to 18 kJ mol^{-1} in the non-substituted system. The 1 kJ mol^{-1} difference between these values is insufficient to cause a dramatic shift in the relative abundance of the two reaction pathways (the MI mass spectra exhibit ratios for dissociation to isomerization of 1.0 : 0.5 for $(CH_3CN)(CH_3OH)H^+$ [1] and 0.1 : 1.0 for $(ClCH_2CN)(CH_3OH)H^+$). Chloro-substitution does reduce the relative energy of the initial transition state leading from the proton-bound pair to the intermediate $(ClCH_2CN\bullet\bullet\bullet CH_3\bullet\bullet\bullet OH_2)^+$ ion (TSa) by 13 kJ mol^{-1}. While this step in the isomerization reaction is not rate limiting it may influence the relative abundance of the two product channels.

To examine this possibility, the MP2/6-31+G(d) reaction surface was kinetically modeled with RRKM theory. Four elementary reactions were addressed: the reaction leading from **30** to $CH_3OH_2^+ + ClCH_2CN$ (k_1), the forward isomerization of **30** to **31** (k_2), the reverse isomerization of **31** to **30** (k_3) and the forward isomerization of **31** to **32** (k_4). The individual rate constants are plotted as a function of the internal energy of **30** in Figure 36a. Due to its small density of states the rate constants for the reactions leading out from ion **31** (k_3 and k_4) are similar to each other

and significantly greater than those for reactions from ion **30**. The two potential energy wells on the surface means that products will be formed with a biexponential rate consisting of fast and slow components. The fast component of the rate (having a rate constant k_{fast}) will be due to the immediate dissociation of ion **30** to products via k_1 prior to any isomerization reaction and will only be significant during the early stages of the reaction before the ions arrive in the 2FFR. Only the slow component of the rate (having a rate constant k_{slow}) will be important in the 2FFR of the mass spectrometer. The values of k_{fast} and k_{slow} are plotted in Figure 36b and were calculated following the treatment developed by Baer et al. [14] for a two-well reaction surface. It turns out that k_{fast} and k_{slow} have similar magnitudes in the present system. The equation for k_{slow} in terms of k_1 - k_4 is [14]:

$$k_{slow} = k_1\left(\frac{k_3 + k_4}{k_2}\right) + k_4 \qquad (2)$$

The ratio of water-loss products to simple-dissociation products, Ratio (iso/diss), will be determined by the following equation:

$$Ratio\left(\frac{iso}{diss}\right) = \frac{k_4}{k_1\left(\frac{k_3 + k_4}{k_2}\right)} \qquad (3)$$

This ratio is plotted in Figure 36b. At internal energies below 1.5 eV, the isomerization channel dominates the chemistry of the proton-bound pair. The ratio drops to ~ 0.6 at an internal energy of 3.5 eV. This is at least qualitatively consistent with the MI mass spectrum which reflects the

dissociation of low-internal energy ions on the microsecond timescale. Since there is considerable uncertainty about the internal energy distribution of metastable ions, a quantitative correlation cannot be made. In equation (3) as k_2 decreases so does the ratio between isomerization and simple-bond cleavage. The relative energy of TSa is larger for the $(CH_3CN)(CH_3OH)H^+$ ion than it is for the chloro-substituted ion (Figure 35) and thus a greater fraction of the $(ClCH_2CN)(CH_3OH)H^+$ ions undergo dehydration.

6.4.2 $(ClCH_2CN)(ROH)H^+$ (R = CH_3CH_2, $CH_3CH_2CH_2$, $(CH_3)_2CH$))

The 2FFR MI mass spectrum (Figure 33b) of the chloroacetonitrile-ethanol proton-bound dimer ion $(ClCH_2CN)(CH_3CH_2OH)H^+$ (**34**), *m/z* 122, exhibits the same four basic reaction pathways as its methanol analogue, except that the simple dissociation to protonated ethanol dominates the spectrum. Methyl-substitution does not reduce the relative energy of TSb [3]. Chloro-substitution acts only to lower TSa and thus favors the isomerization reaction. Dominance of the simple-bond dissociation in the MI mass spectrum must therefore be due to the greater PA of ethanol (776.4 vs 754.3 kJ mol^{-1} for methanol [13]) and hence lower dissociation-product energy.

The 2FFR MI mass spectra of the proton-bound pairs $(ClCH_2CN)(CH_3CH_2CH_2OH)H^+$ (**35**) and $(ClCH_2CN)((CH_3)_2CHOH)H^+$ both exhibit peaks at *m/z* 118 ($-H_2O$) and *m/z* 61 ($-ClCH_2CN$), Figures 33c,d. The relative intensities of the two competing channels in the n-propanol

containing proton-bound pair are similar to those for the ethanol-containing analogue. Ethyl-substitution of the central carbon in the $(CH_3CN\bullet\bullet\bullet R\bullet\bullet\bullet OH_2)^+$ion does not reduce the relative energy of TSb [3] and again the dominance of simple-bond dissociation products in Figure 2c is due to the PA of the alcohol (PA of n-propanol is 786.5 vs 754.3 kJ mol^{-1} for methanol [13]). Dimethyl-substitution (i-propanol) does reduce the energy of TSb [3], and this effect is also apparent in the chloro-substituted system (Figure 33d).

6.5 Conclusion

Proton-bound pairs of chloroacetonitrile and alcohols exhibit a competition on the microsecond timescale between simple-bond cleavage and isomerization leading to dehydration. The effect of chloro-substitution on acetonitrile does not significantly affect the height of the highest isomerization barrier governing the dehydration reaction. In the case of $(CH_3CN)(CH_3OH)H^+$ the barrier lies approximately 18 kJ mol^{-1} below the lowest dissociation threshold (CH_3CNH^+ + CH_3OH) while it is 19 kJ mol^{-1} lower for $(ClCH_2CN)(CH_3OH)H^+$. Chloro-substitution does reduce the proton affinity of acetonitrile resulting in the lowest energy simple-bond cleavage reaction products to be ROH_2^+ + $ClCH_2CN$ in all cases. Kinetic modeling of the unimolecular reactions with RRKM theory showed that a key step in governing the ratio of the two types of reactions observed in the MI mass spectra is the initial rearrangement of the proton-bound pairs to the high energy intermediate structure $(CH_3CN\bullet\bullet\bullet R\bullet\bullet\bullet OH_2)^+$, even though it is not the rate limiting step for the overall isomerization reaction leading to dehydration.

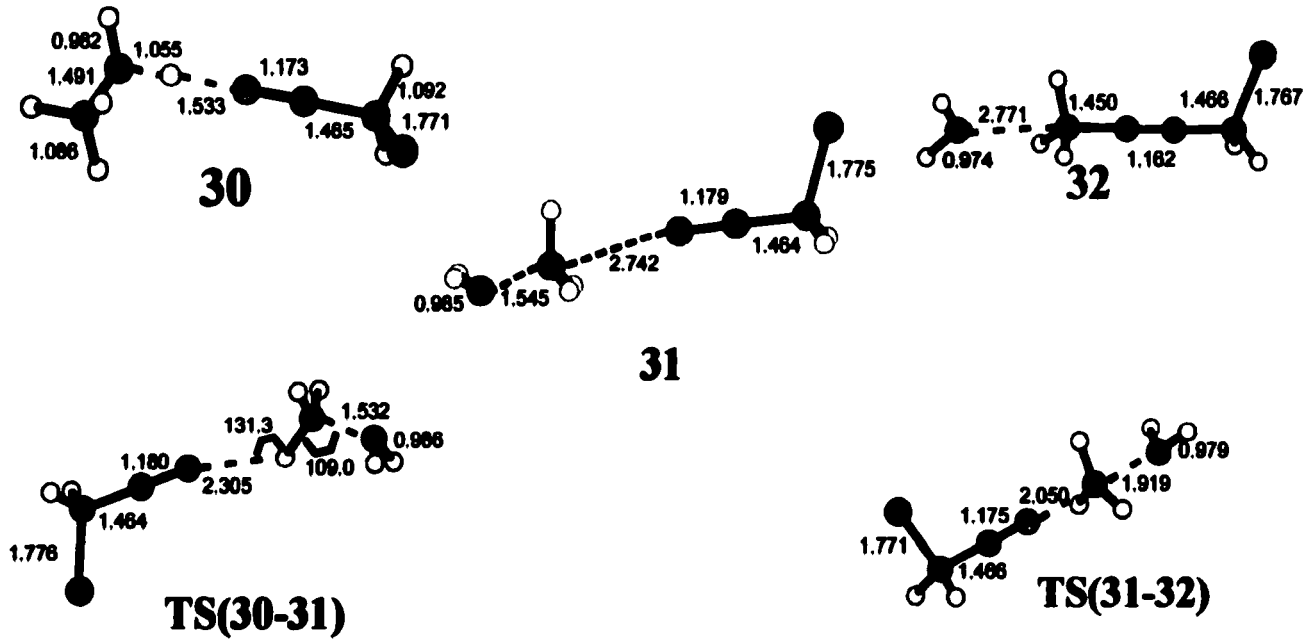

Figure 34: Selected geometric parameters for the proton-bound dimer ($ClCH_2CN)(CH_3OH)H^+$ (30), its isomers (31,32) and transition state structures TS(30-31) and TS(31-32). All geometries were fully optimized at the MP2/6-31+G(d) level of theory. Bond lengths are in angstroms, bond angles in degrees.

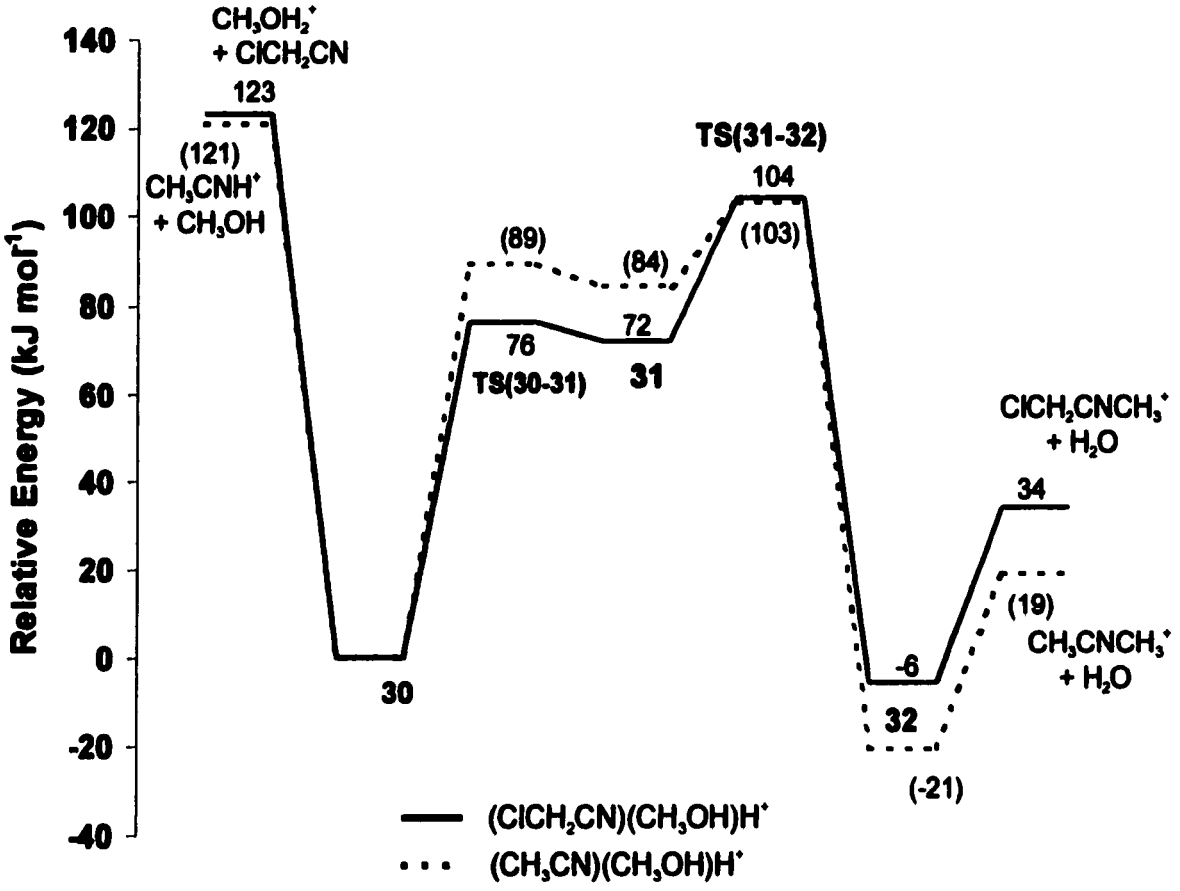

Figure 35: Comparison of the minimum energy reaction pathways of the proton-bound pairs $(ClCH_2CN)(CH_3OH)H^+$ (solid line), $(CH_3CN)(CH_3OH)H^+$ (dashed line). All values are in kJ mol^{-1}

a)

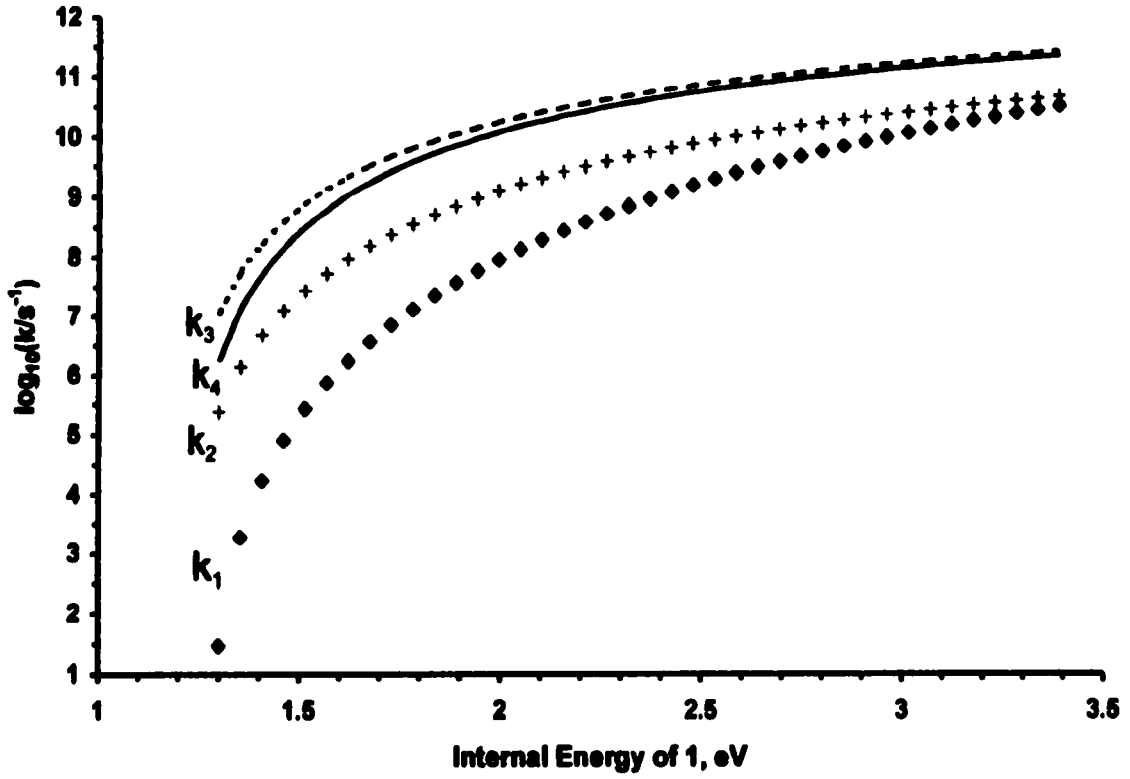

Figure 36: Plot of log (k) vs E curves for the four principle unimolecular reactions on the $(ClCH_2CN)(CH_3OH)H^+$ surface k_1 (◆), k_2 (✚), k_3 (- - -) and k_4 (—)

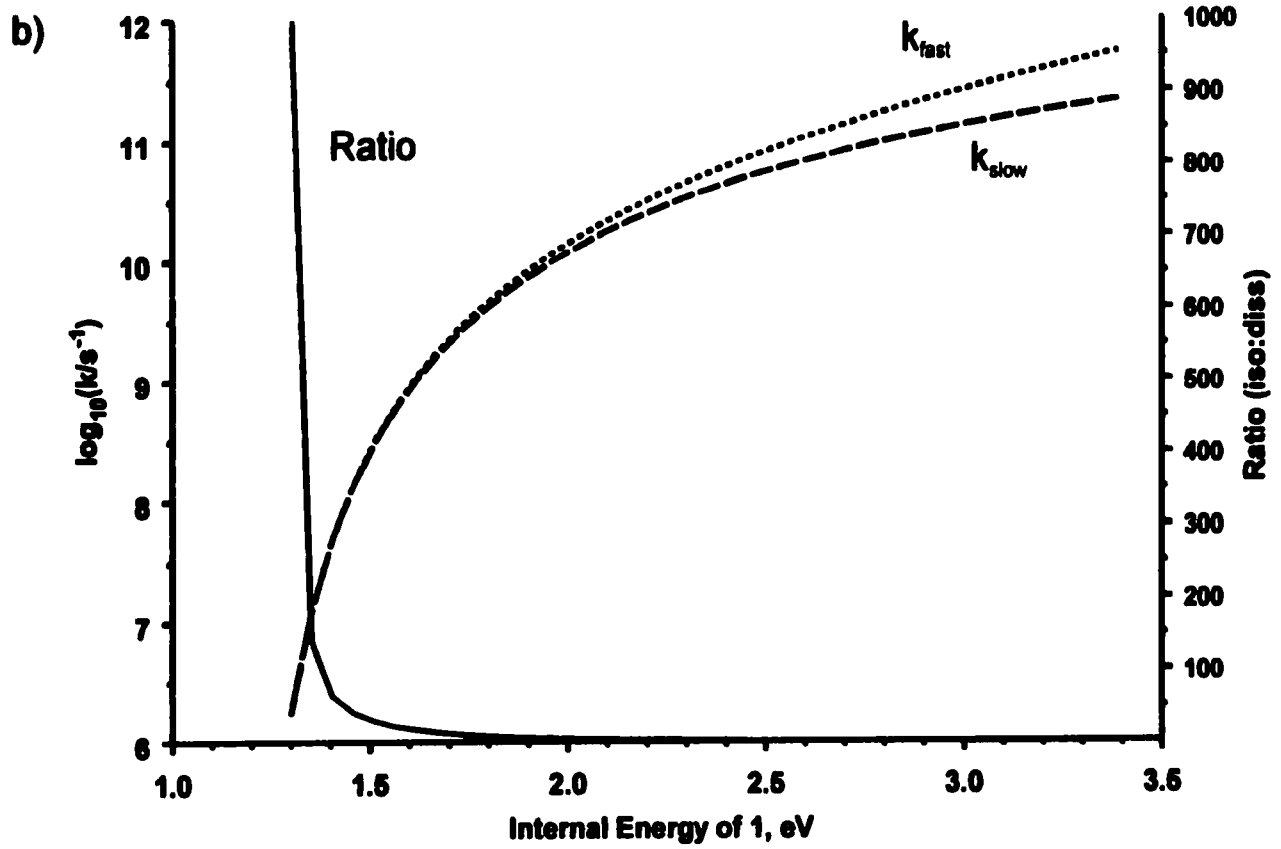

Figure 36: Plot of log (k) vs E for k_{fast} (— —) and k_{slow} (- - -) and the ratio of dehydration to simple-bond dissociation (—).

References

[1] P. M. Mayer, J. Phys. Chem. A 103 (1999) 3687.

[2] R. A. Ochran, A. Annamalai, and P. M. Mayer, J. Phys. Chem. A 104 (2000) 8505.

[3] R. A. Ochran, and P. M. Mayer, European Mass Spectrom. 7 (2001) 267.

[4] T. D. Fridgen, J. D. Keller, and T. B. McMahon, J. Phys. Chem. A (2001) 3816.

[5] J. L. Holmes, and P. M. Mayer, J. Phys. Chem. 99 (1995) 1366.

[6] K. L. Busch, G. L. Glish, and S. A. McLuckey, Mass Spectrometry/Mass Spectrometry Editor, ed. (New York, VCH Publishers, 1988).

[7] W. J. Hehre, L. Radom, P. v. R. Schleyer, and J. A. Pople, Ab Initio Molecular Orbital Theory Editor, ed. (New York, Wiley, 1986).

[8] M. J. Frisch, G. W. Trucks, H. B. Schlegel, G. E. Scuseria, M. A. Robb, J. R. Cheeseman, V. G. Zakrzewski, J. A. Montgomery, R. E. Stratmann, J. C. Burant, S. Dapprich, J. M. Millam, A. D. Daniels, K. N. Kudin, M. C. Strain, O. Farkas, J. Tomasi, V. Barone, M. Cossi, R. Cammi, B. Mennucci, C. Pomelli, C. Adamo, S. Clifford, J. Ochterski, G. A. Petersson, P. Y. Ayala, Q. Cui, K. Morokuma, D. K. Malick, A. D. Rabuck, K. Raghavachari, J. B. Foresman, J. Cioslowski, J. V. Ortiz, B. B. Stefanov, G. Liu, A. Liashenko, P. Piskorz, I. Komaromi, R. Gomperts, R. L. Martin, D. J. Fox, T. Keith, M. A. Al-Laham, C. Y. Peng, A. Nanayakkara, C. Gonzalez, M. Challacombe, P. M. W. Gill, B. Johnson, W. Chen, M. W. Wong, J. L. Andres, C. Gonzalez, M. Head-Gordon, E. S. Replogle, J. A. Pople *GAUSSIAN 98 Rev. A.7*; Gaussian Inc.: Pittsburgh PA, 1998.

[9] P. M. Mayer, Chem. Phys. Lett. 314 (1999) 311.

[10] T. Baer, and W. L. Hase Unimolecular Reaction Dynamics, Theory and Experiments

Oxford University Press, New York, 1996.

[11] T. Beyer, and D.R. Swinehart, ACM Commun. 16 (73) 379.

[12] A.P. Scott, and L. Radom, J. Phys. Chem. 100 (1996) 16502.

[13] E.P. Hunter, and S.G. Lias, "Proton Affinity Evaluation" NIST Chemistry WebBook, NIST Standard Reference Database Number 69, Eds. P.J. Linstrom and W.G. Mallard, July 2001, National Institute of Standards and Technology, Gaithersburg MD, 20899 (http://webbook.nist.gov).

[14] T. Baer, W. A. Brand, T. L. Bunn , and J. J. Butler, Faraday Discuss. Chem . Soc. 75 (1983) 45.

CHAPTER 7

Does Oxygen Catalyze the Formation of Distonic Ions in $(CH_3CN)(O_2)^{+\bullet}$?

7.1 Introduction

The ionic composition of the troposphere and stratosphere is determined by trace quantities of neutral compounds such as acetonitrile and methanol. There have been several speculations regarding the origin of these molecules [1]. An active chemical ionization mass spectrometry (ACIMS) method has been developed for atmospheric trace gas measurements employing balloon-borne and aircraft-borne instruments [2]. Trace abundances of acetonitrile and acetone have been quite conclusively determined. However, while ions at mass-to-charge ratios m/z = 33 + n18 have been observed, their conclusive identification as protonated methanol and its hydrates has been problematic [2].

Measured ion profiles in the ionosphere exhibit a clear chemical boundary between 82 and 85 km. The nature of this boundary is such that the region above 85 km (the E-region) is dominated by the ions O_2^+, NO^+, and M^+ (where M^+ is either Na^+, Mg^+, Al^+, or Fe^+), whereas below 82 km (the D-region), the dominant ions are of the form $H^+(H_2O)_n$, with n=1-8 being the most abundant [3]. This study focuses on a combined experimental and theoretical investigation of the dissociation and isomerization pathways of $(CH_3CN)(O_2)^{+\bullet}$ ions and identifies the effect of oxygen on the isomerization of $CH_3CN^{+\bullet}$ in the $(CH_3CN)(O_2)^+$ dimer ion.

7.2 Experimental Procedures

The experiments were performed on a modified triple sector VG ZAB-2HF mass spectrometer [4] incorporating a magnetic sector followed by two electrostatic sectors (BEE geometry). Cluster ions were generated in the chemical ionization ion source of the instrument by co-introduction of O_2 and CH_3CN. The pressures in the ion source chamber, read with an ionization gauge located above the ion source diffusion pump, were typically between 10^{-5} and 10^{-4} Torr (the pressure in the ion source itself being approximately two orders of magnitude higher). Cluster ions were not observed when the pressure was below 10^{-5} Torr, and there was no evidence of higher order clusters at any of the pressures used in these experiments. For mass analysed ion kinetic energy (MI) spectra, the magnetic field was set to select the ions of desired m/z value under investigation, ionic products of their decomposition were recorded in the second and third field-free regions (2FFR and 3FFR respectively) of the instrument [5]. Helium collision gas was used in all CID experiments and was introduced into the collision cells to achieve 10% reduction in the ion flux (i.e., single collision conditions). All chemicals were commercially obtained and used without further purification. Isotopically labelled compounds (CDN Isotopes Ltd) were of 99% purity.

7.3 Computational Procedures

Standard ab initio molecular orbital calculations [6] were performed using the GAUSSIAN 98

[7] suites of programs. Geometries were optimized at both the HF/6-31G(d) and B3-LYP/6-31+G(d) levels of theory.

7.4. Results and Discussion

7.4.1 Ions Formed in the Ion Source

The main signals observed in the mass spectrum when CH_3CN and O_2 are added are m/z 32 ($O_2^{+\bullet}$), m/z 41 ($C_2H_3N^{+\bullet}$) and m/z 73 $(C_2H_3N)(O_2)^{+\bullet}$. While the identity of the m/z 32 ions is easily deduced, a question which arises is the nature of the m/z 41 ions. Ions having the composition $C_2H_3N^{+\bullet}$ can either be ionized acetonitrile, $CH_3CN^{+\bullet}$, or the distonic ion $^{\bullet}CH_2CNH^{+}$. Calculations place the distonic 195 kJ mol^{-1} lower in energy than $CH_3CN^{+\bullet}$ at the B3-LYP/6-31+G(d) level of theory and 227 kJ mol^{-1} lower at the MP2/6-31+G(d) level of theory. The conversion of ionized $CH_3CN^{+\bullet}$ to $^{\bullet}CH_2CNH^{+}$ requires a 1,3-Hydrogen shift, which normally is a very high energy process [8]. Our calculations place the transition state at 108 kJ mol^{-1} (B3-LYP/6-31+G(d)) and 130 kJ mol^{-1} (MP2/6-31+G(d)) above $CH_3CN^{+\bullet}$. RRKM calculations predict that the forward isomerization of $CH_3CN^{+\bullet}$ to $^{\bullet}CH_2CNH^{+}$ is approximately 1000 times faster than the reverse reaction and the rate constant is greater than $10^{8} s^{-1}$, just 1 kJ mol^{-1} above threshold. So any high internal energy $CH_3CN^{+\bullet}$ ions will spontaneously isomerize to $^{\bullet}CH_2CNH^{+}$.

It has been shown that a second molecule can assist the proton transfer [9] if the proton affinity of the "catalyst' lies in between the PA's of the two ends of the radical (in this case, $^{\bullet}CH_2CN$).

The PA of the carbon atom with the singly occupied p-orbital in $^{\bullet}CH_2CN$ is 524 kJ mol^{-1} (determined from the $\Delta_f H$ values for $CH_3CN^{+\bullet}$, and $^{\bullet}CH_2CN$ and H) while that of the nitrogen is 763 kJ mol^{-1} [10]. The PA of O_2 is 421 kJ mol^{-1} [11] , which lies outside these two values, and so nominally O_2 should not assist the 1-3 shift. To test this, the CID mass spectra of source generated m/z 41 ions were obtained under a variety of experimental conditions and compared to literature data for the $CH_3CN^{+\bullet}$ and $^{\bullet}CH_2CNH^{+}$ ions (Table 14). All the spectra show three distinct groups of fragments; 40-38, 28-25, and 15-12. The key distinguishing factor in the CID mass spectra for $CH_3CN^{+\bullet}$ and $^{\bullet}CH_2CNH^{+}$ is the m/z 15 : m/z 14 ratio which have values 1:4 [12] and 1:3 [8] for CH_3CN^{+} and 1:7 [12], 1:7 [8] and 1:20 [13] for CH_2CNH^{+}. Experiments performed with only acetonitrile in the ion source at low, medium and high pressures were compared to the literature values (Table 14). The ratio for m/z 15 : m/z 14 were approximately 1:2 indicating that only the $CH_3CN^{+\bullet}$ structure is present in the ion source under these conditions.

When low, medium and high oxygen pressures are also present in the ion source (CH_3CN pressure = 1 x 10^{-5} Torr), the ratio of the intensities for m/z 15 : m/z 14 were 1:2 for low oxygen pressure, 1:2 for medium oxygen pressure and 1:8 for high oxygen pressure, this result is consistent with a distonic ion structure. The CID mass spectrum of metastably generated m/z 41 ions is listed in Table 14. The mass spectrum is consistent with that of the distonic isomer $^{\bullet}CH_2CNH^{+}$ isomer. Based on these experimental results, it is very likely that oxygen is promoting the isomerization of $CH_3CN^{+\bullet}$ to its distonic isomer $CH_2CNH^{+\bullet}$. The implications of this will be discussed below.

Table 14: CID spectra of m/z 41.

Precursor	m/z											Structure
	40	39	38	28	27	26	25	15	14	13	12	
CH_3CN [11]	100	25	14	63	35	32	10	22	80	25	10	$CH_3CN^{+\bullet}$
Butyronitrile[11]	100	26	9	57	39	27	12	12	85	23	15	$^{\bullet}CH_2CNH^{+}$
CH_3CN [8]	100	32	20	55	36	36	17	23	68	32	29	$CH_3CN^{+\bullet}$
Butyronitrile[8]	100	23	14	51	33	27	18	11	74	29	23	$^{\bullet}CH_2CNH^{+}$
Butanonitrile [12]	Not given							5	100	24	14	$^{\bullet}CH_2CNH^{+}$
CH_3CN only in source												
Low Pres. (10^{-7}) Torr	100	27	23	24	19	19	11	5	11	5	4	$CH_3CN^{+\bullet}$
Medium Pres.(10^{-5}) Torr	100	27	17	25	15	15	7	6	11	5	4	$CH_3CN^{+\bullet}$
High Pres.(10^{-4}) Torr	100	22	18	25	15	16	9	5	11	5	5	$CH_3CN^{+\bullet}$
CH_3CN/ O_2 in source												
Low Pres.(10^{-7}) Torr	100	32	30	37	26	32	17	13	24	7	5	$CH_3CN^{+\bullet}$
Medium Pres.(10^{-5}) Torr	100	46	34	40	32	32	17	9	21	6	5	$CH_3CN^{+\bullet}$/ $^{\bullet}CH_2CNH^{+}$
High Pres.(10^{-4}) Torr	100	28	21	35	26	17	11	3	24	9	5	$^{\bullet}CH_2CNH^{+}$
Metastably generated 41*	100	42	27	14	5	6	5	1	5	1	1	$^{\bullet}CH_2CNH^{+}$

* metastably generated ion from the unimolecular dissociation of $(CH_3CN)(O_2)^{+\bullet}$ m/z 73

Metastable $(C_2H_3N)(O_2)^{+\bullet}$ The 2FFR MI mass spectrum (Figure 37a) of the acetonitrile-oxygen dimer ion $(C_2H_3N)(O_2)^{+\bullet}$ (37), m/z 73, exhibits three peaks, m/z 56 (-17 amu), m/z 41 ($C_2H_3N^+$), and m/z 32 ($O_2^{+\bullet}$) having relative intensities of 0.58 : 1.0 : 0.76. The loss of 17 amu is attributed to loss of OH to form $(C_2H_2NO)^+$, loss of oxygen (to form $C_2H_3N^+$) and loss of acetonitrile (to form $O_2^{+\bullet}$). The MI mass spectrum of isotopically labelled dimer ion is similar (Figure 38). The m/z 41 ion is a dish-shaped peak indicating a large kinetic energy release in the dissociation, which implies that the dissociation occurs over a barrier. The kinetic energy release (KER) values for the processes (reported from the full width at half-height of the three peaks, $T_{0.5}$) are 2 meV (m/z 32), 132 meV (m/z 56) and 543 meV (m/z 41). The first value is consistent with a simple bond dissociation reaction occurring at threshold, while the latter is consistent with the formation of m/z 41 with a large reverse energy barrier. The CID mass spectrum of the dimer ion (Figure 37b) shows a significant increase in the intensity of m/z 32, the superposition of a gaussian peak atop the dish-shaped signal m/z 41 and a reduction in the intensity of m/z 56. This is consistent with the first channel involving a simple dissociation reaction and the formation of m/z 41 involving a rearrangement of the initially formed dimer ion. Each of the fragment ions in Figure 37a was transmitted to the 3FFR for identification.

The CID mass spectrum of the metastably generated m/z 56 formed by loss of OH ($C_2H_2NO^{+\bullet}$), exhibits three peaks at m/z 55(-H), m/z 30 (NO^+) and m/z 26 ($CN^{+\bullet}$ or $C_2H_2^{+\bullet}$) and having relative intensities of 0.09:1.0:0.11 (Figure 39a). The CID mass spectrum of metastably generated m/z 58 from $(CD_3CN)(O_2)^{+\bullet}$ also exhibited three peaks (Figure 39b) at m/z 56 (-D), m/z 30 ($NO^{+\bullet}$) and m/z 28 thus confirming the latter ion to be $C_2D_2^{+\bullet}$. These results are consistent with a

CH_2CNO^+ or $CHCHNO^+$ structure for this ion.

Table 15 shows the relative abundances of m/z 56, m/z 41 and m/z 32 ions at medium and high pressure conditions in the ion source on different days. At 10^{-5} Torr source pressure, the 56 : 41 : 32 ratio is consistent at approximately 30 : 100 : 40, while at 10^{-4} Torr source pressure the ratio changes to ca 80 : 100 : 55, except for trial 3 in which the ratio is 85 : 100 : 26. These results are indicative of a mixture of ion structures being formed in the source in different amounts depending on pressure. In particular, m/z 56 is affected by pressure the most, and so we propose that m/z 32 and 41 arise from the dissociation of one structure, while m/z 56 arises from the dissociation of a second structure. To learn more about these potential isomers, we probed the surface with DFT calculations.

7.5 Computational Details.

7.5.1 $(C_2H_3N)(O_2)^{+\bullet}$ Isomers

The first possible ion structure formed in the source is an electrostatically bound pair. When O_2 (triplet ground state) encounters a $CH_3CN^{+\bullet}$ or $^{\bullet}CH_2CNH^+$ ion, the resulting complex $(C_2H_3N)(O_2)^{+\bullet}$ can take on either a doublet or quartet character. When a neutral CH_3CN molecule encounters the doublet $O_2^{+\bullet}$ ion, a doublet complex will be formed. For this reason we have calculated the relative energies for some doublet and quartet complexes (Table 16a, Figure 40). The dissociation energies of these complexes were also calculated (Table 16a). It must be noted however, that the B3-LYP/6-31+G(d) level of theory does not perform well for these

simple dissociation products. For example, the NIST value for the IE of O_2 is 12.02 eV [11], while that obtained at the B3-LYP level of theory is 12.75 eV. This discrepancy has been observed previously by Curtiss et. al [14]. In addition, IE for CH_3CN is calculated to be 11.83 eV while the NIST value is 12.20 eV [11]. The relative energy of singlet oxygen is also poorly represented because the molecular orbital configuration from GAUSSIAN 98 is for the b $^1\sum_g^+$ state (157 kJ mol^{-1} [15] and 162 kJ mol^{-1} calculated, above the triplet ground state) and not the lower a $^1\Delta g$ state (94 kJ mol^{-1} above $^3O_2$). Therefore, the calculated product energies have been adjusted by these experimental values and are listed in Table 16 in parenthesis. They result in the reversing of the dissociation products $CH_3CN^{+\bullet}$ + $^2O_2^{+\bullet}$ and $CH_3CN^{+\bullet}$ + $^3O_2$, consistent with the experimental IE's.

The initial formation of **38/40**, can be ruled out for two reasons. The large KER for distonic ion formation requires a barrier in the dissociation which would be absent for a $(CH_2CNH)(O_2)^{+\bullet}$ structure. The dissociation energy of **38/40** is only 12 kJ mol^{-1} and it is doubtful that a significant amount of this ion would be formed under the experimental conditions. The fact that $O_2^{+\bullet}$ formation, a process that lies at least 214 kJ mol^{-1} higher in energy (Table 16a), is competitive means that **38/40** cannot be the main component of the flux out of the source. It is undoubtedly involved on the reaction surface, however, as the process forming CH_2CNH^+ likely involves this ion. As for the complex ion between CH_3CN and O_2, the calculations on the doublet surface reveal only one stable isomer, **37** in which O_2 is bound to the nitrogen in CH_3CN (Figure 40).

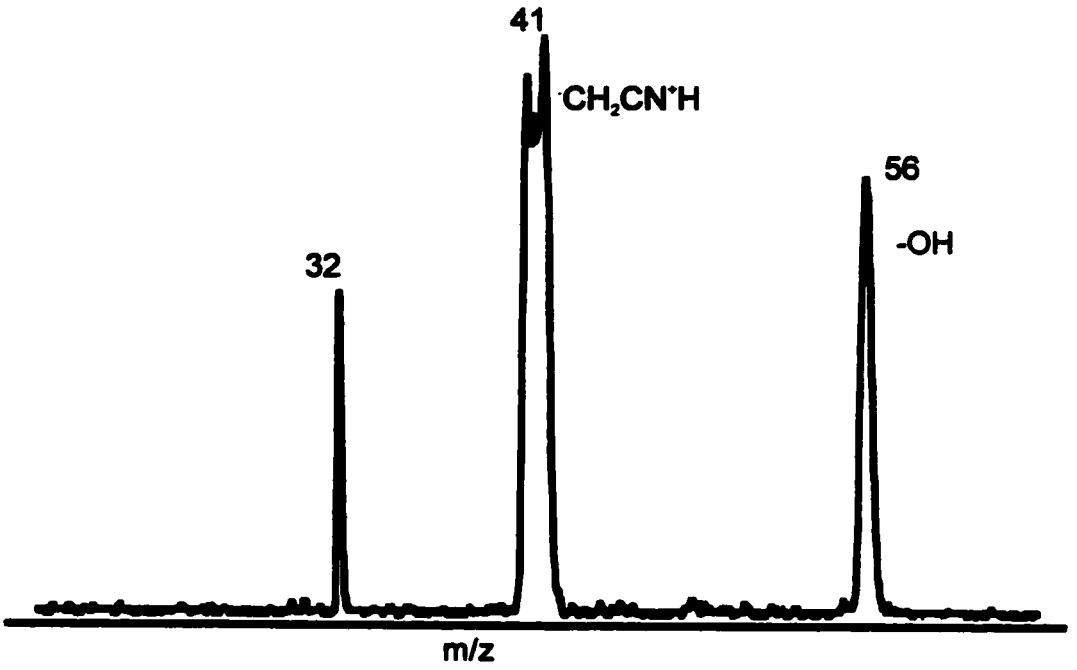

Figure 37a :2FFR MI mass spectrum of $(CH_3CN)(O_2)^{+\cdot}$

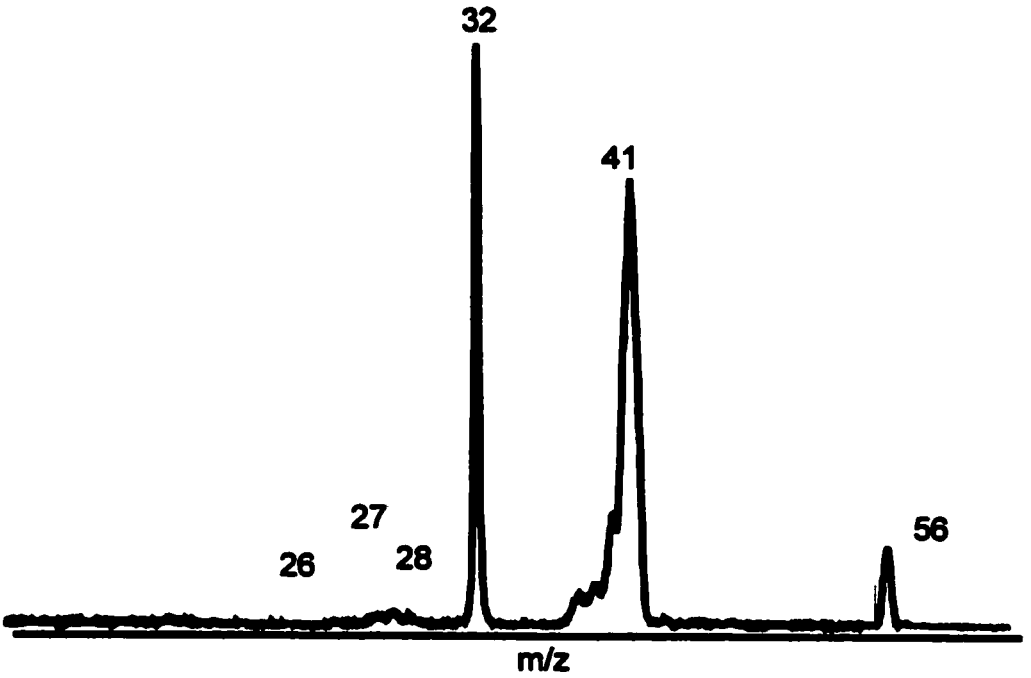

Figure 37b : 2FFR CID mass spectrum of $(CH_3CN)(O_2)^{+\cdot}$

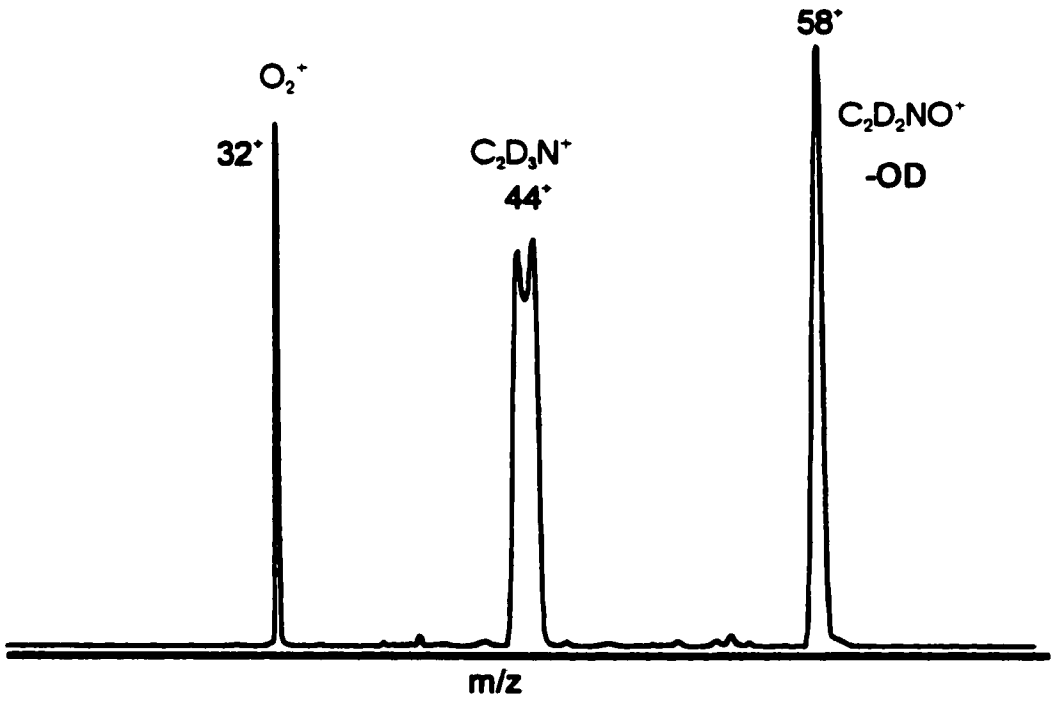

Figure 38: 2FFR MI mass spectrum of $(CD_3CN)(O_2)^{+\cdot}$

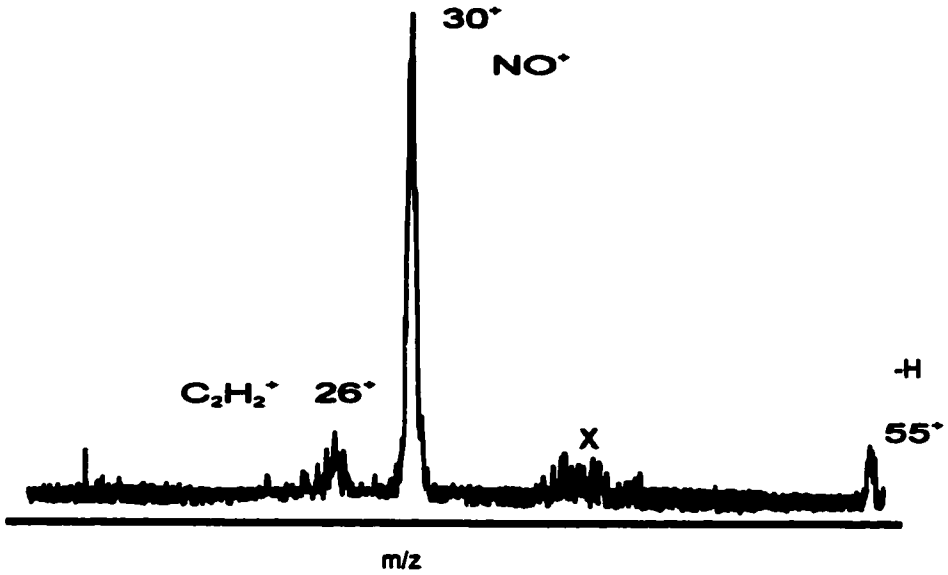

Figure 39a: 3FFR CID of metastably generated m/z 56

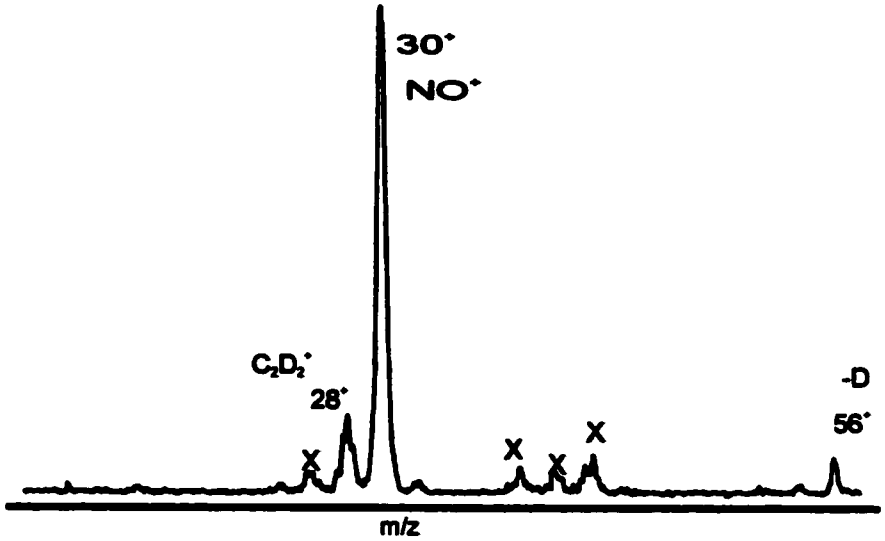

Figure 39b: 3FFR CID of metastably generated m/z 58

Artifacts are denoted with an (X)

Placing O_2 on the methyl end results in a dissociating structure. On the quartet surface exactly the reverse is found. The quartet $^4[O_2 \bullet\bullet\bullet CH_3CN]^{+\bullet}$ ion cannot be a major component of the ion flux due to its low dissociation energy (27 kJ mol^{-1}) and so we are left with the major complex ion being $^2[O_2 \bullet\bullet\bullet CH_3CN]^{+\bullet}$. Distonic ion formation must involve the 1,3-H shift in the complex. No transition state could be located on the B3-LYP surface that involved O_2 mediating the hydrogen motion. This may be a deficiency of the DFT, method and further work should examine the surface with other methods. It should be noted however, that for odd electron systems, UMP2 is particularly poor [16]. To get an idea of the relative rates for dissociation of ion **37** to $O_2^{+\bullet} + CH_3CN$ and $CH_3CN^{+\bullet} + {}^3O_2$ and isomerization to form CH_2CNH^+, we performed RRKM calculations assuming the same 1,3-H shift barrier as was found for $CH_3CN^{+\bullet} \rightarrow {}^{\bullet}CH_2CNH^+$ isomerization (108 kJ mol^{-1}). The results are presented in Figure 41. From the figure it is apparent that the rate constants for isomerization, k_3, increases very rapidly with internal energy. The relative values of the two lowest energy process, k_1 and k_3 indicate that, $O_2^{+\bullet}$ formation should not be observed as competing in the MI mass spectrum. The two thresholds would have to be virtually identical for this to happen. Alternatively, if the relative thresholds are indeed reasonable, the fact that dissociation and isomerization compete on the microsecond timescale could be indicative that the reactions are not occurring statistically (in which case RRKM does not apply). This requires further study.

7.5.2 Insertion Reaction Products

It is known that $O_2^{+\bullet}$ inserts in the CH bond in methane [17]. Isomer **41** reflects the insertion

of oxygen into the C—H bond in CH_3CN, to make a covalently bonded isomer lying 10 kJ mol^{-1} above isomer **37**. Any $HOOCH_2CN^{+\bullet}$ formed should immediately dissociate (a process that only requires 35 kJ mol^{-1} Table 16b) to form $HO^{\bullet} + OCH_2CN^{+}$ which has the wrong connectivity as observed from the CID mass spectrum. $HOCH_2CNO^{+\bullet}$ (**43**) has a threshold for dissociation to $CH_2CNO^{+} + {}^{\bullet}OH$ of 205 kJ mol^{-1} but the formation of this ion might be expected to be difficult due to the connectivity. Another covalent structure results from the insertion into the N—H bond of CH_2CNH^{+}, CH_2CNOOH^{+} (**42**), which can also dissociate to form $CH_2CNO^{+} + {}^{\bullet}OH$, a process requiring 18 kJ mol^{-1}. Other isomers of the OH loss fragment ion m/z 56 were located, but do not have the connectivity suggested by the CID mass spectrum ($CHCNOH^{+}$, NH_2CCO^{+}, $HNCCOH^{+}$ and $HCNCHO^{+}$). We were unable to find an equilibrium $CHCHNO^{+}$ ion structure.

7.6 Conclusion

The dimer ion of acetonitrile and oxygen exhibit three peaks at m/z 32 (O_2), m/z 41 (CH_3CN and ${}^{\bullet}CH_2CNH^{+}$) and m/z 56 (-OH) in its MI mass spectrum. When O_2 (triplet ground state) encounters a $CH_3CN^{+\bullet}$ or ${}^{\bullet}CH_2CNH^{+}$ ion, the resulting complex $(C_2H_3N)(O_2)^{+\bullet}$ can take on either a doublet or quartet character. RRKM calculations predict a fast forward isomerization of $CH_3CN^{+\bullet}$ to ${}^{\bullet}CH_2CNH^{+}$. The fact that the dissociation and isomerization compete on the microsecond timescale is an indication that the reactions do not occur statistically and that RRKM theory does not apply.

Table 15: MI spectra of m/z 73

Trial	Precursor	m/z		
		56	41	32
	CH_3CN/O_2 in source[a]			
1	Medium Pres.(10^{-5}) Torr	26	100	46
2	Medium Pres.(10^{-5}) Torr	30	100	30
3	Medium Pres.(10^{-5}) Torr	34	100	43
1	High Pres.(10^{-4}) Torr	85	100	60
2	High Pres.(10^{-4}) Torr	75	100	56
3	High Pres.(10^{-4}) Torr	85	100	26
4	High Pres.(10^{-4}) Torr	68	100	54
5	High Pres.(10^{-4}) Torr	82	100	48

[a] Trials reflect same relative ion source pressures for the two neutrals, experiments performed on different days.

Table 16a: Relative B3-LYP/6-31+G(d) Energies

ion	relative energy [a] B3-LYP/6-31+G(d)
$^2[CH_3CN \bullet\bullet\bullet O_2]^{+\bullet}$ **(37)**	0
$^2[CH_2CNH \bullet\bullet\bullet O_2]^{+\bullet}$ **(38)**	-89
$^4[O_2\bullet\bullet\bullet CH_3CN]^{+\bullet}$ **(39)**	110
$^4[CH_2CNH\bullet\bullet\bullet O_2]^{+\bullet}$ **(40)**	-89
$CH_3CN + {}^2O_2^{+\bullet}$	207 **(137)**[b]
$CH_3CN^{+\bullet} + {}^1O_2$	280 **(212)**[b]
$CH_3CN^{+\bullet} + {}^3O_2$	118 **(154)**[b]
$^{\bullet}CH_2CNH^{+} + {}^3O_2$	-77
$CH_2CNH^{+\bullet} + {}^1O_2$	85

[a] Values are in kJ mol $^{-1}$.

[b] Values in parentheses converted by the experimental IE values (see text).

Table 16b: Relative B3-LYP/6-31+G(d) Energies

ion	relative energy [a] B3-LYP/6-31+G(d)
$HOOCH_2CN$ **(41)**	10
CH_2CNOOH **(42)**[b]	54
$HOCH_2CNO$ **(43)**	-133
$[CH_2CNO]^+ + {}^{\bullet}OH$	72
$OCH_2CN + {}^{\bullet}OH$	45

[a] Values are in kJ mol $^{-1}$.

[b] Could not get rid of the -16 mode probably due to B3-LYP.

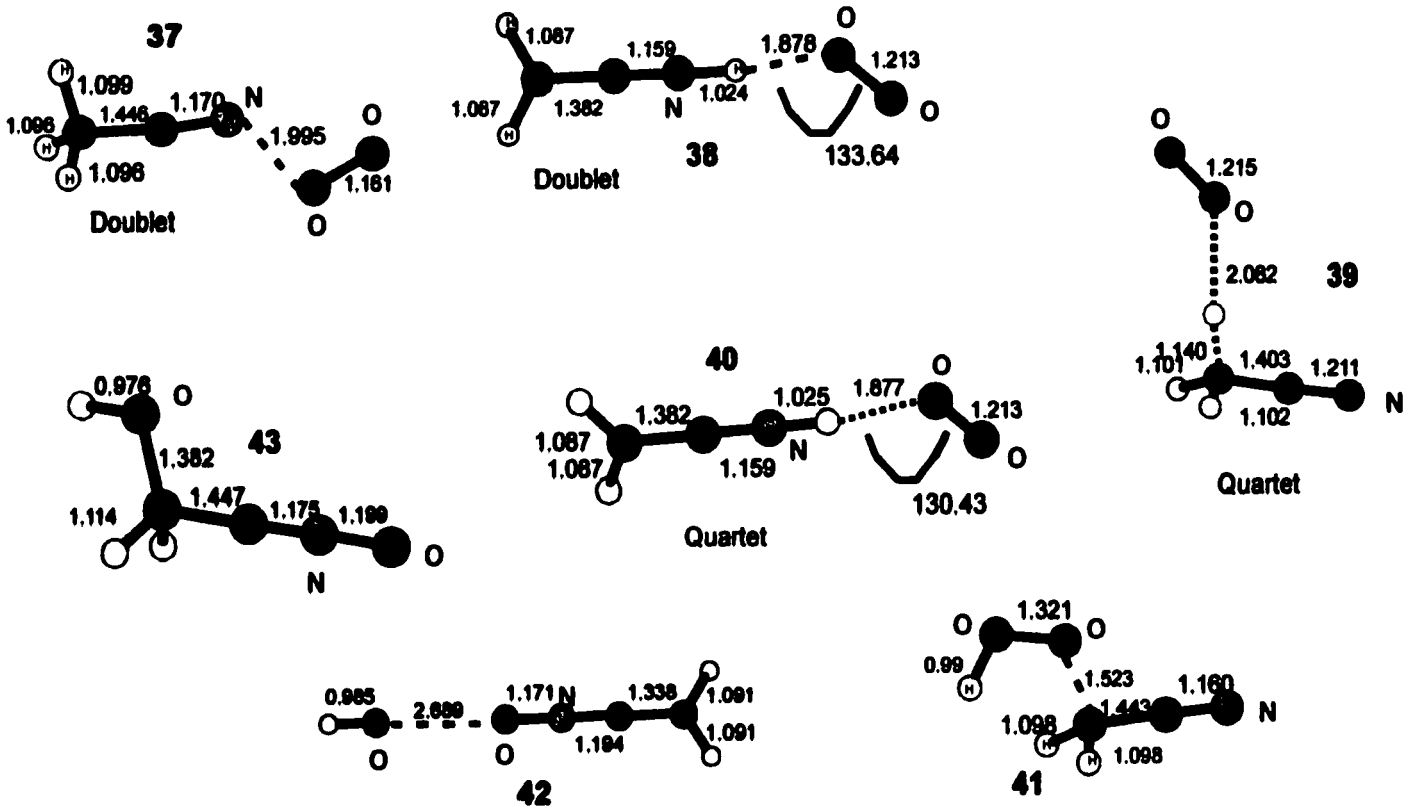

Figure 40: B3-LYP/6-31+G(d) optimized isomers of $(CH_3CN)(O_2)^{\cdot}$

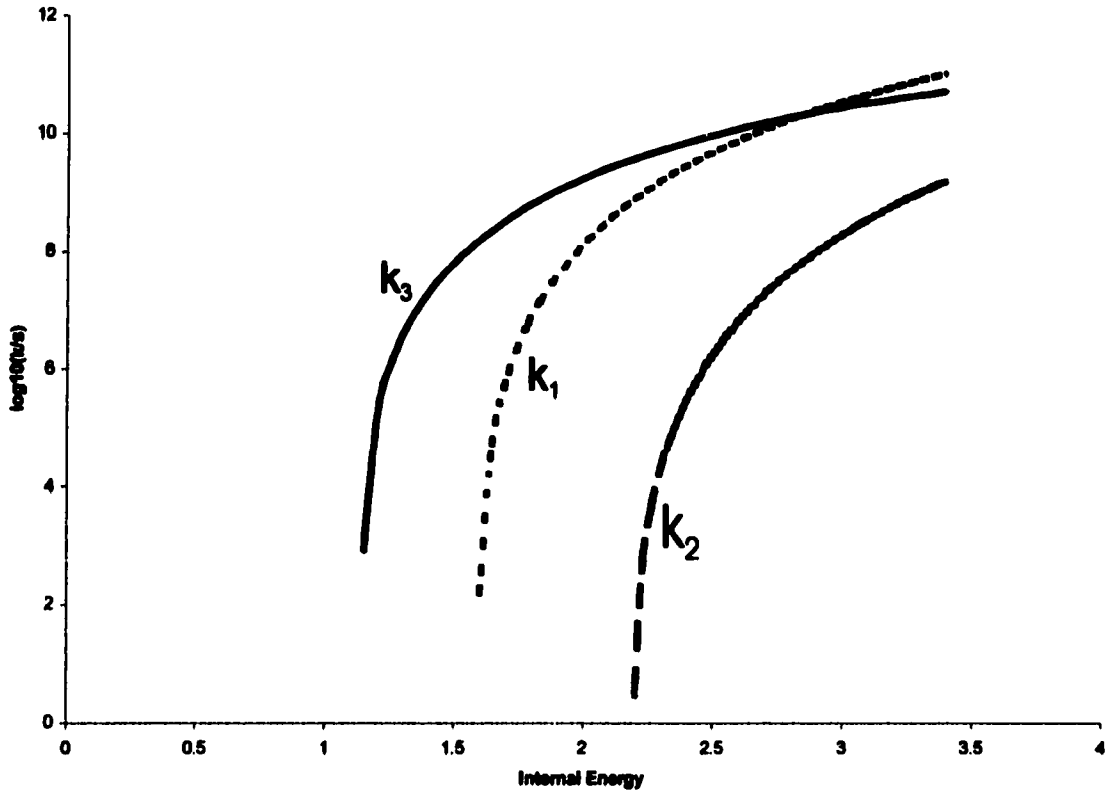

Figure 41: A plot of log (k) vs E curves for the dissociation of 37 to form $^2O_2^{\cdot}$ + CH_3CN(k_1), $CH_3CN^{\cdot}$ + $^3O_2$(k_2) and for the isomerization to 38 (k_3).

References

[1] E. Murad, W. Swider, R. A. Moss and S. Toby, Geophys. Res. Lett. 11 (1984) 147.

[2] M. Iraqi and C. Liftshitz, Int. J. of Mass Spectrom. and ion Pro. 88 (1989) 45.

[3] L. .Angel and A. J. Stace, J. Phys Chem. A 103 (1999) 2999.

[4] P. M. Mayer, J. Phys. Chem. A 103 (1999) 5905.

[5] K. L. Busch, G. L. Glish and S. A. McLuckey, Mass Spectrometry/Mass Spectrometry Editor, ed. (New York, VCH Publishers, 1988).

[6] W. J. Hehre, L. Radom, P. v. R. Schleyer and J. A. Pople, Ab Initio Molecular Orbital Theory Editor, ed. (New York, Wiley, 1986).

[7] M. J. Frisch, G. W. Trucks, H. B. Schlegel, G. E. Scuseria, M. A. Robb, J. R. Cheeseman, V. G. Zakrzewski, J. A. Montgomery, R. E. Stratmann, J. C. Burant, S. Dapprich, J. M. Millam, A. D. Daniels, K. N. Kudin, M. C. Strain, O. Farkas, J. Tomasi, V. Barone, M. Cossi, R. Cammi, B. Mennucci, C. Pomelli, C. Adamo, S. Clifford, J. Ochterski, G. A. Petersson, P. Y. Ayala, Q. Cui, K. Morokuma, D. K. Malick, A. D. Rabuck, K. Raghavachari, J. B. Foresman, J. Cioslowski, J. V. Ortiz, A. G. Baboul, B. B. Stefanov, G. Liu, A. Liashenko, P. Piskorz, I. Komaromi, R. Gomperts, R. L. Martin, D. J. Fox, T. Keith, M. A. Al-Laham, C. Y. Peng, A. Nanayakkara, C. Gonzalez, M. Challacombe, P. M. W. Gill, B. Johnson, W. Chen, M. W. Wong, J. L. Andres, C. Gonzalez, M. Head-Gordon, E. S. Replogle and J. A. Pople *GAUSSIAN 98, Rev A.7*; Gaussian, Inc: Pittsburgh, PA, 1998.

[8] E. K. Chess, R. L. Lapp and M. L. Gross, Org. Mass Spectrom. 17 (1982) 475.

[9] G. v. d. Rest, H. Nedev, J. Chamot-Rooke, P. Mourgues, T. B. McMahon and H. E. Audier, Int. J. of Mass Spectrom. 202 (2000) 161.

[10] P. M. Mayer, M. Glukhovtsev, J. W. Gauld and L. Radom, J. Am. Chem. Soc. 119 (1997) 12889.

[11] NIST Chemistry WebBook, NIST Standard Reference Database Number 69 Editor, ed. (Gaithersburg MD, National Institute of Standards and Technology, 2000).

[12] J. v. Thuiji, J. J. v. Houte, A. Maquestiau, R. Flammang and C. D. Meyer, Organic Mass Spectrometry 12 (1977) .

[13] B. v. Baar, W. Koch, C. Lebrilla, J. K. Terlouw, T. Weiske and H. Schwartz, Angnew. Chem., Int. Ed. Engl. 25 (1986) 827.

[14] L. A. Curtis, P. Redfern, K. Raghavachari and J. Pople, J. Chem. Phys. 109 (1998) 42.

[15] P. H. Krupenie, The Spectrum of molecular oxygen J. Phys. Chem. Ref. Data (1972) 423.

[16] P. M. Mayer, C. J. Parkinson, D. M. Smith and L. Radom, J. Chem. Phys. 108 (1998) 604.

[17] P. Lin and H. I. Kenttamaa, Organic Mass Spectrometry 27 (1992) 1155.

SUPPORTING INFORMATION

Appendix A GAUSSIAN Archive Entries for MP2/6-31+G(d) Optimized Geometries (Acetonitrile-Ethanol)

(CH_3CN)(CH_3CH_2OH)H(dimer)(2)

1\1\GINC-FRED\FOpt\RMP2-FC\6-31+G(d)\C4H10N1O1(1+)\RICHARD\19-Aug-1999
\0\\# MP2/6-31+G(D) OPT FREQ=NORAMAN GEOM=CHECK GUESS=CHECK\\Geometry
optimization of acetonitrile/ethanol/proton\\1,1\N,-0.2556485314,0.177
1607285,1.2828430578\C,-0.1405693657,0.2682995159,2.4473327774\C,0.004
0151206,0.3761672757,3.8951643171\H,-0.4419663105,0.158331178,-0.22465
16899\O,-0.5537015215,0.1647349387,-1.2790537105\H,-1.4010528949,-0.26
95918653,-1.5233746293\C,0.6118398388,-0.4598579775,-2.0047704187\C,0.
3412405139,-0.3858498129,-3.4833577554\H,0.2941748119,1.3963057362,4.1
569797249\H,0.7722767933,-0.3203855687,4.2384833765\H,-0.9470544456,0.
1344649924,4.375232687\H,1.4494354163,0.159218112,-1.6880166414\H,0.71
69203599,-1.4767623954,-1.6236245897\H,1.2099128151,-0.7891156261,-4.0
122968359\H,0.1923210405,0.6469907474,-3.8040338384\H,-0.5249723397,-0
.9900139267,-3.7683828064\\Version=SGI-G98RevA.6\HF=-286.3588348\MP2=-
287.2271223\RMSD=3.859e-09\RMSF=8.253e-06\Dipole=-0.241756,-0.3883662,
0.257989\PG=C01 [X(C4H10N1O1)]\\@

$CH_3CNCH_2CH_3^+$ (16)

1\1\GINC-FRED\FOpt\RMP2-FC\6-31+G(d)\C4H8N1(1+)\RICHARD\23-Sep-1999\0\
\# MP2/6-31+G(D) OPT FREQ=NORAMAN GEOM=CHECK GUESS=CHECK\\Geomertry
op
timization of mz70_2\\1,1\N,0.2451611315,0.2439059385,0.0111758387\C,0
.0965497577,0.1721487349,1.1629157565\C,-0.0884640911,0.0885455542,2.6
040094654\H,0.8550839485,-0.2086643786,3.0698449766\H,-0.8603779465,-0
.6538928782,2.8243028907\H,-0.396467771,1.0669400301,2.9828425062\C,0.
4107639323,0.3062809353,-1.4345501173\H,1.4627249975,0.0761494919,-1.6
195413346\H,0.2168574562,1.3463044761,-1.7075667938\C,-0.5365759657,-0
.6702048374,-2.1177388216\H,-0.3784299301,-0.5907357702,-3.1962512964\
H,-1.5789025198,-0.4253333211,-1.904423742\H,-0.3302579542,-1.69873154
12,-1.8152557753\\Version=SGI-G98RevA.7\HF=-210.3322586\MP2=-211.00208
\RMSD=4.053e-09\RMSF=4.919e-05\Dipole=0.1668509,0.2218691,0.878331\PG=
C01 [X(C4H8N1)]\\@

$(CH_3CN)(C_2H_4)H^+$ (18)

1\1\GINC-FRED\FOpt\RMP2-FC\6-31+G(d)\C4H8N1(1+)\RICHARD\26-Jul-1999\0\
\# MP2/6-31+G(D) OPT FREQ=NORAMAN\\Geometry Optimization of Acetonitri
le-ethene ion\\1,1\H,-0.5942022348,-0.0024373069,0.0010389462\N,0.4656
36228,-0.0039223235,-0.006711567\C,1.627325031,-0.0051593241,-0.014734
2144\C,3.0799061804,-0.0066712335,-0.0242344684\H,3.4295335676,-0.0079
478854,-1.0603907296\H,3.4407254909,0.8887319374,0.4894614168\H,3.4388
653438,-0.9019191541,0.4910340154\C,-2.5725863258,0.0083794314,-0.6516
98094\C,-2.5617084258,0.0067734806,0.696524112\H,-2.619791946,-0.9175
337556,-1.219472123\H,-2.6071291981,0.9359890869,-1.2176494128\H,-2.59
88423588,-0.9204771736,1.2628091381\H,-2.5862310199,0.9331163886,1.265
0057106\\Version=SGI-G98RevA.6\HF=-210.2821558\MP2=-210.9544288\RMSD=6
.983e-09\RMSF=3.556e-05\Dipole=1.794485,-0.0054599,-0.0148704\PG=C01 [
X(C4H8N1)]\\@

CH_3CN

1\1\GINC-FRED\FOpt\RMP2-FC\6-31+G(d)\C2H3N1\RICHARD\26-Sep-1999\0\\# M
P2/6-31+G(D) OPT FREQ=NORAMAN\\(mp2/6-31+G(d) Geometry Optimization of
CH3CN\\0,1\N,0.0037071189,0.,-1.4548192102\C,0.0007568636,0.,-0.27415
73191\C,-0.0030623911,0.,1.1898932112\H,-1.0312202559,0.0000000042,1.5
604159686\H,0.5095517966,0.8895667497,1.564451575\H,0.5095517893,-0.88
9566754,1.5644515749\\Version=SGI-G98RevA.7\State=1-A'\HF=-131.9258095
\MP2=-132.3453598\RMSD=1.772e-09\RMSF=2.213e-04\Dipole=-0.0040165,0.,1
.5674061\PG=CS [SG(C2H1N1),X(H2)]\\@

CH_3CNH^+

1\1\GINC-FRED\FOpt\RMP2-FC\6-31+G(d)\C2H4N1(1+)\RICHARD\26-Sep-1999\0\
\# MP2/6-31+G(D) OPT FREQ=NORAMAN\\(mp2/6-31+G(d) Geometry Optimizatio
n of CH3CNH+\\1,1\N,-0.0020192406,0.,-1.3255622922\C,-0.0002831029,0.,
-0.166547063\C,0.0019808698,0.,1.2844768913\H,1.0382603273,0.,1.636083
4455\H,-0.5153308103,-0.8969667445,1.6385118235\H,-0.5153308103,0.8969
667444,1.6385118235\H,-0.0036506241,0.,-2.3417500173\\Version=SGI-G98R
evA.7\State=1-A'\HF=-132.233304\MP2=-132.641023\RMSD=9.106e-09\RMSF=1.
837e-04\Dipole=-0.0009688,0.,-0.5968725\PG=CS [SG(C2H2N1),X(H2)]\\@

CH_3CH_2OH

1\1\GINC-FRED\FOpt\RMP2-FC\6-31+G(d)\C2H6O1\RICHARD\17-Aug-1999\0\\# M
P2/6-31+G(D) OPT FREQ=NORAMAN\\Geometry Optimization of Ethanol\\0,1\O
,-0.426448325,0.,-1.1388641752\C,-0.4779222743,0.,0.2971045367\C,0.951
4189145,0.,0.7924604964\H,-1.3356776498,0.,-1.4855713322\H,-1.01065331

64,-0.890078148,0.6572660459\H,-1.0106533164,0.890078148,0.6572660459\
H,1.4754986002,0.8875036727,0.4288161246\H,1.4754986002,-0.8875036727,
0.4288161246\H,0.9765938414,0.,1.8869301945\\Version=SGI-G98RevA.6\Sta
te=1-A'\HF=-154.0799912\MP2=-154.5301505\RMSD=2.775e-09\RMSF=2.637e-05
\Dipole=-0.605731,0.,0.448328\PG=CS [SG(C2H2O1),X(H4)]\\@

$CH_3CH_2OH_2^+$

1\1\GINC-FRED\FOpt\RMP2-FC\6-31+G(d)\C2H7O1(1+)\RICHARD\17-Aug-1999\0\
\# MP2/6-31+G(D) OPT FREQ=NORAMAN GEOM=CHECK GUESS=CHECK\\Geometry
Optimization of ethanolH\\ 1, 1\O, -0.4756324374,
0.0378026305,-1.1223708508\C,-0.4586261085,0.0140384834,0.4307929058\C,
0.9810857016,0.0259782267,0.8476423063\H,-1.3823731413,0.009031931,
-1.5125205778\H,0.0617811421,-0.6889157066,-1.5198257172\H,-1.0152880296,
-0.8779017616,0.7170435117\H,-1.0022310976,0.9266993993,0.6666663775\H,
1.501645517,0.9053308159,0.4641035674\H,1.505244056,-0.8866169362,
0.5510911841\H,1.0015234942,0.0698509537,1.9417971879\\Version=SGI-G98
RevA.6\HF=-154.3871908\MP2=-154.8299829\RMSD=9.247e-09\RMSF=3.142e-05\
Dipole=-0.8713,-0.5297162,-0. 9411112\PG=C01 [X(C2H7O1)]\\@

C_2H_4

1\1\GINC-FRED\FOpt\RMP2-FC\6-31+G(d)\C2H4\RICHARD\19-Jul-1999\0\\# MP2
/6-31+G(D) OPT FREQ=NORAMAN GEOM=CHECK GUESS=CHECK\\Geometry Optimizat
ion of ethene\\0,1\C,-0.6384363351,0.,0.203451598\H,-0.8998099849,0.,1
.2573467635\C,0.6384359511,0.,-0.2034513921\H,1.4613889875,0.,0.504898
7005\H,0.899810936,0.,-1.2573464074\H,-1.461387635,0.,-0.504900292\\Ve
rsion=SGI-G98RevA.6\State=1-A'\HF=-78.0350747\MP2=-78.2911797\RMSD=6.4
84e-09\RMSF=3.261e-05\Dipole=0.0000002,0.,-0.0000001\PG=CS [SG(C2H4)]\
\@

H_2O

1\1\GINC-FRED\FOpt\RMP2-FC\6-31+G(d)\H2O1\RICHARD\18-Aug-1999\0\\# MP2
/6-31+G(D) OPT FREQ=NORAMAN GEOM=CHECK GUESS=CHECK\\Geometry
Optimization of Water\\0,1\O,-0.0960134418,0.,-0.0678555919\H,-0.0618518486,0.,
0.9023642205\H,0.829959383,0.,-0.3595194851\\Version=SGI-G98RevA.6\Sta
te=1-A1\HF=-76.0166449\MP2=-76.2097766\RMSD=2.225e-09\RMSF=3.560e-05\D
ipole=0.7476121,0.,0.52836\PG=C02V [C2(O1),SGV(H2)]\\@

Appendix B GAUSSIAN Archive Entries for MP2/6-31+G(d) Optimized Geometries (Acetonitrile-Propanols)

$((CH_3)_2CHOH)^+$

N-N= 1.346508125963D+02 E-N=-7.214288753593D+02 KE= 1.926787076719D+02
1\1\GINC-FRED\FOpt\RMP2-FC\6-31+G(d)\C3H8O1\RICHARD\03-Feb-2000\0\\# M
P2/6-31+G(D) OPT FREQ=NORAMAN\\Geometry Optimization of nproh @mp2/6-3
1+G(d)\\0,1\H,-0.8825987918,1.7791732885,0.0816499957\O,-0.0357335081,
1.3687173425,-0.1703194294\C,0.0013749657,0.0338082411,0.3709660882\H,
-0.0065056519,0.0934369931,1.4700407304\C,1.3192516057,-0.5566702336,-
0.0879614939\H,1.4506247662,-1.5651767753,0.3169314637\H,1.3405550165,
-0.6087676963,-1.1809662579\H,2.1508190789,0.0691292918,0.2465195987\C
,-1.1979457508,-0.7743093564,-0.1008328367\H,-2.1378338224,-0.31820797
43,0.2312656571\H,-1.2038251607,-0.8225437288,-1.1942717127\H,-1.16145
22934,-1.793754045,0.2983554146\\Version=SGI-G98RevA.7\HF=-193.1195694
\MP2=-193.7043054\RMSD=2.974e-09\RMSF=3.165e-05\Dipole=-0.5158587,-0.3
787413,0.3914739\PG=C01 [X(C3H8O1)]\\@

$((CH_3)_2CHOH_2)^+$

1\1\GINC-FRED\FOpt\RMP2-FC\6-31+G(d)\C3H9O1(1+)\RICHARD\03-Feb-2000\0\
\# MP2/6-31+G(D) OPT FREQ=NORAMAN\\Geometry Optimization of nprohH @mp
2/6-31+G(d)\\1,1\H,-0.0964598104,1.5208334627,0.9910391447\O,-0.233452
4697,1.3809621184,0.0233798263\H,-1.1411408121,1.6961438005,-0.2033317
457\C,0.0226082954,-0.123868789,-0.4019745761\H,-0.006713894,-0.005131
5179,-1.4860811051\C,-1.0995275893,-0.966547446,0.1379834239\H,-2.0775
325199,-0.6488174349,-0.2344598401\H,-0.9397162731,-1.9933387849,-0.20
81316566\H,-1.1028429123,-0.9827492349,1.2317261832\C,1.4053519947,-0.
4203134905,0.1061681999\H,1.4348913127,-0.4629496664,1.1997375127\H,1.
6907462134,-1.4093536465,-0.2662207757\H,2.1357922488,0.3020444289,-0.
2643786134\\Version=SGI-G98RevA.7\HF=-193.4334505\MP2=-194.0099149\RMS
D=5.415e-09\RMSF=1.413e-05\Dipole=-0.6546433,0.9236518,0.2704145\PG=C0
1 [X(C3H9O1)]\\@

(14)

1\1\GINC-FRED\FOpt\RMP2-FC\6-31+G(d)\C5H12N1O1(1+)\RICHARD\29-Mar-2000
\0\\# MP2/6-31+G(D) OPT FREQ=NORAMAN\\Geometry Optimization of mz84c+H
2O @mp2/6-31+G(d)\\1,1\N,0.3741976209,0.0002716621,0.0796763383\C,0.45
57082928,0.0008932465,1.2401018129\C,0.5529070061,0.0003649705,2.69005
56176\O,-2.3955582735,-0.0021240982,1.2056656492\H,-2.9900076315,-0.77
12560825,1.273466005\H,-2.991058578,0.7665847233,1.268927711\H,-0.4643

389933,0.0016563954,3.0895262733\H,1.0909751148,0.8928197166,3.0199992
326\H,1.0883493578,-0.8939498988,3.0192681817\C,0.1674419298,0.0002355
114,-1.3645728216\H,-0.9234577002,-0.0003324557,-1.4632663003\C,0.7664
596984,1.2795007073,-1.936345216\H,0.5635521811,1.302296982,-3.0102485
571\H,0.3208797957,2.1684652323,-1.4832211395\H,1.8498363999,1.3001257
12,-1.7900628565\C,0.7677191908,-1.2783746277,-1.9364757799\H,0.564845
4921,-1.3012487657,-3.0103840795\H,1.8511124047,-1.2979735301,-1.79018
12019\H,0.3229782897,-2.167815725,-1.4834645084\\Version=SGI-G98RevA.7
\HF=-325.4053336\MP2=-326.4075627\RMSD=3.484e-09\RMSF=1.598e-05\Dipole
=-0.3186676,0.0001911,1.0232487\PG=C01 [X(C5H12N1O1)]\\@

(6)

1\1\GINC-FRED\FOpt\RMP2-FC\6-31+G(d)\C5H10N1(1+)\RICHARD\25-Feb-2000\0
\\# MP2/6-31+G(D) OPT=TIGHT FREQ=NORAMAN\\Geometry Optimization of mz8
4 @mp2/6-31+G(d)\\1,1\N,0.5783979379,-0.3533553643,0.3479331095\C,0.49
42058784,-0.1035587156,1.4813673888\C,0.6453462041,-0.66001711,-1.0733
151588\C,0.3995015241,0.2108896069,2.8991594732\C,-0.7016789206,-0.390
7898032,-1.7402786421\H,0.9506999798,-1.7079071906,-1.135452867\H,1.44
15181923,-0.0256266313,-1.4738745895\H,-0.644387752,0.135785276,3.2155
460027\C,-1.1334710964,1.0695289622,-1.6580562647\H,0.7648423044,1.227
8972214,3.0658746447\H,1.0092761444,-0.4987305065,3.4650938169\H,-0.57
48800405,-0.693826716,-2.7856531836\H,-1.4580105905,-1.0555111351,-1.3
093276892\H,-2.0646814881,1.2167367869,-2.2100061535\H,-0.3795723094,1
.7318581601,-2.0948195699\H,-1.3170115428,1.3864946429,-0.6261729564\\
Version=SGI-G98RevA.7\HF=-249.3682983\MP2=-250.1715175\RMSD=6.517e-09\
RMSF=2.590e-08\Dipole=0.6519496,-0.2904125,1.3852241\PG=C01 [X(C5H10N1
)]\\@

$CH_3CH_2CH_2OH$

1\1\GINC-FRED\FOpt\RMP2-FC\6-31+G(d)\C3H8O1\RICHARD\17-Dec-1999\0\\# M
P2/6-31+G(D) OPT FREQ=NORAMAN\\Geometry Optimization of nproh @mp2/6-3
1+G(d)\\0,1\H,2.5809923152,0.3896944132,0.0018904894\O,1.8428222585,-0
.2445695935,-0.0002757981\C,0.6066041558,0.486357701,0.0000770177\H,0.
5402306818,1.1272003695,-0.8907292312\H,0.5405578807,1.1270459907,0.89
10120576\C,-0.5218695093,-0.5243500329,0.0001877705\H,-0.4106430634,-1
.1655716174,0.8814988737\H,-0.4103595424,-1.1659844275,-0.8807927011\C
,-1.8921008633,0.1503189862,-0.0002159294\H,-2.6946875547,-0.592967125
2,-0.0000617442\H,-2.0221172241,0.781281099,-0.8861240212\H,-2.0223542
606,0.7818981198,0.8852195095\\Version=SGI-G98RevA.7\HF=-193.1147847\M
P2=-193.6968852\RMSD=3.505e-09\RMSF=2.365e-05\Dipole=-0.1180736,0.7002
319,0.0017138\PG=C01 [X(C3H8O1)]\\@

C_3H_6

1\1\GINC-MS1\FOpt\RMP2-FC\6-31+G(d)\C3H6\RICHARD\17-May-2000\0\\#MP2/6
-31+G(D) OPT FREQ=NORAMAN\\Geomertry of iproh/ch3cn@mp2\\0,1\H,0.51420
81669,0.,-1.7711555828\C,1.0204758131,0.,-0.8087639886\H,2.1060005541,
0.,-0.8242095864\C,0.334327795,0.,0.344367455\H,0.8862486697,0.,1.2847
285981\C,-1.1623939045,0.,0.4447069544\H,-1.6213143146,0.,-0.548617124
2\H,-1.5198006489,0.8815641321,0.9886955854\H,-1.5198006489,-0.8815641
321,0.9886955854\\Version=x86-Linux-G98RevA.7\State=1-A\HF=-117.07453
16\MP2=-117.4629407\RMSD=4.793e-09\RMSF=2.585e-05\Dipole=-0.1120763,0.
,0.0833004\PG=CS [SG(C3H4),X(H2)]\\@

$CH_3CH_2CH_2OH_2^+$

1\1\GINC-FRED\FOpt\RMP2-FC\6-31+G(d)\C3H9O1(1+)\RICHARD\20-Dec-1999\0\
\# MP2/6-31+G(D) OPT FREQ=NORAMAN\\Geometry Optimization of nprohH @mp
2/6-31+G(d)\\1,1\H,2.6202081366,-0.4609323519,-0.011160507\O,1.8525223
25,0.1535976686,-0.1012068634\H,1.9651066018,0.8940464331,0.5420488051
\C,0.4685320347,-0.5425563822,0.0367685486\H,0.5030771831,-1.084619629
,0.9825965774\H,0.4762448315,-1.2153285603,-0.8196338025\C,-0.58069583
69,0.5300010649,-0.0345302283\H,-0.4685651431,1.0918168534,-0.96666378
5\H,-0.4699987775,1.2240002612,0.8072366275\C,-1.9675865336,-0.1271495
53,0.0247849491\H,-2.7344240058,0.6483639097,-0.0214752258\H,-2.109950
149,-0.6845944871,0.9544189272\H,-2.1233752622,-0.8033045556,-0.819852
3262\\Version=SGI-G98RevA.7\HF=-193.4244178\MP2=-193.9990021\RMSD=4.73
1e-09\RMSF=1.286e-05\Dipole=2.1913258,-0.164043,0.4994237\PG=C01 [X(C3
H9O1)]\\@

CH_3CN

1\1\GINC-FRED\FOpt\RMP2-FC\6-31+G(d)\C2H3N1\RICHARD\26-Sep-1999\0\\# M
P2/6-31+G(D) OPT FREQ=NORAMAN\\(mp2/6-31+G(d) Geometry Optimization of
CH3CN\\0,1\N,0.0037071189,0.,-1.4548192102\C,0.0007568636,0.,-0.27415
73191\C,-0.0030623911,0.,1.1898932112\H,-1.0312202559,0.0000000042,1.5
604159686\H,0.5095517966,0.8895667497,1.564451575\H,0.5095517893,-0.88
9566754,1.5644515749\\Version=SGI-G98RevA.7\State=1-A\HF=-131.9258095
\MP2=-132.3453598\RMSD=1.772e-09\RMSF=2.213e-04\Dipole=-0.0040165,0.,1
.5674061\PG=CS [SG(C2H1N1),X(H2)]\\@

CH_3CNH^+

1\1\GINC-FRED\FOpt\RMP2-FC\6-31+G(d)\C2H4N1(1+)\RICHARD\26-Sep-1999\0\
\# MP2/6-31+G(D) OPT FREQ=NORAMAN\\(mp2/6-31+G(d) Geometry Optimizatio
n of CH3CNH+\\1,1\N,-0.0020192406,0.,-1.3255622922\C,-0.0002831029,0.,

-0.166547063\C,0.0019808698,0.,1.2844768913\H,1.0382603273,0.,1.636083
4455\H,-0.5153308103,-0.8969667445,1.6385118235\H,-0.5153308103,0.8969
667444,1.6385118235\H,-0.0036506241,0.,-2.3417500173\\Version=SGI-G98R
evA.7\State=1-A'\HF=-132.233304\MP2=-132.641023\RMSD=9.106e-09\RMSF=1.
837e-04\Dipole=-0.0009688,0.,-0.5968725\PG=CS [SG(C2H2N1),X(H2)]\\@

(19')

1\1\GINC-MS1\FOpt\RMP2-FC\6-31+G(d)\C5H10N1(1+)\RICHARD\11-Jul-2000\0\
\#MP2/6-31+G(D) OPT FREQ=NORAMAN\\Geometry optimization of isomer\\1,1
\H,0.0501594957,-0.0486507856,-0.3232080807\C,1.0841500483,-0.01881875
78,0.0781527257\N,2.1784236526,0.0065422249,0.4623208292\C,3.542624562
8,0.0378308359,0.9356401876\H,3.524521894,-0.1359680528,2.0115957577\H
,3.9508440819,1.0210203148,0.7008651931\H,4.0889919036,-0.7503659275,0
.4172422348\C,-2.2145086934,-0.4741491415,-0.6041009029\H,-2.249921583
1,-1.5645633672,-0.63637116\C,-2.8340580811,0.1829819174,0.5919237226\
H,-3.9029851365,-0.0530178473,0.6330694455\H,-2.7291316824,1.271069847
1,0.552696967\H,-2.3996312103,-0.1856877719,1.528518899\C,-1.676211853
2,0.184485187,-1.6507249591\H,-1.3150033041,-0.3460382071,-2.528226579
2\H,-1.6787859268,1.2724259774,-1.6977731257\\Version=x86-Linux-G98Rev
A.7\HF=-249.3057232\MP2=-250.108341\RMSD=6.902e-09\RMSF=3.844e-05\Dipo
le=2.8397953,-0.0400733,0.6570718\PG=C01 [X(C5H10N1)]\\@

(8)

1\1\GINC-FRED\FOpt\RMP2-FC\6-31+G(d)\C5H12N1O1(1+)\RICHARD\12-Jul-2000
\0\\# MP2/6-31+G(D) OPT FREQ=NORAMAN\\Optimization of CH3CN-Propene+H2
O @mp2\\1,1\H,-0.5640650464,-0.0703037858,0.0071809039\N,0.3994287787,
-0.0225130072,0.4475084508\C,1.4964746597,0.032924323,0.8253205598\O,2
.6371544442,0.2629226109,-1.7812499288\H,2.7300303977,1.0809067729,-2.
3018712077\H,2.9548911144,-0.4398608318,-2.3763633411\C,2.8467916041,0
.101759309,1.3519107423\H,2.9317495558,0.9702129065,2.0104798988\H,3.5
245622021,0.1974150522,0.5004223058\H,3.0603030398,-0.811042181,1.9143
562073\C,-2.6059975689,-0.5970584002,-0.2255030319\H,-2.566526799,-1.6
758895289,-0.3858333231\C,-3.2363946848,-0.1282831084,1.0499141869\H,-
4.2846373235,-0.4446214419,1.0802680841\H,-3.2068935166,0.9613187915,1
.1379202085\H,-2.7516783363,-0.5732955294,1.9263111323\C,-2.1287196834
,0.214992911,-1.1938360847\H,-1.7500287189,-0.1847876335,-2.130969029\
H,-2.203869533,1.2981473658,-1.1112997989\\Version=SGI-G98RevA.7\HF=-3
25.356961\MP2=-326.3590566\RMSD=4.057e-09\RMSF=2.337e-05\Dipole=1.8234
528,0.0468276,0.2361754\PG=C01 [X(C5H12N1O1)]\\@

$(CH_3CN)((CH_3)_2CHOH)H^+$(4)

1\1\GINC-MS2\FOpt\RMP2-FC\6-31+G(d)\C5H12N1O1(1+)\RICHARD\17-Jul-2000\
0\\#MP2/6-31+G(D) OPT=TIGHT FREQ=NORAMAN\\Geomertry of iproh/ch3cn@mp2
\\1,1\H,-0.1642756759,-0.5839851988,-0.3005419526\N,-1.6195194655,-0.0
613426139,-0.0775078578\C,-2.7314551207,0.3074574377,0.0060187957\C,-4
.1127844659,0.7655289143,0.1154917806\H,-4.3597820682,1.3889372736,-0.
7468955372\H,-4.781914486,-0.0975603234,0.1424916001\H,-4.2338943139,1
.3477512899,1.0317721889\O,0.8081225589,-0.9450603436,-0.4495396904\H,
0.8199233916,-1.9065695809,-0.2415571334\C,1.8513149245,-0.1896543683,
0.3778936238\H,1.4728040666,-0.2162842451,1.403591705\C,3.13930094,-0.
9585797562,0.2263801853\H,3.9183530469,-0.4484969088,0.800238296\H,3.0
603653651,-1.9771523141,0.6200969255\H,3.449157665,-0.9918470095,-0.82
13036053\C,1.862358442,1.2066362912,-0.1898767914\H,2.5807557951,1.804
8965604,0.3781611702\H,2.1727910495,1.1932259823,-1.2376191647\H,0.884
963633,1.6886344076,-0.105007529\\Version=x86-Linux-G98RevA.7\HF=-325.
4024427\MP2=-326.4050361\RMSD=5.722e-09\RMSF=2.735e-07\Dipole=0.631029
8,0.5150784,0.3548343\PG=C01 [X(C5H12N1O1)]\\@

$(CH_3CN)(CH_3CH_2CH_2OH)H^+$ (3)

1\1\GINC-FRED\FOpt\RMP2-FC\6-31+G(d)\C5H12N1O1(1+)\RICHARD\26-Jul-2000
\0\\#MP2/6-31+G(D) OPT=TIGHT FREQ=NORAMAN\\Geometry Optimization of ch
3cnproh trial 3 @mp2/6-31+G(d)\\1,1\H,0.4264919892,0.6586494088,-0.302
4997829\O,0.4046413781,0.6681320955,0.7548776245\H,1.3216532002,0.7439
636323,1.1012780339\C,-0.2997952433,-0.5293006606,1.3440894278\H,0.182
987407,-1.4195291906,0.9351504337\H,-1.3136254865,-0.4276338589,0.9579
350133\C,-0.2293536999,-0.4422075859,2.8481392088\H,0.8183035175,-0.47
1116944,3.1728976658\H,-0.6583008014,0.5105560122,3.1737892244\C,-0.99
25862539,-1.6130892222,3.474795548\H,-0.9367968272,-1.5507985309,4.563
5406852\H,-0.5693936503,-2.5753012135,3.1724504855\H,-2.0489443574,-1.
593152693,3.1924730247\N,0.4214475326,0.6511583511,-1.8291666621\C,0.3
982647977,0.725026324,-3.0003973223\C,0.3722986502,0.8124425033,-4.456
6603362\H,1.383584406,0.680395806,-4.8480469061\H,-0.2779277445,0.0317
655721,-4.8579323694\H,-0.0082649104,1.791808626,-4.7556890263\\Versio
n=SGI-G98RevA.7\HF=-325.3952558\MP2=-326.3954055\RMSD=4.389e-09\RMSF=1
.750e-08\Dipole=0.6921217,0.2621372,-1.1400566\PG=C01 [X(C5H12N1O1)]\\
@

(19)

1\1\GINC-FRED\FOpt\RMP2-FC\6-31+G(d)\C5H10N1(1+)\RICHARD\09-Aug-2000\0
\\# MP2/6-31+G(D) OPT=TIGHT FREQ=NORAMAN\\Geometry Optimization of mz8
4 @mp2/6-31+G(d)\\1,1\N,0.7170231706,-0.3769413488,0.0000555128\C,1.83

86031477,-0.0668907809,0.0000244485\C,-0.6977233101,-0.7135275182,0.00
0865269\C,3.2436956662,0.3121893242,-0.0000170302\H,-0.8595600624,-1.
3258172692,0.8916248169\H,-0.8595449184,-1.3260443332,-0.891298537\C,-
1.5528419701,0.5523225143,-0.0000815179\H,3.7242434952,-0.092811677,-0
.8947490504\H,3.7245584077,-0.0937818833,0.8941059697\H,3.3217139568,1
.4027830621,0.0005609509\H,-1.3132123032,1.1497192655,-0.8857342179\H,
-1.313228636,1.14994329,0.8854244606\C,-3.0329871083,0.1702554931,-0.0
00046698\H,-3.2943607548,-0.4121150981,0.8881947739\H,-3.2943443949,-0
.4123401601,-0.888145387\H,-3.6479055368,1.0729600503,-0.000166745\\Ve
rsion=SGI-G98RevA.7\HF=-249.369012\MP2=-250.1711721\RMSD=2.341e-09\RMS
F=3.329e-08\Dipole=1.9271262,-0.1641216,0.000035\PG=C01 [X(C5H10N1)]\\
@

(14)
1\1\GINC-FRED\FOpt\RMP2-FC\6-31+G(d)\C5H12N1O1(1+)\RICHARD\14-Feb-2001
\0\\# MP2/6-31+G(D) OPT FREQ=NORAMAN\\Isomerization barrier\\1,1\C,1.4
979537396,0.005857724,-0.1131822404\N,-1.5497314458,-0.0429367071,-0.0
410926263\C,-2.7288874068,-0.0209946893,-0.088772139\C,-4.1901920003,0
.0062793782,-0.1471486848\H,-4.5994038028,0.1054724614,0.8606456904\H,
-4.5208766398,0.853191467,-0.7523868839\H,-4.5603731227,-0.9190531779,
g -0.5939554916\H,0.7773452521,-0.0158265152,-0.9280385129\C,1.498694415
5,-1.2443289721,0.7180102923\H,2.2906094175,-1.2309578738,1.4730940162
\H,1.5765064651,-2.1502560337,0.1097319826\H,0.5332963623,-1.280956450
4,1.2315012663\O,2.8566050901,0.0370419832,-0.9577711202\H,2.999241638
2,-0.7968858345,-1.4644455067\H,3.6419967038,0.1717138365,-0.376479663
\C,1.4980072152,1.3136033976,0.6215282858\H,2.2670886816,1.3446330848,
1.4004929928\H,1.6149493895,2.1595264827,-0.0593198631\H,0.5214432751,
1.4011186068,1.106364236\\Version=SGI-G98RevA.7\HF=-325.3794404\MP2=-3
26.3779265\RMSD=3.908e-09\RMSF=4.380e-06\Dipole=2.2119028,-0.4383512,-
0.5429876\PG=C01 [X(C5H12N1O1)]\\@

(13)
1\1\GINC-MS1\FOpt\RMP2-FC\6-31+G(d)\C5H12N1O1(1+)\RICHARD\21-Feb-2001\
0\\# MP2/6-31+G(D) OPT FREQ=NORAMAN\\Isomerization barrier\\1,1\C,-1.5
459464798,-0.3546582981,-0.01993419\N,1.4860871561,-0.5318063896,-0.10
16617123\C,2.6638518386,-0.4919529378,-0.0340814723\C,4.1230016651,-0.
4382368816,0.0551943039\H,4.4839303703,0.5133878703,-0.3410908145\H,4.
4331881201,-0.5317273515,1.0982830023\H,4.5608084328,-1.2551260885,-0.
5225552428\H,-0.9431604977,-0.6623392311,0.8302206085\H,-1.0654921849,
-0.62697824,-0.9581032372\O,-2.7868174918,-1.3039444192,0.1119363717\H
,-2.5479699197,-2.2575736546,0.0292103364\H,-3.4816331458,-1.098981992

7,-0.5574444328\C,-2.0714328302,1.0496618489,0.0510888211\H,-2.7576829
881,1.2397906972,-0.7836667448\H,-2.6206860829,1.1890602398,0.98737948
39\C,-0.8945024716,2.0332252716,-0.0252324633\H,-0.2015586393,1.882244
5045,0.8052439848\H,-1.2773247422,3.0546549789,0.0262632479\H,-0.34031
9213,1.9195543297,-0.9598091753\\Version=x86-Linux-G98RevA.7\HF=-325.3
695799\MP2=-326.3656646\RMSD=4.919e-09\RMSF=2.798e-05\Dipole=-2.098479
2,-1.4893492,-0.3880266\PG=C01 [X(C5H12N1O1)]\\@

N-Propanol / Acetonitrile Dimer
TS dimer to complex MP2/6-31+G(d)

1\1\GINC-MS2\PTS\RMP2-FC\6-31+G(d)\C5H12N1O1(1+)\PMM\03-Mar-2001\1\\#N
MP2/6-31+G(D) OPT=(TS,EF,RCFC) FREQ GEOM=CHECK GUESS=CHECK\\npropanio
l - dimer to complex ts\\1,1\X\X,1,1.\O,2,0.7435,1,90.\N,2,nx,3,a,1,d1
,0\C,2,cx,1,90.,3,180.,0\X,4,1.,2,90.,5,0.,0\C,4,cn,6,cnx,2,cnxx,0\X,7
,1.,4,90.,6,0.,0\C,7,cc,8,ccx,4,ccxn,0\H,9,hc,7,hcc,8,hccx,0\H,9,hc2,7
,hcc2,10,hcch,0\H,9,hc3,7,hcc3,10,hcch1,0\H,3,oh1,2,ohx,1,ohxx,0\H,3,o
h2,2,ohx2,1,ohxx2,0\H,5,ch,2,chx,1,chxx,0\H,5,ch2,2,chx2,15,chxh,0\C,5
,cc3,2,ccx3,15,ccxh1,0\H,17,ch4,5,hcc4,3,hcco,0\H,17,ch5,5,hcc5,18,hcc
h5,0\C,17,cc6,5,ccc6,18,ccch6,0\H,20,1.09383476,17,hcc7,5,hccc7,0\H,20
,1.09222878,17,hcc8,21,hcch8,0\H,20,ch9,17,hcc9,21,hcch9,0\\ch9=1.0923
903\hcc7=111.13711194\hcc8=109.25474561\hcc9=111.33635263\hccc7=61.721
64984\hcch8=119.19809568\hcch9=-121.06186505\ch4=1.09455276\ch5=1.0969
1117\cc6=1.53607364\hcc4=109.92275122\hcco=-55.82145395\hcc5=110.18041
683\hcch5=119.50176926\ccc6=108.69598176\ccch6=-120.70981702\ohxx=95.9
975228\ohxx2=-142.18216939\cnx=93.41983999\cnxx=175.64291935\hc3=1.092
19149\hcc3=109.84671412\cc3=1.50061233\ccx3=106.97766985\ccxh1=120.257
43866\cx=0.82334689\ccx=89.97715395\ccxn=180.02255877\hccx=107.5042406
9\cn=1.18031931\cc=1.4628605\hc=1.09219348\hc2=1.09218316\oh1=0.986792
37\oh2=0.98635162\ch=1.08838792\ch2=1.08763567\hcc=109.81709862\hcc2=1
09.83627478\ohx=112.47877081\ohx2=111.65735482\chx=101.34622783\chx2=1
05.98450221\hcch=120.00204603\hcch1=-119.99675954\chxx=-31.3593337\chx
h=-115.93543265\nx=3.72459633\d1=-110.02494536\a=142.20650871\\Version
=x86-Linux-G98RevA.7\HF=-325.3697689\MP2=-326.3656496\RMSD=2.308e-09\R
MSF=1.099e-04\Dipole=2.4442713,-0.1365543,0.2405045\PG=C01 [X(C5H12N1O
1)]\\@

TS intermediate complex to isomer MP2/6-31+G(d)

1\1\GINC-MS2\PTS\RMP2-FC\6-31+G(d)\C5H12N1O1(1+)\PMM\29-Jan-2001\1\\#N
MP2/6-31+G(D) OPT=(TS,EF,RCFC) FREQ\\ts complex to iso2 for n-propyl
system\\1,1\C\H,1,R2\H,1,R3,2,A3\C,1,r4,2,a4,3,d4,0\O,1,R5,2,A5,3,D5,0
\H,5,R6,1,A6,2,D6,0\H,5,R7,1,A7,6,D7,0\N,1,R8,2,A8,3,D8,0\X,8,1.,1,90.
,2,0.,0\C,8,R9,9,A9,1,D9,0\X,10,1.,8,90.,9,0.,0\C,10,R10,11,A10,8,D10,
0\H,12,R11,10,A11,11,D11,0\H,12,R12,10,A12,13,D12,0\H,12,R13,10,A13,13
,D13,0\H,4,r14,1,a14,2,d14,0\H,4,r15,1,a15,16,d15,0\C,4,r16,1,a16,16,d
16,0\H,18,r17,4,a17,1,d17,0\H,18,r18,4,a18,19,d18,0\H,18,1.0938288,4,a
19,19,d19,0\\r17=1.09475432\r18=1.09237205\a17=111.74604469\a18=110.20
497978\a19=110.87586092\d17=59.71162842\d18=119.57876303\d19=-120.9102
7516\r16=1.52465333\a16=114.01611721\d16=-124.39282022\r4=1.48953271\a
4=121.84525437\d4=174.04091094\r14=1.09711405\r15=1.09440048\a14=106.8
7229817\a15=107.26378381\d14=121.40140426\d15=111.80361129\R2=1.080303
62\R3=1.08184356\R6=0.97837212\R7=0.97873262\R9=1.17728127\R10=1.46104
05\R11=1.09233947\R12=1.09235216\R13=1.09235047\A3=117.41864908\A5=89.
57210489\A6=117.65125994\A7=117.35016517\A8=82.33745758\A11=109.601337
21\A12=109.63398469\A13=109.62150423\D5=-86.77916944\D6=-67.60576511\D
7=128.64168783\D8=80.9706743\D9=175.67658178\D10=180.41307878\D11=-9.3
1791847\D12=120.00847628\D13=-119.99397224\R5=2.02120472\R8=2.19467236
\A9=90.62844277\A10=89.92823322\\Version=x86-Linux-G98RevA.7\HF=-325.3
590361\MP2=-326.3519305\RMSD=6.265e-09\RMSF=7.076e-05\Dipole=0.7142294
,0.7040046,0.5073063\PG=C01 [X(C5H12N1O1)]\\@

ISO-Propanol / Acetonitrile Dimer System
TS Complex to isomer MP2/6-31+G(d)

1\1\GINC-MS2\PTS\RMP2-FC\6-31+G(d)\C5H12N1O1(1+)\PMM\13-Feb-2001\1\\#N
MP2/6-31+G(D) OPT=(TS,EF,RCFC) GEOM=CHECK GUESS=CHECK\\ts complex to
iso2 for n-propyl system\\1,1\C\H,1,R2\C,1,R3,2,A3\C,1,r4,2,a4,3,d4,0\
O,1,R5,2,A5,3,D5,0\H,5,R6,1,A6,2,D6,0\H,5,R7,1,A7,6,D7,0\N,1,R8,2,A8,3
,D8,0\X,8,1.,1,90.,2,0.,0\C,8,R9,9,A9,1,D9,0\X,10,1.,8,90.,9,0.,0\C,10
,R10,11,A10,8,D10,0\H,12,1.0923,10,A11,11,D11,0\H,12,R12,10,A12,13,D12
,0\H,12,R13,10,A13,13,D13,0\H,4,r14,1,a14,2,d14,0\H,4,r15,1,a15,16,d15
,0\H,4,r16,1,a16,16,d16,0\H,3,r17,1,a17,2,d17,0\H,3,r18,1,a18,19,d18,0
\H,3,r19,1,a19,19,d19,0\\r17=1.08877253\r18=1.09427648\r19=1.09751394\
a17=112.91854389\a18=109.49580718\a19=107.22073858\d17=9.50579205\d18=
123.46671983\d19=-121.50796716\r16=1.08962439\a16=112.76024652\d16=-12
5.49891472\r4=1.4707637\a4=119.1696965\d4=177.36392728\r14=1.09350542\
r15=1.09768221\a14=110.42625973\a15=106.56544858\d14=144.06475702\d15=
115.81997223\R2=1.0806923\R3=1.4712578\R6=0.9762067\R7=0.97639677\R9=1

.17913393\R10=1.46171821\R12=1.09229605\R13=1.0922962\A3=119.78763128\
A5=81.7469278\A6=123.89116678\A7=123.37356492\A8=74.86723157\A11=109.7
0194007\A12=109.72914051\A13=109.69152838\D5=-92.82474486\D6=-85.59196
589\D7=145.95247347\D8=85.24290299\D9=179.05815253\D10=179.97605276\D1
1=-291.45947658\D12=120.01862416\D13=-119.98957531\R5=2.27136716\R8=2.
44966309\A9=87.02990111\A10=90.06253827\\Version=x86-Linux-G98RevA.7\H
F=-325.3751263\MP2=-326.3628344\RMSD=4.792e-09\RMSF=1.759e-06\Dipole=-
0.1121027,0.7848475,0.299026\PG=C01 [X(C5H12N1O1)]\\@

Appendix C GAUSSIAN Archive Entries for MP2/6-31+G(d) Optimized Geometries (Chloroacetonitrile-methaol)

($ClCH_2CN$)(CH_3OH)H^+ M/Z 108 (15)

1\1\GINC-MS5\FOpt\RMP2-FC\6-31+G(d)\C3H7Cl1N1O1(1+)\RICHARD\10-Sep-200
1\0\\# MP2/6-31+G(D) OPT FREQ=NORAMAN\\Meoh-CLCH2CN Dimer Optimization
\\1,1\N,0.4447510016,-0.7458212181,-0.1699903086\H,1.9642594507,-0.893
5199124,-0.3147080294\O,3.0085755793,-0.9737359637,-0.4415492823\H,3.3
967729659,-1.4790522026,0.3064316901\C,3.6759082201,0.345955161,-0.636
4627221\H,3.1842753124,0.7804684331,-1.5020492792\H,4.7190040882,0.125
26377,-0.8459558819\H,3.5457305017,0.9490569659,0.2598816443\C,-0.7182
340165,-0.6164124882,-0.0765420409\C,-2.1699998336,-0.457175603,0.0408
531493\Cl,-2.5612886077,1.1592161997,0.6509556459\H,-2.5541665208,-1.2
137071512,0.7291130649\H,-2.6218773337,-0.5987514802,-0.9437230883\\Ve
rsion=x86-Linux-G98RevA.7\HF=-706.1934527\MP2=-707.0606984\RMSD=4.411e
-09\RMSF=1.519e-06\Dipole=3.0174818,-1.1870649,-0.2470874\PG=C01 [X(C3
H7Cl1N1O1)]\\@

$ClCH_2CNCH_3$ M/Z 90 (20)

1\1\GINC-MS1\Freq\RMP2-FC\6-31+G(d)\C3H5Cl1N1(1+)\RICHARD\25-Jul-2001\
0\\# MP2/6-31+G(D) OPT=(TIGHT,CALCALL)\\clch2cnch3 optimization\\1,1\N
,-1.475022075,-0.0003320767,0.5765746414\C,-0.3129849149,0.0000089377,
0.5985205691\C,1.1530840174,0.0004335206,0.5954054021\Cl,1.7382206961,
0.000326101,-1.071392658\H,1.498951274,-0.8932178945,1.1231406729\H,1.
4984329685,0.8944607641,1.1228434734\C,-2.9189091883,-0.0007582084,0.5
335509135\H,-3.2155926183,-0.0009054915,-0.5159507901\H,-3.2670282123,
0.8989978228,1.0413271656\H,-3.2665002053,-0.9006597869,1.0414308674\\
Version=x86-Linux-G98RevA.7\HF=-630.165185\MP2=-630.8338935\RMSD=5.667
e-09\RMSF=1.241e-07\

ClCHCN M/Z 74

1\1\GINC-MS5\FOpt\RMP2-FC\6-31+G(d)\C2H1Cl1N1(1+)\RICHARD\09-Apr-2001\
0\\# MP2/6-31+G(D) OPT FREQ=NORAMAN\\CLCHCN Optimization\\1,1\N,2.3292
852244,-0.4665568042,0.\C,1.249288714,0.0237656424,0.\C,-0.0110914324,
0.6647065212,0.\H,-0.0648532866,1.7570224615,0.\Cl,-1.3923133514,-0.15
42328126,0.\\Version=x86-Linux-G98RevA.7\State=1-A\HF=-589.8462566\MP
2=-590.3849559\RMSD=4.914e-09\RMSF=1.014e-04\Dipole=-0.9757984,0.91820
31,0.\PG=CS [SG(C2H1Cl1N1)]\\@

CH_2CHNCH_2 m/z 55

N-N= 1.032034613870D+02 E-N=-5.966091448220D+02 KE= 1.703350887022D+02
1\1\GINC-MS4\FOpt\UMP2-FC\6-31+G(d)\C3H5N1(1+,2)\RICHARD\13-Apr-2001\0
\\# MP2/6-31+G(D) OPT FREQ=NORAMAN\\CH3CNCH2 Optimization\\1,2\N,-0.64
52329777,0.0002598632,-0.0000009522\C,0.5025336466,0.000488941,0.00001
40189\C,1.9511899703,-0.0000935328,0.0000171588\H,2.3074154279,-0.5178
950818,0.8959726279\H,2.3074201585,-0.5179087658,-0.8959282496\H,2.307
1398251,1.0342777024,0.0000100693\C,-2.0182250386,-0.0002816842,-0.000
017695\H,-2.5095714466,0.961243851,-0.000067278\H,-2.508764591,-0.9622
190922,-0.0000614006\\Version=x86-Linux-G98RevA.7\HF=-170.6639451\MP2=
-171.1612095\PUHF=-170.6762152\PMP2-0=-171.171206\S2=0.857703\S2-1=0.8
16347\S2A=0.756583\RMSD=7.197e-09\RMSF=1.517e-05\Dipole=0.179833,-0.00
08263,-0.000029\PG=C01 [X(C3H5N1)]\\@

C_2H_4 M/Z 28

1\1\GINC-MS1\FOpt\RMP2-FU\6-31+G(d)\C2H4\RICHARD\19-Jul-2001\0\\# MP2(
FULL)/6-31+G(D) OPT FREQ=NORAMAN\\Geometry Optimization of ethene\\0,1
\C,-0.6377658475,0.,0.2033702574\H,-0.8989813164,0.,1.2569212376\C,0.6
377059156,0.,-0.203274733\H,1.4606905708,0.,0.5045135477\H,0.898825082
8,0.,-1.2568781908\H,-1.4601747456,0.,-0.5051297413\\Version=x86-Linux
-G98RevA.7\State=1-A\HF=-78.0351585\MP2=-78.3005567\RMSD=6.307e-09\RM
SF=3.271e-05\Dipole=0.0000521,0.,-0.0000463\PG=CS [SG(C2H4)]\\@

CH_3CN M/Z 41

1\1\GINC-MS4\FOpt\RMP2-FC\6-31+G(d)\C2H3N1\RICHARD\09-Sep-2001\0\\# MP
2/6-31+G(D) OPT FREQ=NORAMAN\\CH3CN Optimization\\0,1\N,-1.4546883303,
0.,-0.0004324022\C,-0.2738785522,0.,-0.000071349\C,1.1896049982,0.,0.0

003588512\H,1.5630927413,0.,-1.0259889815\H,1.5626834472,-0.8889627892
,0.5136453919\H,1.5626834472,0.8889627892,0.5136453919\\Version=x86-Li
nux-G98RevA.7\State=1-A'\HF=-131.9258033\MP2=-132.3453604\RMSD=5.092e-
09\RMSF=1.051e-04\Dipole=1.5674769,0.,0.0004476\PG=CS [SG(C2H1N1),X(H2
)]\\@

$ClCH_2CN$-CH_3OH-ISOM (32)

1\1\GINC-MS1\FOpt\RMP2-FC\6-31+G(d)\C3H7Cl1N1O1(1+)\RICHARD\22-Sep-200
1\0\\# MP2/6-31+G(D) OPT=TIGHT FREQ=NORAMAN\\Optimization of H2O compl
ex 3\\1,1\N,0.5313499035,0.3940595569,-0.0264616257\C,-0.6100048661,0.
6101903914,0.0143806265\C,-2.0538067762,0.8580245266,0.0656020423\H,-2
.3256082304,1.4940097406,-0.7815729157\H,-2.2824358824,1.3763131544,1.
001106765\Cl,-2.9229199586,-0.6785193822,-0.0148785717\C,1.9530586369,
0.1107915537,-0.0764672068\H,2.3694998252,0.644167417,-0.9288395127\H,
2.0698163906,-0.9647527733,-0.1983754648\H,2.4001409398,0.450158335,0.
8555048795\O,4.6829262989,-0.3482280698,0.044230754\H,5.1368444475,-1.
1415889248,0.379850627\H,5.4030401235,0.2298913792,-0.2644460828\\Vers
ion=x86-Linux-G98RevA.7\HF=-706.1957028\MP2=-707.060508\RMSD=3.445e-09
\RMSF=4.948e-08\Dipole=1.3903457,1.0207629,0.0324884\PG=C01 [X(C3H7Cl1
N1O1)]\\@

CH_3OH M/Z 32

1\1\GINC-MS3\FOpt\RMP2-FC\6-31+G(d)\C1H4O1\RICHARD\16-Sep-2001\0\\# MP
2/6-31+G(D) OPT=TIGHT FREQ=NORAMAN\\Methanol Optimization\\0,1\H,-0.86
56911055,-1.0776872931,0.\O,0.0525450077,-0.7596403882,0.\C,0.04210507
38,0.6717383139,0.\H,1.0874008396,0.978536729,0.\H,-0.4473501195,1.072
9218933,0.894652528\H,-0.4473501195,1.0729218933,-0.894652528\\Version
=x86-Linux-G98RevA.7\State=1-A\HF=-115.0394923\MP2=-115.3578389\RMSD=
8.174e-09\RMSF=2.893e-06\Dipole=-0.6473294,0.4885311,0.\PG=CS [SG(C1H2
O1),X(H2)]\\@

CH_3OH_2 M/Z 33

1\1\GINC-MS3\Freq\RMP2-FC\6-31+G(d)\C1H5O1(1+)\RICHARD\17-Sep-2001\0\\
MP2/6-31+G(D) OPT=(TIGHT,CALCALL)\\CH3OH2+ Optimization\\1,1\H,1.150
4748495,0.8028292985,0.2745920625\O,0.7182919205,0.0000006511,-0.10424
05203\H,1.1504751809,-0.8028314635,0.2745843358\C,-0.7970916223,-0.000
000309,0.0297969828\H,-1.1092702711,-0.9002971602,-0.490976189\H,-1.04
6194728,-0.0000053153,1.0879098209\H,-1.1092706619,0.9003012824,-0.490

9677643\\Version=x86-Linux-G98RevA.7\HF=-115.3389419\MP2=-115.6501621\
RMSD=8.757e-09\RMSF=3.251e-07\Dipole=0.559956,-0.0000026,0.5619178\Dip
oleDeriv=0.3745804,0.0851439,0.0050434,0.1382751,0.4686842,0.0084182,0

T. S proton-bound dimer to intermediate complex (C_3H,ClNO) TS(15-19)

1\1\GINC-MS1\Freq\RMP2-FC\6-31+G(d)\C3H7Cl1N1O1(1+)\RICHARD\23-Oct-200
1\1\\# MP2/6-31+G(D) FREQ GEOM=CHECK GUESS=CHECK\\T. S proton-bound di
mer to intermediate complex\\1,1\X\X,1,1.\O,2,0.7435,1,90.\N,2,nx,3,a,
1,d1,0\C,2,cx,1,90.,3,180.,0\X,4,1.,2,90.,5,0.,0\C,4,cn,6,cnx,2,cnxx,0
\X,7,1.,4,90.,6,0.,0\C,7,cc,8,ccx,4,ccxn,0\Cl,9,clc,7,hcc,8,hccx,0\H,9
,hc2,7,hcc2,10,hcch,0\H,9,hc3,7,hcc3,10,hcch1,0\H,3,oh1,2,ohx,1,ohxx,0
\H,3,oh2,2,ohx2,1,ohxx2,0\H,5,ch,2,chx,1,chxx,0\H,5,ch2,2,chx2,15,chxh
,0\H,5,ch3,2,chx3,15,chxh1,0\\cx=0.78856489\cnx=96.1717167\cnxx=179.95
030278\ccx=89.66097025\ccxn=180.00627616\hccx=180.30569675\d1=-110.268
81096\a=149.8809874\cn=1.18019796\cc=1.46461973\clc=1.7765726\hc2=1.09
173578\oh1=0.98640193\oh2=0.98639956\ch=1.08573696\ch2=1.08573846\hcc=
110.75295487\hcc2=109.37910849\ohx=112.76755028\ohx2=112.76901251\chx=
103.80778438\chx2=103.80739935\hcch=120.15650223\hcch1=-120.1559132\oh
xx=48.86299897\ohxx2=-188.10065998\chxx=10.9444311\chxh=117.348491\chx
h1=-121.32287972\nx=3.78722421\hc3=1.09173686\hcc3=109.38104847\ch3=1.
08525642\chx3=109.0417669\\Version=x86-Linux-G98RevA.7\HF=-706.1689394
\MP2=-707.0314213\RMSD=2.788e-09\RMSF=3.687e-06\Dipole=4.5758118,-3.26
64465,-1.1957702\DipoleDeriv=-1.0184821,0.0709074,0.0260145,-0.0297026

Claims to Original Research

1. Proton-bound dimers of acetonitrile and alcohols were studied to identify possible rearrangements that occur in the course of their unimolecular chemistry, employing mass spectrometry and ab initio theory. The main isomerization channel is an internal S_N2 reaction that involves the formation of an intermediate complex $(CH_3CN{\bullet\bullet\bullet}ROH_2)^+$ prior to the loss of water to form $(CH_3CNR)^+$. Methyl substitution of the carbon atom adjacent to the OH_2 moiety lowers the energy of the intermediate complex and hence, the barrier to the isomerization.

2. The effect of chlorine substitution on acetonitrile on the three systems methanol, ethanol and propanol were investigated and compared with the acetonitrile-alcohol proton-bound dimer ions. Chloro-substitution does reduce the proton affinity of the acetonitrile resulting in the lowest energy simple-bond cleavage reaction products $ROH_2^+ + ClCH_2CN$ in all cases. Kinetic modelling of the unimolecular reactions with RRKM theory showed that a key step in governing the ratio of the two type of reactions observed in the MI mass spectra is the initial rearrangement of the proton-bound pairs to the high energy intermediate structure $(CH_3CN{\bullet\bullet\bullet}R{\bullet\bullet\bullet}OH_2)^+$, even though it is not the rate limiting step for the overall isomerization reaction leading to water loss.

3. The dissociation pathway of the acetonitrile-oxygen dimer ion complex was investigated. A mass spectrometric investigation and density functional theory calculation showed that there is a large kinetic energy release in the dissociation which implies the dissociation occurs over a barrier.

(1) R.A. Ochran, A. Annamalai and P. M. Mayer, "Unimolecular Reactions of Proton-Bound Cluster Ions: Competition between Dissociation and Isomerization in the Ethanol-Acetonitrile Dimer" J. Phys. Chem. A 104 (2000) 8505.

(2) R.A. Ochran and P.M. Mayer, "Ion Rearrangement at the Beginning of Cluster Formation: Methyl-Substitution Effects on the Internal S_N2 Reaction in the Proton-Bound Dimers of CH_3CN and Alcohols" European Mass Spectrom. 7 (2001) 267.

(3) R.A. Ochran and P. M. Mayer, "How Does Chlorine Substitution on Acetonitrile affect the internal S_N2 isomerization of Proton-bound dimers $(ClCH_2CN)(ROH)H^+$ [R=CH_3, C_2H_5, C_3H_7]" ? Submitted.

(4) R.A. Ochran and P.M. Mayer, "Does Oxygen Catalyze Distonic ion Formation in $(CH_3CN)(O2)^{+\bullet}$" ? In preparation.